UNIVERSIDAD DE GUANAJUATO

CAMPUS IRAPUATO – SALAMANCA
DIVISIÓN DE INGENIERÍAS

Study of modal coupling in tapered optical fibers

TESIS

QUE PARA OBTENER EL GRADO DE:

DOCTOR EN INGENIERÍA ELÉCTRICA

PRESENTA:
Luis Alejandro Herrera Piad

DIRECTORES:
Dr. Roberto Rojas Laguna
Dr. Daniel Jáuregui Vázquez

SALAMANCA, GTO. Marzo, 2019

La educación empieza con la vida y no acaba sino con la muerte.

José Martí.

AGRADECIMIENTOS

-Por el apoyo brindado mediante la beca con número (CVU/Becario): 546217/300665 y demás beneficios que conlleva ser un becario CONACYT.

-Este trabajo de Tesis fue apoyado por el CONACyT a través del Proyecto de Ciencia Básica, "Investigación Experimental de Láseres Sintonizables de Longitudes de Onda múltiples utilizando Interferómetros tipo Mach-Zehnder Fabricados con Fibra de Cristal Fotónico", No 286916 y "Estudio de las No linealidades en Fibras de Cristal fotónico para la obtención de Fuentes de luz de amplio espectro y la propagación de pulsos de alta energía", No A1-S-33363.

-A la DAIP por el apoyo otorgado mediante el complemento de beca mixta para realizar mi estancia de investigación.

-A todo el cuerpo académico de Telecomunicaciones y Fotónica, en especial a mis asesores Dr. Rojas, Dr. Jáuregui y Dr.Haus (q. e. p. d.) por guiarme durante todo el trabajo de tesis y permitirme realizar una estancia de investigación. Al Dr. Cisneros, Dr. Juan Manuel, Dr. Juan Carlos, Dr. Estudillo, Dr. Juan Pablo y al Dr. Alvarado por apoyarme en todo lo que me hizo falta.

-Al Dr. Miguel Andrés y Dr. José Luis por acogerme en sus laboratorios y permitirme ampliar mis conocimientos en esta área durante la estancia de investigación, agradecer también a todos los estudiantes y demás profesores de la Universidad de Valencia.

-A todos los integrantes del claustro de profesores y trabajadores de la parte administrativa, que contribuyeron a mi formación estudiantil en especial al Dr. Aviña por su apoyo incondicional en todo momento como profesor y coordinador del posgrado en su etapa. Agradecer también a todos los estudiantes del posgrado que me ayudaron en cualquier labor esté o no relacionada con el trabajo escolar, porque me hicieron sentir parte de una gran familia. Agradecer especialmente a Regulo y Gaby, a los cuales considero mis padres en México. Disculpas si alguien se me olvida.

-A mis familiar fundamentalmente mis padres, por formarme desde la cuna y guiarme hasta el día de hoy, para poder cumplimentar otra parte de este sueño de toda la vida.

-A Yanelis por apoyarnos mutuamente en todo momento.

Muchas gracias a todos.

Luis Alejandro

DEDICATORIA

-A mi familia (la que puede verme hoy y la que no), en especial a mis padres Luis y Patricia, por apoyarme en todo momento y llevarme por el buen camino para que lograra crecer profesionalmente cada día.

-A mi hija Eva Laura para que un futuro lo más cercano posible se sienta orgullosa de su padre.

Al Dr. Haus (q. e. p. d.) por su apoyo incondicional, de las pocas veces que he conocido tanta inteligencia y sencillez reunida en una misma persona. Fue un verdadero placer conocerlo.

Luis Alejandro

ABSTRACT

Optical fiber communication is a way of transmitting information by sending pulses of light through an optical fiber. Firstly developed in the 70s, fiber-optic communication systems have revolutionized the communication industry due to their advantages over electrical transmission.

Telecommunications and laser technologies have been recently related with few-mode, Large Modal Area (LMA) and multimode fibers (MMF). More specifically, photonic lanterns, pump combiners and MMF have been newly proposed for high power lasers and communications. Another device frequently used in lasers, sensing and other systems communications is the tapered optical fiber. It was necessary to maximize the optical power collected in a waveguide from the diffracting field of a semiconductor laser; therefore the conformal mapping technique permitted the reshaping of the captured field into the fundamental mode of the output waveguide. Additionally, tapered fiber sensors are able to measure refractive index, strain, magnetic field, temperature and acoustic signals. Then, compared with the conventional fiber structures, tapered optical fibers can provide a number of useful features including another like a large evanescent field, strong mode confinement capability, small-scale diameter, and Supercontinuum generation.

In this work, an investigation about the modal interaction in tapered optical fibers is proposed to observe this device under physical changes, with the objective to propose the optimum geometry to be implemented in laser and sensing applications from our laboratory.

RESUMEN

La comunicación por fibra óptica es una forma de transmitir información mediante el envío de pulsos de luz a través de una fibra óptica. Desarrollados por primera vez en la década de los 70s, los sistemas de comunicación de fibra óptica han revolucionado la industria debido a sus ventajas sobre la transmisión eléctrica.

Las tecnologías de telecomunicaciones y láseres se han relacionado recientemente con fibras de pocos modos, de área modal grande y multimodo. Más específicamente, se han propuesto linternas fotónicas, combinadores de fuentes y fibras multimodo para láseres de alta potencia y comunicaciones. Otro dispositivo que se usa frecuentemente en los láseres, sensores y otras sistemas de comunicaciones es la fibra óptica cónica o estrechada. Fue necesario maximizar la potencia óptica recolectada en una guía de onda desde el campo de difracción de un láser semiconductor; por lo tanto, la técnica de mapeo permitió la remodelación del campo capturado en el modo fundamental de la guía de onda de salida. Además, los sensores de fibra estrechada son capaces de medir diversas variables como índice de refracción, tensión, campo magnético, temperatura y señales acústicas. En comparación con las estructuras de fibra convencionales, las fibras ópticas estrechadas pueden proporcionar una serie de características útiles como un gran campo evanescente, capacidad de confinamiento, diámetro a pequeña escala y generación de supercontinuo, entre muchas otras.

En este trabajo se propone una investigación sobre la interacción modal en fibras ópticas estrechadas para observar este dispositivo bajo diversos cambios físicos con el objetivo de proponer la geometría óptima que se implementará en las aplicaciones de detección y láseres de nuestro laboratorio.

CONTENTS

Chapter I: Introduction

Optical fiber communication [1] emerged around 30 years ago and it is seen as one of the most consistent telecommunication technologies to achieve consumers needs for present and future applications. Optical transmission systems are based on the principle that light can carry more information over longer distances in a glass medium than the electrical signals by copper or coaxial cable. Light is an electromagnetic wave and optical fiber is a waveguide, in order to compensate the loss of this wave-guide, an optical amplifier is needed [2]. First, light-wave communications systems operated near 0.8 μm at a bit rate up to 2.3 Mb/s, and electronic repeaters spaced at about 32 km. The signal regeneration has been traditionally implemented using repeaters in which the optical signal is converted into an optical current by a photodiode; the electronic current is then amplified and converted back into an optical signal by a laser diode. Since then, one of the biggest researching activities within the area of optical communications is devoted for reducing the attenuation in the signal path between the transmitter and receiver, as well as reducing the dispersion. These problems were solved by using laser sources with ultra-narrow line width and dispersion shifted fibers. However, the real limitation has been the necessity to regenerate optical signals, typically every 70-100 km. Other disadvantages of electronic repeaters are their high cost and complexity, especially for multi-channel light-wave systems, as many parallel repeaters are needed to regenerate several optical channels in the same fiber [3].

As it is seen, optical fibers have developed into a mature and ubiquitous technology primarily for optical communications systems. The field of optical fiber sensors has concurrently grown because of the wide availability and low-cost of the fibers, photonic devices and electronics. In particular, tapered optical fibers (TOFs) are a specific class that has been developed for diverse applications [4–6]; they have found application in fiber lasers [5], non-linear optical elements [7], low-level biomolecule or chemical species sensing [8] and thermodynamic variable sensing such as temperature [9]. Specifically, tapered fiber sensors are able to measure refractive index [10,11], strain [12], magnetic field [13], temperature [14] and acoustic signals [15]. Moreover, it has been demonstrated that several parameters can be simultaneously detected by modifying fiber optic structures

such as temperature and curvature [16], fiber bending and strain [17], temperature and strain [18], and temperature and refractive index [14,19].

Then, compared with the conventional fiber structures above, TOFs can provide a number of useful features including a large evanescent field, strong mode confinement capability and small-scale diameter. Thus, TOFs exhibits great potential for applications in communication systems and optical sensing, since it was reported for the first time in 2003 [20,21].

Explaining more about TOFs, the initial motivation of tapering fibers was to provide field access for coupling to a second fiber [6]. This was an alternative to both side-polishing [22], and etching [23] (which may be combined with tapering [24]). Opposite to polished couplers which rely on evanescent field coupling, Bures et al. showed that fused tapered couplers typically act as cladding-mode devices [25]. For example, the cladding and external medium provide the guidance coupling between the fibers could be considered as a beating of the modes of the total structure. Furthermore a first model neglecting the core offered good agreement with experiment data except for small taper elongations [26].

Cassidy et al. demonstrated that if the taper transition is not small enough, the fundamental mode could couple to higher order modes resulting in oscillatory responses in the fundamental mode output power of a bi-tapered fiber [27]. Furthermore, Stewart et al. introduced the way to work with the taper slope for avoiding substantial higher-modes coupling [28]. Higher-mode oscillations, which should be avoided for couplers, could be exploited to obtain numerous applications such as sensing, filtering, modulation and laser applications.

Based on the literature review, tapered optical fibers were chosen as the main topic to be studied in this thesis.

The goal is to get a good performance of TOFs in sensing and laser applications, allowing the upgrading in this field of investigation and the obtained results can be inclusively improved for future work.

1.1 Justification

Nowadays, TOFs provide several advantages over other filter devices. Its design can be different depending on the application the user needs to use. For example for couplers ideally the tapering should be slow enough to avoid higher-order mode coupling, meanwhile single mode fiber devices can be abruptly tapered to exploit the non-adiabatic coupling effect, also the adiabaticity sometimes is required to obtain a good interference pattern for sensing, laser applications and communications systems. This demands new challenges for the performance of all system modules, including the TOFs, which is the main topic of this thesis. In this case, the optimum geometry is founded, improving laser technologies and sensing applications and introducing this new field of investigation in our campus.

1.2 General Objective

Design tapered optical fibers analyzing the modal interaction under physical changes in order to propose the optimum geometry for further applications in diverse fields.

1.3 Specific Objectives

TOFs have been playing a crucial role, acting like filters for lasers and sensing devices are one of the devices with a great future in the world of optics. Therefore one of the specific objectives of this work is to completely understand the modal coupling in TOFs, in order to obtain the optimum geometry to be used with a nice performance in laser and sensing applications. Moreover, it is expected that the systems presented have better stability and offer more quality of the output signal and other parameters, approaching the advantages that tapers provide.

1.4 Thesis Structure

This work is oriented to the study of modal coupling in TOFs to its implementation in novelty laser and sensing applications.

Chapter 2 develops the study of the TOFs and possible important applications. The TOFs functioning and its theoretical properties are described. Chapter 3 deals with the procedure for systems implementation, the main parameters of each part of the system and the experimental methods used for characterization are presented. On the other hand, the functioning of the setups is explained. Chapter 4, 5, 6 and 7 presents the final results and comparison with other research groups. Finally, the conclusions of the work, promising applications and the possible improvement and implementation for a possible future work are provided.

Chapter II: Overview, Theory and State of the Art of Tapered Optical Fibers and Components

This chapter will introduce the main topic of this work, the tapered optical fibers, presenting the theory about tapers and other components. The equations of light propagation of optical fibers will be described; more specifically about tapered optical fibers, its functioning and applications using the evanescent field. We start with a brief introduction about the importance of the optical fiber in our life due to its important use in communications systems.

The appearance of telegraphy in the 1830s replaced the use of light by electricity and opened the era of electrical communications. The bit rate could be improved to approximately 10 b/s by using new coding methods like the Morse code. The creation of the telephone in 1876 caused a technological revolution and the electric signals were transmitted in analog form through a constantly varying electric current. Analog electrical techniques were controlling the communications systems for a century or maybe more. The expansion of worldwide telephone networks run to many signs of progress in the design of electrical communications systems. The use of coaxial cables instead of wire pairs increased significantly system capacity. However the bandwidth of those systems is limited by the frequency-dependent cable losses, so this limitation led to the growth to microwave communication systems, in which an electromagnetic carrier wave with frequencies in the range of 1–10 GHz, is used to transmit the signal by using suitable modulation techniques.

The first microwave system operating at the carrier frequency of 4 GHz was put into service in 1948. Since then, coaxial and microwave systems have evolved considerably and are able to operate at bit rates up to 100 Mb/s. The problematic for high-speed coaxial systems is their small repeater spacing (around 1 km), which makes the system expensive to operate. Microwave communication systems generally allow a larger repeater spacing, but their bit rate is also limited by the carrier frequency of such waves.

The invention of the laser solved the problem of the signal attenuation in the system. Therefore the attention was focused on finding ways for using laser light for optical communications. There were many advanced ideas during the 1960s, it was suggested in 1966 that optical fibers might be the greatest choice, but the main problem was the high losses of approximately 1000 dB/km. An innovation occurred in 1970 when fiber loss could be reduced to below 20 dB/km in the wavelength region near 1 μm. At the same time, GaAs semiconductor lasers were discovered. Hence the availability of compact optical sources and low-loss optical fibers were the guide for developing the new fiber-optic communication systems.

The evolution has been rapidly evident considering an increment in the bit rate by a factor of 100,000 in a period of less than 25 years. Transmission distances increased from 10 to 10,000 km and the bit rate-distance product (b/s by km commonly called BL product) of modern light-wave systems can exceed by a factor of 107 compared with the first-generation light-wave systems.

This 25-year period of huge progress extended from 1975 to 2000 can be grouped into several distinctive generations. In every generation, BL increases initially but then starts to saturate as the technology matures. Therefore each new generation brings an essential change that helps to improve the system performance.

The first generation of light-wave systems operated near 0.8 μm and used GaAs semiconductor lasers. They operated at a bit rate of 45 Mb/s and allowed repeater spacing up to 10 km.

During the 1970s the repeater spacing could be bigger by working with the light-wave system in the wavelength region near 1.3 μm, where fiber loss is below 1 dB/km; additionally, optical fibers exhibit minimum dispersion in this wavelength region. This realization led to a worldwide effort for the development of InGaAsP semiconductor lasers and detectors operating near 1.3 μm. The second generation of fiber-optic communication systems became available in the early 1980s, but the bit rate of early systems was limited to below 100 Mb/s due to dispersion in multimode fibers. This limitation was overcome by the use of single-mode fibers. By 1987, second-generation light-wave systems, operating

at bit rates up to 1.7 Gb/s with a repeater spacing about 50 km, were commercially available.

Nevertheless, the repeater spacing continued being a problem due to the fact that it was limited by the fiber loss at the operating wavelength of 1.3 μm (typically 0.5 dB/km).

Losses of silica fibers become minimum near 1.55 μm. However, the introduction of third-generation light-wave systems operating at 1.55 μm was extensively postponed by a large fiber dispersion near 1.55 μm. Conventional InGaAsP semiconductor lasers could not be used because of pulse spreading occurring as a result of simultaneous oscillation of several longitudinal modes.

The dispersion problem could be solved by using dispersion-shifted fibers designed to have minimum dispersion near 1.55 μm or by limiting the laser spectrum to a single longitudinal mode. Third-generation light-wave systems operating at 2.5 Gb/s became commercially available in 1990. Such systems are capable of operating at a bit rate up to 10 Gb/s. One more time the problem of third-generation 1.55 μm systems is that the signal is regenerated periodically by using repeaters spaced apart typically by 60–70 km [29].

The fourth generation of light-wave systems makes use of optical amplification to increase the repeater spacing and in the case of wavelength-division multiplexing (WDM) for raising the bit rate. The arrival of the WDM technique started a revolution that resulted in light-wave systems operating at a bit rate of 10 Tb/s by 2001.

The fifth and last generation of fiber-optic communication systems are concerned with extending the wavelength range, which a WDM system can operate simultaneously. The conventional wavelength window, known as the C-Band, covers the wavelength range of 1.53–1.565 μm. It is being extended on both the long- and short-wavelength sides, resulting in the L and S bands, respectively. Raman amplification technique can be used for signals in all three wavelength bands. Moreover, a new kind of fiber known as the dry fiber has been developed with the property that fiber losses are small over the entire wavelength region extending from 1.30 to 1.65 μm. Availability of such fibers and new amplification schemes may lead to light-wave systems with thousands of WDM channels.

Starting in 2000, many channels used in experiments operate at 40 Gb/s; migration toward 160 Gb/s is also likely in the future [29].

Well, after this extensive description of system communications history, having the fiber optic as the main element, sensing and laser technologies still developing new methods and improving their performance. Then, optical waveguides find applications in integrated optical devices as well as various forms of communication systems. The study of electromagnetic (EM) wave propagation through various types of optical fibers and waveguides has been investigated by several research groups, as appeared in the literature. In this context, several forms of optical waveguides implementing different composite materials [30] and/or new forms of geometrical cross-sections [31,32] have been developed, most of which are now widely recognized for their use in the fabrication of integrated optical circuits and in the laser beam technology. These include unconventional types of waveguide geometries too.

Therefore, among the various types of fiber structures, fibers with tapers have received considerable attention over the years because of their promising applicability in the area of fused fiber couplers. These TOFs are of practical interest for the fabrication of all-optical components as these miniaturized find enormous potential applications in the areas related to optical sensors as well as other integrated optics applications where directional couplers and beam expanders are being used.

It is noted that TOFs can be used with much efficiency in evanescent wave fiber-optic absorption sensors, then TOFs become one of the most promising means in high-speed transmission systems. Optically, the taper transitions transform the local fundamental mode from a core mode in the untapered fiber to a cladding mode in the taper waist, the basis of many of its applications including multiplexing and modulation. It is desirable for the transition to be as short as possible, allowing the resulting component to be compact and insensitive to the degradation of the environment [33]. Hence, in this chapter, the theoretical fundamentals of optical fibers (including TOFs) and other system components will be presented.

2.1 Erbium-Doped Fiber Amplifier

Before to describe TOFs, we need to know the basic concepts and properties of optic elements, starting with the erbium doped fiber (EDF). In the next figure, the energy levels of erbium ions in silica glasses are shown. The transition corresponding to the 1520-1570 nm signal band, known as the third telecommunications window, includes the metastable state ($^4\mathbf{I}_{13/2}$) and the ground state ($^4\mathbf{I}_{15/2}$). The population inversion between these two levels is achieved by optically pumping the erbium ions from the ground level to some higher state and then ions relax to that metastable state. The metastable state is an excited state with a longer lifetime than the other excited states. However, it has a shorter lifetime than the stable ground state. Atoms in the metastable state continue in an excited state for a considerable time. A large number of excited atoms are accumulated in the metastable state and the population of metastable state can exceed the population at the lower level thereby establishing population inversion in a lasing medium. After that, signal amplification in this band is accomplished by stimulated emission.

By choosing many pump wavelengths for experiments, an efficient high gain operation of erbium-doped fiber amplifiers is possible and it was demonstrated [29,34]. Practical pump wavelengths of 532 nm and 980 nm are identified as optimal, especially 980 nm pump band ($^4\mathbf{I}_{15/2}$ to $^4\mathbf{I}_{11/2}$ transition) because it offers the highest gain efficiencies. For that reason, 980 nm pumping will be the selected wavelength for this work for some of our applications.

Furthermore, it is important to mention that the EDF allows creating an ASE (Amplified Spontaneous Emission) light source to characterize some devices to see the spectrum response. ASE light source is one type of optical light sources, where the emission is generated by Amplified Spontaneous Emission via stimulated emission. An optical gain medium emits light spontaneously when it is optically/electrically pumped, and if the pumping of the gain medium is strong enough, the “spontaneous” emission is amplified via the “stimulated” emission. ASE light sources generally possess broadband spectrum and low coherence, and have been used in various optical measurement and sensing systems. In particular, ASE light sources made by rare-earth (RE) doped optical fiber are widely used due to the following reasons: ASE is generated in the fiber core and therefore can be

coupled to a single mode fiber with a very low coupling loss. Also, the core of an optical fiber is usually circular thus the output is inherently unpolarized and the emission from a RE-doped optical fiber is generally very broad, resulting in a very broadband light source.

ASE from a RE-doped optical fiber is generated in a similar way as fiber lasers and fiber amplifiers. Indeed, fiber lasers below threshold and fiber amplifiers with no signal input are both ASE sources. Another example of an amplified spontaneous emission source is the superluminescent diode (SLED or SLD), is a semiconductor light source based on superluminescence. It combines the high power and brightness of laser diodes with the low coherence of conventional light-emitting diodes. Its emission band is 5–100 nm wide.

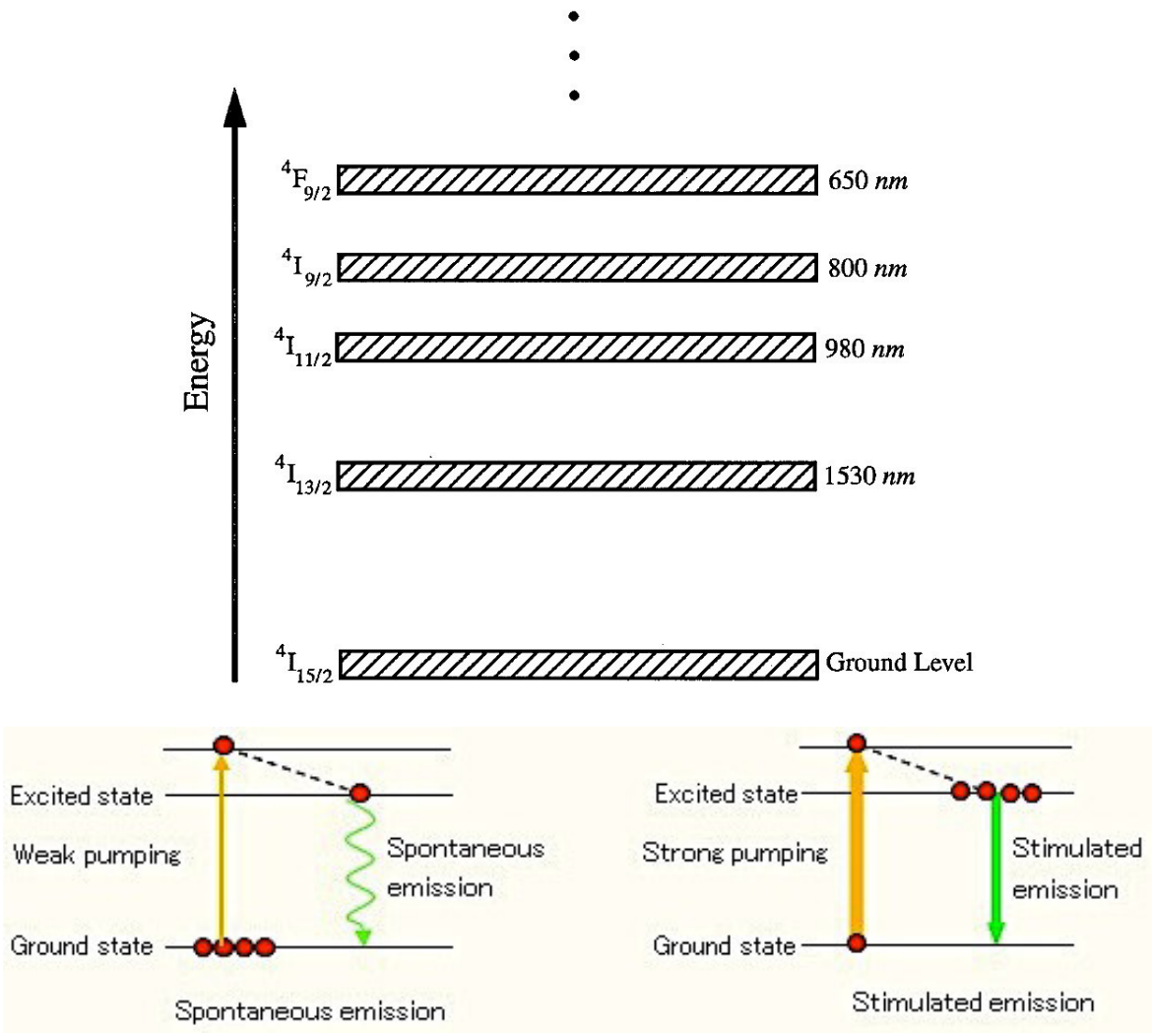

Figure 2.1: Energy levels of erbium ions in silica glass [3] and differences between Spontaneous and Stimulated Emission.

Figure 2.1 also shows a scheme of spontaneous emission and stimulated emission. When the pump intensity is increased enough, the initial spontaneous emission is amplified by stimulated emission and the optical power increases.

2.2 Refraction Index Profiles

This section will show a simple historical development of the properties of optical fiber, especially the refraction index. Three parameters are basically responsible for these properties. The core and cladding materials used determine the attenuation and chromatic dispersion, the refractive index profile defines the mode dispersion and the core diameter is responsible for the number of modes. Particularly the core material and the index profile are at least identifiable from the name of the fiber.

2.2.1 Step-Index Fibers (SI)

The first optical fibers were pure step index profile (SI). This means that a simple optical cladding surrounds a uniform core. For this reason, a protective material is always included in the cable. Figure 2.2 represents the refractive index curve.

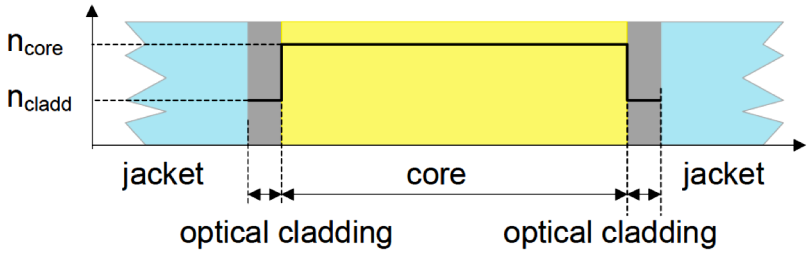

Figure 2.2: Structure of a step index profile fiber [35].

As it is known from the basic theory of optical fibers, when the core diameter is small, only a single mode is supported and the fiber is said to be a single-mode fiber. Fibers with large core diameters are multimode fibers (MMF). One of the problems associated with the propagation of light in a MMF arises from the differences between the group velocities of the modes. This ends in a spread of travel times and consequences in the expansion of a light pulse as it travels through the fiber. This effect, called modal dispersion, establishes a limit of how often adjacent pulses can be launched without resulting in pulse overlap at the

end of the fiber. Also, it limits the speed at which multimode optical fiber communication systems can operate.

Modal dispersion can be reduced by grading the refractive index of the fiber core from a maximum value at its center to a minimum value at the core-cladding frontier (figure 2.3). The fiber is then called a graded-index fiber (GI).

2.2.2 Graded Index Fibers (GI)

In a graded-index fiber (GI) the travel velocity increases with radial distance from the core axis (since the refractive index decreases), although rays of bigger inclination to the fiber axis must travel farther, they thus travel faster. This permits the travel times of the different modes to be equalized [36].

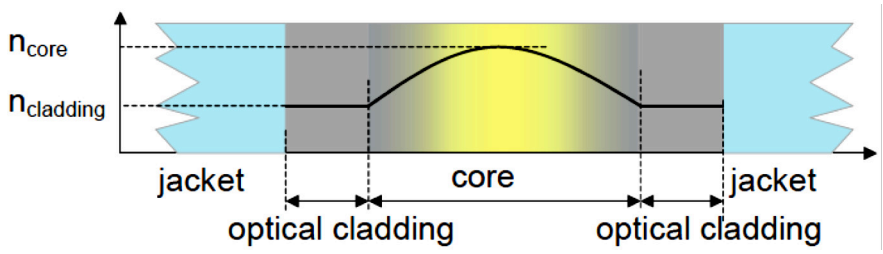

Figure 2.3: Structure of a graded index profile fiber [35].

Explaining a little more, due to the continually changing refractive index, the light rays in a GI fiber do not propagate in a straight line but are constantly refracted towards the fiber axis. Light rays that are launched at the center of the fiber and do not exceed a certain angle are completely prevented of leaving the core area. This behavior is illustrated in figure 2.4. The geometric path of the rays running on a parallel to the axis is still considerably smaller than the path of rays that are launched at a bigger angle. However, as can be seen, the index is smaller in the regions distant from the core. This means a greater propagation speed. If an ideal combination of parameters is used, the different path lengths and different propagation speeds may cancel each other out completely so the modal dispersion disappears. In reality, this is not totally possible. However, it is possible to increase bandwidths by two to three orders of magnitude compared with the SI fiber [36].

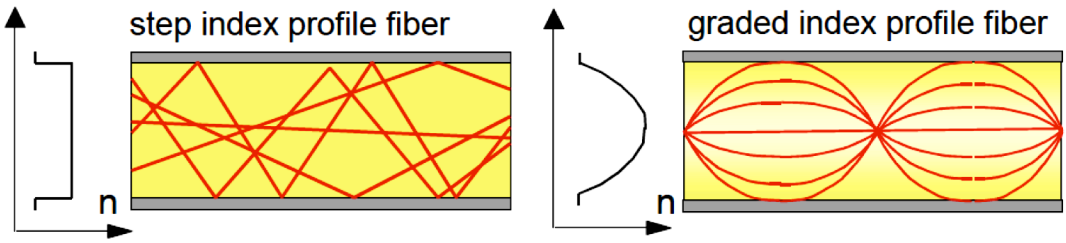

Figure 2.4: Comparison of step and graded index profile [35].

2.3 Propagation Modes in Optical Fibers

An optical propagation mode refers to a specific solution of the wave equation that satisfies the appropriate boundary conditions and has the property that its spatial distribution does not change with propagation. It is important to mention that the analysis realized in this section, is for Step-Index Fibers.

As any electromagnetic phenomena, propagation of optical fields in fibers is ruled by Maxwell equations.

For a non-conducting medium without free charges, these equations are

$$\nabla \mathrm{x}\, \mathbf{E} = -\frac{\partial \mathbf{B}}{\partial \mathrm{t}}, \tag{2.1}$$

$$\nabla \mathrm{x}\, \mathbf{H} = \frac{\partial \mathbf{D}}{\partial \mathrm{t}}, \tag{2.2}$$

$$\nabla \bullet \mathbf{D} = 0\,, \tag{2.3}$$

$$\nabla \bullet \mathbf{B} = 0\,, \tag{2.4}$$

where $\mathbf{E}$ and $\mathbf{H}$ are the electric and magnetic field vectors respectively, and $\mathbf{D}$ and $\mathbf{B}$ are the corresponding flux densities. The flux densities are related to the field vectors by

$$\mathbf{D} = \varepsilon_0 \mathbf{E}\,, \tag{2.5}$$

$$\mathbf{B} = \mu_0 \boldsymbol{H}, \tag{2.6}$$

where ε_0 is the vacuum permittivity and μ_0 is the vacuum permeability.

A necessary condition to that $\mathbf{E}$ and $\mathbf{H}$ satisfy the Maxwell equations is that their components must satisfy the wave equation:

$$\nabla^2 \mathbf{E}(\mathrm{r},\mathrm{t}) - \frac{1}{\mathrm{c}^2}\frac{\partial^2 \mathbf{E}(\mathrm{r},\mathrm{t})}{\partial \mathrm{t}^2} = 0\,, \tag{2.7}$$

where c is the velocity of light in vacuum. If Fourier Transform is applied, the wave equation can be written

$$\nabla^2 \mathbf{E}(\omega,\mathrm{t}) + k_0^2 n^2 \mathbf{E}(\omega,\mathrm{t}) = 0, \tag{2.8}$$

where the free-space wave number k_0 is defined as $k_0 = \frac{\omega}{\mathrm{c}} = 2\pi/\lambda$ and λ is the vacuum wavelength of the optical field oscillating at the frequency ω.

Hence, an optical propagation mode refers to a specific solution of the wave equation that satisfies the appropriate boundary conditions and has the property that its spatial distribution does not change with propagation.

To take advantage of the cylindrical symmetry, the equation is written in the cylindrical coordinates ρ , $\boldsymbol{\phi}$, and z (equation 2.9) and its solution is obtained (equation 2.11).

$$\frac{\partial^2 \mathrm{E}_z}{\partial \rho^2} + \frac{1}{\rho}\frac{\partial \mathrm{E}_z}{\partial \rho} + \frac{1}{\rho^2}\frac{\partial^2 \mathrm{E}_z}{\partial \boldsymbol{\phi}^2} + \frac{\partial^2 \mathrm{E}_z}{\partial \mathrm{z}^2} + k_0^2 n^2 E_z = 0\,, \tag{2.9}$$

where for a SI fiber of core radius a, the refractive index n has the form

$$n = \begin{cases} n_1 & \rho \le a \\ n_2 & \rho > a \end{cases}, \tag{2.10}$$

$$\mathrm{E}_z(\rho, \phi, z) = \mathrm{F}(\rho)\Phi(\phi)\mathrm{Z}(\mathrm{z}), \tag{2.11}$$

By using equation 2.9 and 2.10, three ordinary differential equations are obtained:

$$\frac{\partial^2 \mathrm{Z}}{\partial \mathrm{z}^2} + \beta^2 \mathrm{Z} = 0\,, \tag{2.12}$$

$$\frac{\partial^2 \Phi}{\partial \phi^2} + \mathrm{m}^2 \Phi = 0\,, \tag{2.13}$$

$$\frac{\partial^2 \mathrm{F}}{\partial \rho^2} + \frac{1}{\rho}\frac{\partial \mathrm{F}}{\partial \rho} + \left(k_0^2 n^2 - \beta^2 - \frac{\mathrm{m}^2}{\rho^2}\right)\mathrm{F} = 0\,, \tag{2.14}$$

Equation 2.12 has a solution $\mathrm{Z} = e^{i\beta z}$ where β has the physical significance of the propagation constant. In the same way, equation 2.13 has a solution $\Phi = e^{\mathrm{i}m\phi}$ but the constant m is limited to take only integer values since the field must be periodic in ϕ with a period of 2π.

Equation (2.14) is satisfied by the Bessel functions. Its general solution in the core and cladding regions can be written as

$$E_z = \begin{cases} AJ_m(p\rho) + A'Y_m(p\rho) & \rho \le a \\ CK_m(q\rho) + C'I_m(q\rho) & \rho > a\ , \end{cases} \tag{2.15}$$

where A, A', C, and C' are constants and J_m, Y_m, K_m, and I_m are different kinds of Bessel functions. Then, observing the behavior of the intensity of electromagnetic field in the fiber, the general solution of equation 2.11 is

$$E_z = \begin{cases} AJ_m(p\rho)e^{\mathrm{i}m\phi}e^{i\beta z} & \rho \le a \\ CK_m(q\rho)e^{\mathrm{i}m\phi}e^{i\beta z} & \rho > a\,, \end{cases} \tag{2.16}$$

The same process can be used to obtain H_z and the other four components can be expressed in terms of E_z and H_z by using Maxwell equations.

Moreover, a really important parameter to determine the cutoff condition is the normalized frequency and it is defined as

$$V = \frac{2\pi}{\lambda} a \sqrt{{n_{core}}^2 - {n_{cladding}}^2} = \sqrt{U^2 + W^2}, \tag{2.17}$$

Also it is convenient to introduce a normalized propagation constant b as

$$b = \frac{\beta/k_0 - n_2}{n_1 - n_2}, \tag{2.18}$$

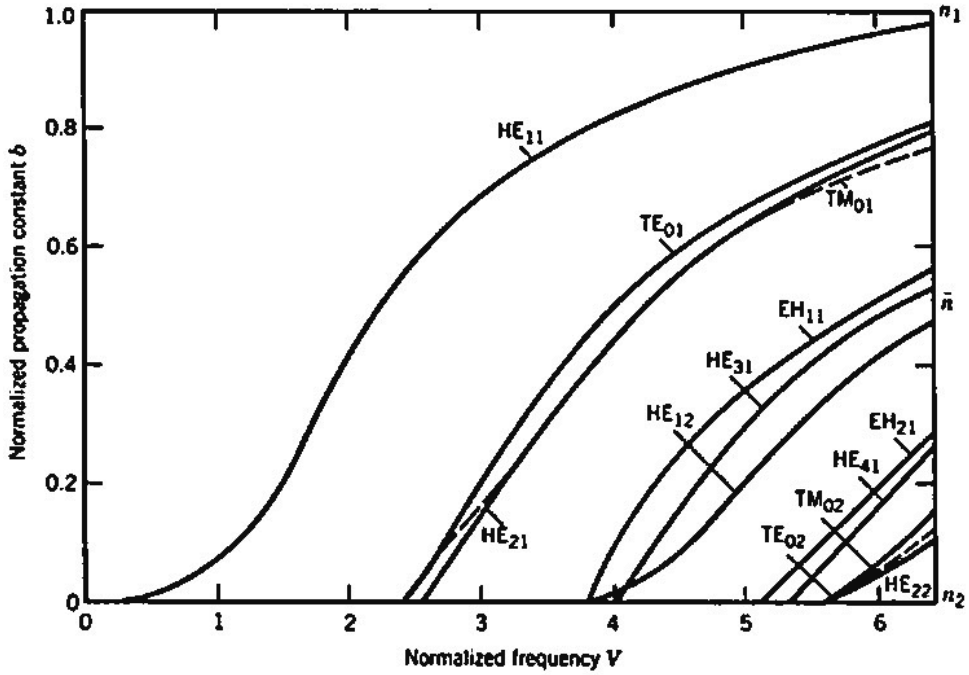

Figure 2.5: Normalized propagation constant b as a function of normalized frequency V for a few low-order fiber modes. The right scale shows the mode index n [29].

Figure 2.5 shows a plot of b as a function of V for a few low-order fiber modes. A fiber with a large value of V supports many modes. However, the number of modes decreases

rapidly as V is reduced. Below a certain value (V =2.405) all modes except the fundamental mode (HE11) reach cutoff (single-mode fiber) [29].

2.4 Optical Fiber Sensors

A sensor is a device capable of detecting magnitudes (physical, chemical or biological) and to transform them into variables that can be manipulated and quantified. In case of an optical sensor, it takes advantage of the interaction of light with matter to detect the characteristics of the measured parameter. The basic concept of a fiber-optic sensing system is demonstrated in Figure 2.6. where the fiber (guided light) interacts with an external parameter and carries the modulated light signal from the source to the detector. The input measured information can be extracted from this modulated optical signal.

A fiber optic sensor uses optical fiber either as the sensing element ("intrinsic sensors"), or signals from a remote sensor to the electronics that process the signals ("extrinsic sensors"). At the moment, four different types of sensors are the most common and are evaluated on the basis of performance criteria such as resolution, dynamic range, cross-sensitivity to multiple ambient perturbations, fabrication, and demodulation processes. The optical fiber sensing methods that have been investigated include well-established technologies like fiber Bragg grating (FBG) and interferometric sensors.

A fiber optic sensor converts a physical parameter to an optical output. The key part of every fiber optic sensor is a transducer device that converts one form of energy associated with the physical parameter into another form of energy. In the case of an extrinsic sensor, the optical fiber serves as a delivery mechanism to guide the optical signal to the sensing region outside the fiber, where it is modulated in response to the physical parameter of interest and then collected by the same (or different) optical fiber and guided to a detector for processing. In an intrinsic sensor, the optical fiber acts both as the means for transporting the optical signal to/from the sensing region and as the transducer (figure 2.6).

Measurements of a wide range of physical parameters by optical fiber sensors have been investigated for many years. Fiber-optic sensors are small in size, are immune to electromagnetic interference, and can be easily integrated with existing optical fiber

communication links. Such sensors can typically be easily multiplexed, resulting in distributed networks that can be used for health monitoring of integrated, high-performance materials and structures [37].

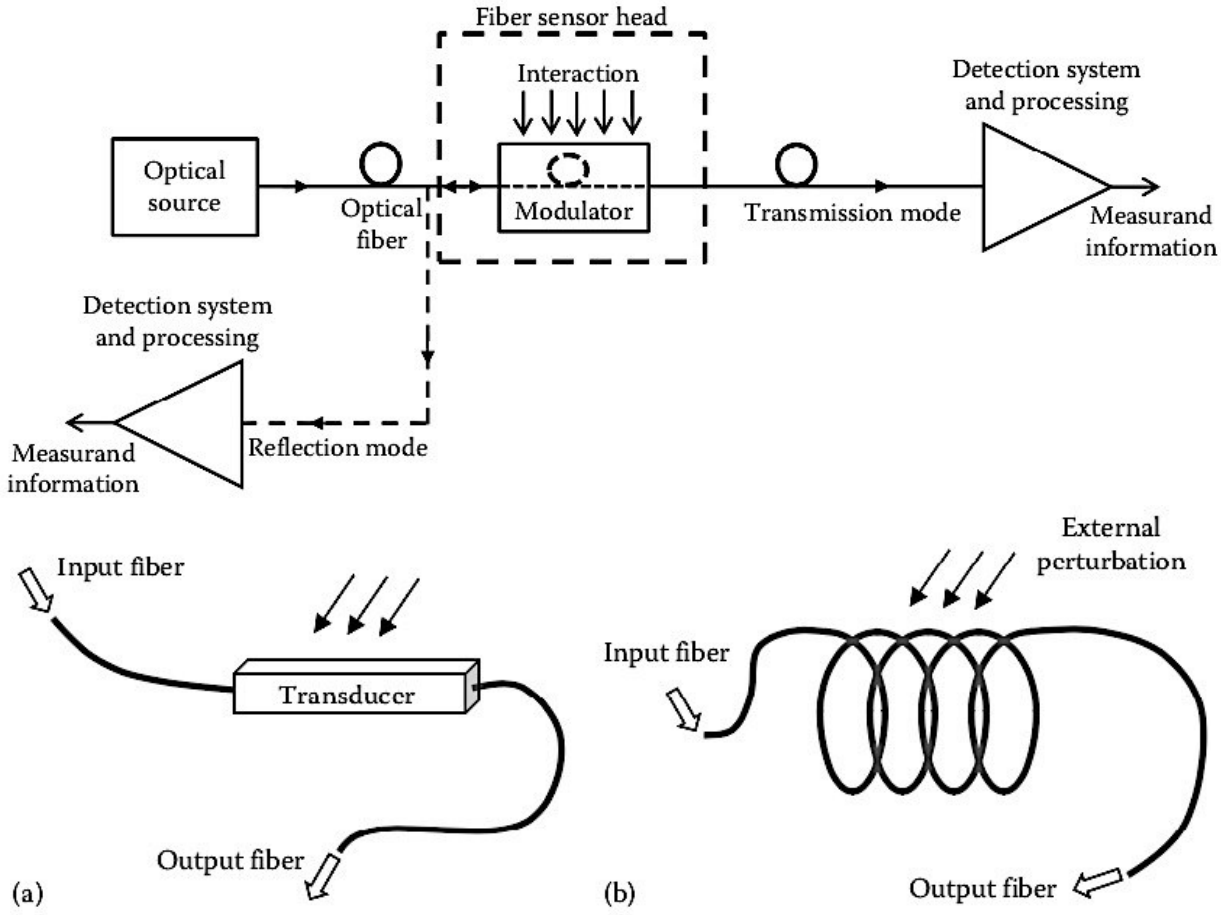

Figure 2.6: Basic concept of an optical fiber sensor. Extrinsic (a) and Intrinsic (b) [37].

Optical fiber sensors of displacement are perhaps the most basic of all fiber sensor types because they may be configured to measure many others related environmental factors. They should possess certain important characteristics. First, they should either be insensitive to ambient fluctuations in temperature and pressure or should employ demodulation techniques that compensate for changes in the output signal due to these additional perturbations. In an embedded configuration, the sensors for axial strain measurements should have minimum cross-sensitivity to other strain states. For environments where large strain magnitudes are expected, the sensor should have a large

dynamic range while at the same time maintaining the desired sensitivity. We now discuss two components for sensing and laser schemes and present their relative advantages and shortcomings [38].

2.4.1 Fiber Bragg Gratings

A fiber Bragg grating (FBG) is produced due to a periodic variation of the refractive index in the fiber core along the length of the fiber. The principal property of FBGs is that they reflect light in a narrow bandwidth that is centered at the Bragg wavelength, λ_B, which is given by $\lambda_B = 2n_{eff}\Lambda$, where Λ is the spatial period (or pitch) of the variation and n_{eff} is the effective refractive index for light propagating in a single mode. The refractive index variations are produced by exposure of the fiber core to an intense optical interference pattern of ultraviolet light (figure 2.7). The capability of light to induce permanent refractive index changes in the core of an optical fiber has been named photosensitivity. The discovery has led to techniques for fabricating Bragg gratings becoming a wide range of FBG-based devices that have applications in optical fiber communications and optical sensor systems [38].

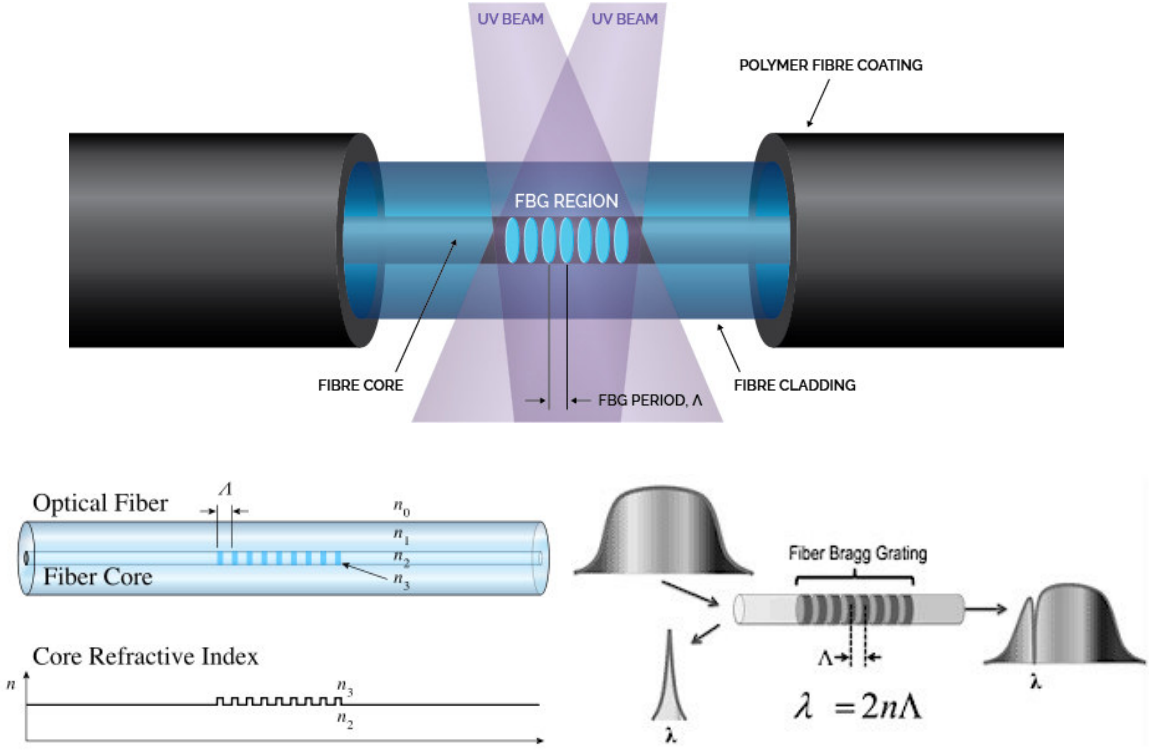

Figure 2.7: Fiber Bragg grating fabrication and spectrum obtained [37].

2.4.2 Fabry-Perot Interferometer

The intrinsic Fabry-Perot interferometric (IFPI) sensor is similar in operation to its extrinsic counterpart. This interferometric technique is based on detecting the optical phase change induced as light propagates along the fiber. Usually, the input light is equally divided between two paths, one of which serves as a reference, while the other one is influenced by the measured parameter. The two fiber paths recombine at the output of the sensor forming an interference pattern, which is directly related to the optical phase difference (OPD) between the two paths. A Fabry-Perot interferometer (FPI) is generally composed of two parallel reflectors separated by a certain distance *L* (cavity length). Mirrors or interfaces between two dielectrics can be used as reflectors. The cavity can also be implemented by introducing two Fresnel or other reflectors along the length of a single fiber. Since the cavity is formed within an optical fiber, changes in the refractive index of the fiber due to the applied perturbation can significantly alter the phase of the sensing signal. Interference occurs due to the multiple superpositions of both reflected and transmitted beams at the two parallel reflectors. As a result, the reflected and transmitted spectra of such an interferometer are functions of cavity length, index of refraction of the medium (n), the reflectivity of the mirrors and wavelength (λ). The phase difference of an FPI is given as

$$\delta_{FPI} = \frac{2\pi}{\lambda} n2L\,, \tag{2.19}$$

External perturbation induces a change in the OPD of the interferometer, resulting in a phase variation. By measuring the shift of the FPI spectrum, the strain applied to it can be qualitatively determined. The free spectral range (FSR) of the interferometer also depends on the variation of the optical path difference, a shorter OPD results in a larger FSR. Despite the fact that a larger FSR gives a wide dynamic range to the sensor, at the same time, it leads to a degraded resolution due to less sharp spectral peaks [37].

The IFPI sensor, like all other interferometric signals, has a nonlinear output that complicates the measurement of large magnitude strain. The main limitation of the IFPI strain sensor is that the photoelastic effect induced a change in the index of refraction

results in a nonlinear relationship between the applied perturbation and the change in cavity length. For most IFPI sensors, the change in the propagation constant of the fundamental mode dominates the change in cavity length. Thus IFPIs are highly susceptible to temperature changes and transverse strain components [39]. In embedded applications, the sensitivity to all of the strain components can result in complex signal output. IFPI sensors also suffer from implication in the output signal due to variations in the polarization state of the input light. The Fabry-Perot interferometric sensors possess nonlinear sinusoidal outputs that complicate signal processing at the detector [38].

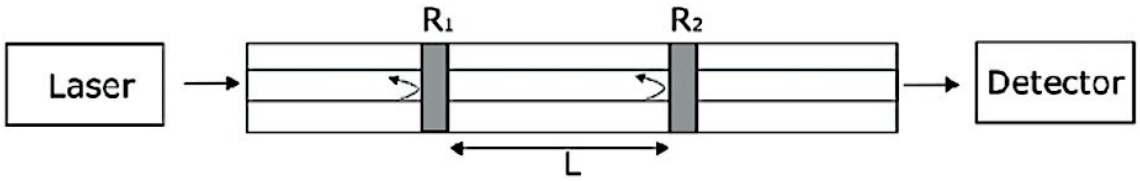

Figure 2.8: Intrinsic Fabry-Perot interferometer [38].

It is important to mention that in this work we use an all-fiber FPI. The FP filter (FPF) is composed of two air intracavities with 50 μm cavity diameter, separated by a silica collapse region around 500 μm. The FPF generated several reflections modes due to the several air-silica refractive index interfaces. Here, the interaction between the fundamental reflected fiber mode and the several reflected higher-order cladding modes provide an interference reflection spectrum. The full manufacturing process and principle operation of this FPF are detailed in [40].

2.5 Lasers

The term laser is an acronym for a radiation source based on Light Amplification by Stimulated Emission of Radiation. In principle, most lasers consist of three parts (figure 2.9): a pump source, an active medium, and a resonator. Almost every source of energy can, in some ways, be used to pump lasers. It is the purpose of the pumping process to establish population inversion in the active medium. Population inversion describes a condition of the active medium where the density of states at higher energy is a larger than the density of states at a lower energy.

Three scattering processes characterize the interaction of light and matter: absorption, stimulated emission and spontaneous emission. In the case of spontaneous emission, a higher excited state decays spontaneously to a state of lower energy, and a photon is emitted. In an absorption event a photon promotes the active medium from a state of lower energy to a higher-energy state. Stimulated emission is the inverse process where photons stimulate an excited state to decay to a state of lower energy, emitting an additional photon. It is important that in all these three processes energy is conserved. In a stimulated-emission process, the energy of the newly generated photons are equal that the stimulating photons. In other words, stimulated light is emitted in the same direction and with the same wavelength as the stimulating light.

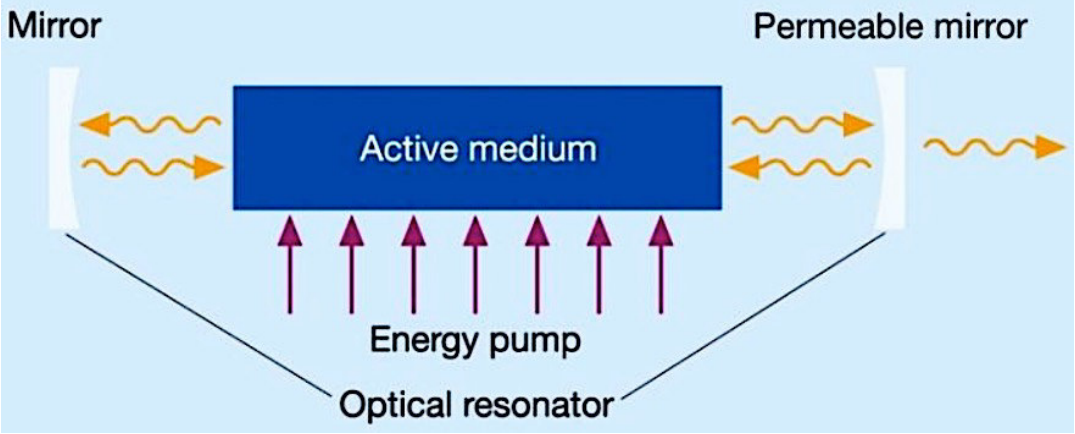

Figure 2.9: Typical parts of a laser [41].

In a medium with population inversion, more stimulated (and spontaneous) emission events than absorption events will occur in any given time interval. Consequently, more photons are generated per time than annihilated and the inverted active medium can amplify either the spontaneously generated photons or light inserted in the medium from the outside.

If the amplification in one pass through the active medium is too small to be useful, the active medium can be artificially lengthened by an optical resonator. In its simplest form, it consists of two highly reflecting mirrors with a small transmission that encloses the active medium. Spontaneously emitted photons in the direction of the resonator axis are amplified in the active medium, and most of the light is directed back into the active

medium by the mirrors, where it is further amplified. When the losses for the light per round trip are smaller than the gain per round trip, the light intensity inside the resonator will grow. The laser has reached a threshold when this condition is fulfilled.

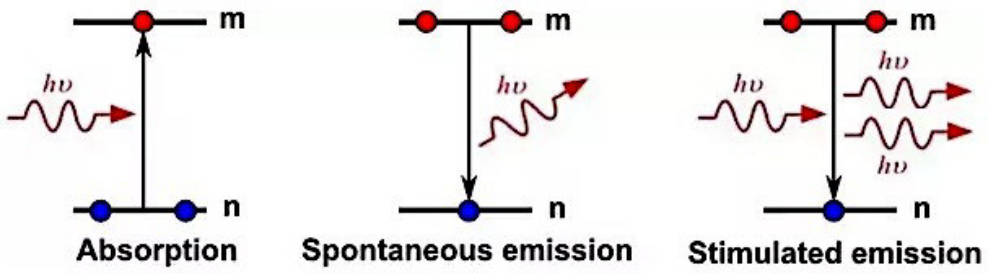

Figure 2.10: Fundamental processes for the interaction of radiation and matter [41].

Fiber lasers are usually meant to be lasers with optical fibers as gain media, although some lasers with a semiconductor gain medium (a semiconductor optical amplifier) and a fiber resonator, have also been called fiber lasers (or semiconductor fiber lasers). Also, devices containing some kind of laser (fiber-coupled laser diodes) and a fiber amplifier are often called fiber lasers (or fiber laser systems).

In most cases, the gain medium is a fiber doped with rare earth ions such as erbium (Er3+), neodymium (Nd3+), ytterbium (Yb3+), thulium (Tm3+), or praseodymium (Pr3+), and one or several fiber-coupled laser diodes are used for pumping. Therefore, most fiber lasers are diode-pumped lasers [41].

2.6 Tapered Optical Fibers Theoretical Analysis

In this section, the theory of operation of TOFs will be described, exploiting multimodal interference and adiabaticity criteria. Moreover, the fundamental principles of light propagation within TOFs structures and related fabrication methods will be introduced, also the range of sensing applications.

Fiber tapers could be categorized into two types: abrupt taper (non-adiabatic) and gradual or non-abrupt taper (adiabatic). The main difference refers to if there is light energy only in the core mode (gradual taper), or if cladding modes are excited (abrupt taper). Hence, the non-abrupt taper is usually fabricated by gradually tapering the optical fiber with small taper angles in order to minimize the insertion loss and normally refers to the adiabatic taper.

However, when the taper angle is large enough, some energy in the core region will be coupled into the cladding region, the tapered structure forms an abrupt taper. In this work, we call our devices, quasi-adiabatic tapers, because we want to obtain a structure with low losses but with the presence of higher order cladding modes, in order to generate an interference pattern.

To produce high-quality tapered fiber-based devices, the tapers should have the following properties: high adiabaticity, uniform microfiber diameter, low surface roughness, and suitable microfiber diameter with large evanescent field. Basically, tapered fibers with thinner diameter have a stronger evanescent field. However, the difficulty in handling these tapered fibers increases with a smaller diameter, as thinner tapered fibers are very fragile and lossy.

Tapered fiber is fabricated by stretching a heated conventional fiber reducing core diameter. As shown in figure 2.11, the smallest diameter part of the tapered fiber is called waist (W). Between the uniform un-stretched fiber and waist are the transition regions (TDOWN and TUP) whose diameters of the cladding and core are decreasing from initial fiber size (d0) down to order micrometer or even nanometer (d1). The power transferred during the tapering process involves an initial adiabatic transfer of the power in the input core to the cladding/air interface [10]. The light is then transferred to the adjacent core-cladding mode. During the up-tapering process, the input light will transfer back to the fiber core.

The light that is transferred to a higher order mode of the core-cladding structure leads to an excess loss because these higher-order modes are not surrounded by the core and are stripped by the higher index of the fiber coating.

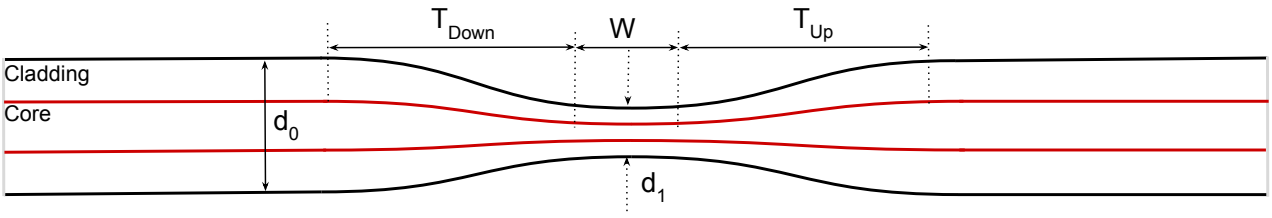

Figure 2.11: Typical profile of a tapered optical fiber.

As the wave propagating through the transition regions, the field distribution varies with the change of core and cladding diameters along the way. Depend on the rate of diameter change, the energy transfer from the fundamental mode to a closest few higher order modes varies, which determines the loss of the propagating wave power. This loss can be minimized if the shape of the fabricated tapered fiber satisfies the adiabaticity criteria along the tapered fiber. Theoretically, an adiabatic tapered fiber is based on the condition that the beat length between fundamental mode LP01 and second local mode is smaller than the taper length, $z_b<z_t$ (figure 2.12):

$$z_t = \frac{\rho}{tan\Omega}, \tag{2.20}$$

$$z_b = \frac{2\pi}{\beta_1 - \beta_2}, \tag{2.21}$$

where $\rho=\rho(z)$ is the core radius, $\Omega=\Omega(z)$ is the taper angle, $\beta_1$and β_2 are the propagation constants of fundamental mode and second local modes respectively.

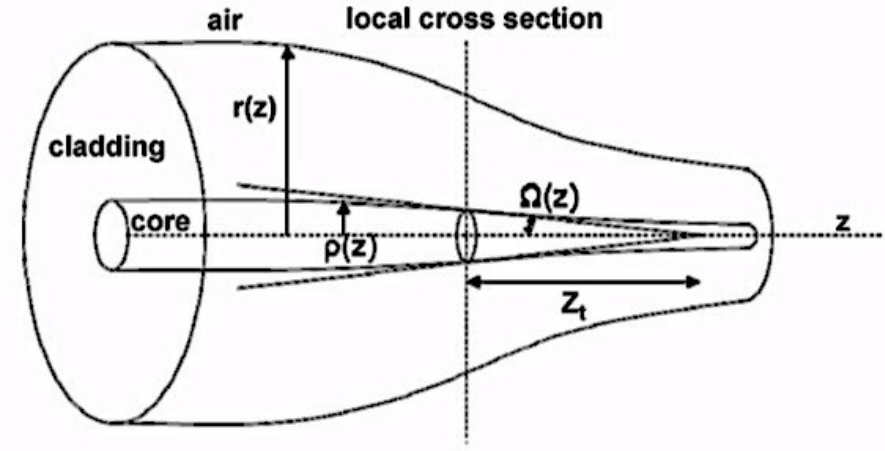

Figure 2.12: Taper transition [42].

Then, to achieve low loss tapered fibers, large transitions lengths are desirable. Based on this condition, adiabatic tapered fiber can be acquired by tapering a fiber at a smaller reduction rate in diameter (two times cladding radius r=r(z) where z is the measured distance of the transition) but this will result to a longer transition length. However,

considering practical limitations in the fabrication of fiber couplers or microfiber based devices, long tapered fiber may aggravate the difficulty in fabrication, and for the purpose of miniaturization, short tapered fiber is preferable. Then, to achieve a balance between taper length and diameter reduction rate, factor F is introduced:

$$\frac{d_r}{d_z} = \frac{\mathrm{F\,r}(\beta_1 - \beta_2)}{2\pi}, \tag{2.22}$$

The optimal profile is achieved when this factor is 1, equations will be described in other section. It is important to mention that tapered fiber with insignificant losses can be achieved with F = 0.5 but the transition length of the tapered fiber is twice longer than the optimal tapered fiber [42]. Furthermore, Birks and Li [43] presented simple mathematical equations to describe the relationship between the shapes of tapered fiber and elongation distance, being the entire radius of the fiber:

$$r(z) = r_0\left(1 + \frac{2\alpha z}{(1-\alpha)L_0}\right), \tag{2.23}$$

Where r_0 denotes the initial fiber radius d_0 (figure 2.11); r_c is the final waist radius d_1 (figure 2.11); $L_0 = L - \alpha x$; is a function dependent of the waist length W (figure 2.11) and the elongation of the fiber, and α is called the transition value, manipulating this last parameter, several shapes of tapered fiber can be produced, decaying-exponential, linear and concave transitions. For example for $\alpha = 1$ we have an abrupt linear transition, these profiles can be useful in some applications like fabrication of wideband chirped fiber Bragg gratings, in which the grating is written on the transitions of the tapered fiber, also long linear shape tapers make good candidates for the fabrication of such devices [44]. On the other hand, they can be used for optical tweezing due to their capability to converge the optical wave to a high intensity at the taper tip, microscopic objects are attracted to the high intensity field driven by the large gradient force at the taper tip [45].

In this work, we use $\alpha = 0$ for a soft exponential transition where $L = L_0$. From the theoretical model presented above, the function for the decaying-exponential profile and the transition length t (T_{down} and T_{up} in figure 2.11) are respectively given by

$$r(z) = r_0 e^{-\frac{z}{L_0}}, \tag{2.24}$$

$$t = L_0 \ln\left(\frac{r_0}{r_c}\right), \tag{2.25}$$

2.6.1 Tapered Optical Fibers Fabrication

Fiber-optic couplers, including splitters and wavelength division multiplexing (WDM), filters, combiners and sensors have been fabricated since the seventies due to easy fabrication, low-cost and stable configuration. The fabrication technologies have included fusion tapering, etching, and polishing. Especially tapered fiber fabrications have been demonstrated by using a wide range of techniques: laser ablation [46], electron beam lithography [47], bottom-up methods such as vapor–liquid–solid techniques [48], and top-down techniques such as fiber pulling [49] or direct draw from bulk materials [50]. Generally, the most common techniques used in practical experiments are the ceramic microheater brushing technique [51] and CO_2 laser irradiation [52]. Among those methods, the flame heating technique has proven to be one of the most versatile, which can fabricate tapered fiber with good physical properties. The taper can be created by stretching the optical fiber while it is heated with a flame, becoming the glass soft. This procedure makes the fiber thinner over some length of a few millimeters or centimeters. The fiber core also gets thinner by the same factor as the total fiber. This type of fabrication employs mainly an oxy-butane torch, a microcontroller for gases mixture (driver), and a linear stage with stepper motors and fiber holders (figure 2.13). The mixing of both gases takes place in the torch chamber. The airflow from the flame is kept at an acceptably low level and the flame temperature is high enough to heat and soften the silica fiber. However, the flame temperature can be further increased by supplying higher pressure of oxygen to the torch, but the flame may go out easily due to the fast weakening

of fuel gas and the fast air flow could result in bending the heated fiber and inducing high insertion loss in the tapered fiber.

The linear stage is used for stretching the heated SMF. To fabricate smooth and low loss tapered fibers, the linear stage is often traveling at a very low velocity (until 50 mm/min). Moreover, the oxy-butane torch is required to travel at higher speed (until 4.5 mm/s) than the linear stage to provide a uniform heat a long tapered fiber. In order to achieve that, the torch is mounted on a custom-made sliding stage that can travel at a very high speed in a linear direction. Again, it is important to emphasize that the quality of the tapered fiber lies on the routine of the torch movement and linear stage pulling length and speed. The microcontroller sits at the top of the motor control system hierarchy, coordinating and controlling the stepper motors. Each stepper motor is equipped with a motor driver and both combinations of motor driver and stepper motor are assigned to the linear stage and the sliding stage for the flame respectively.

To start the process, coating length of several cm is removed from the fiber prior to the fabrication of tapered fiber. Then the fiber is placed horizontally on the translation stage and held by the two fiber holders. During the tapering, the torch moves and heats along the uncoated segment of fiber while the fiber is being stretched. The moving torch provides uniform heat to the fiber so that the tapered fiber is produced with good uniformity along the heat region. Basically, the parameters of the TOF, such as tapered waist diameter and the transition length between regular and tapered fibers, can be determined by controlling the hot region length and heating time.

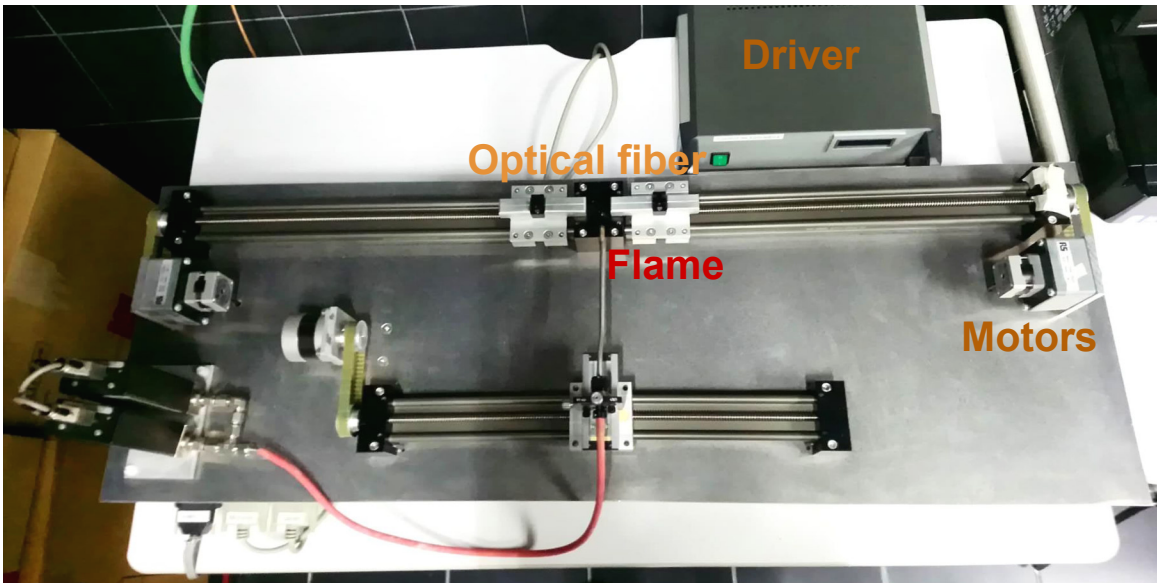

Figure 2.13: Taper fabrication machine.

With the system improved, the problems of high insertion loss due to non-uniformity of tapered fiber can be reduced. Additionally, the system may realize fabrication of tapered fiber with waist diameter until 1 micrometer. As is seen before, in order to fabricate good quality tapered fibers, another important criterion is the adiabaticity. It is commonly known that some tapered fibers suffer loss of power due to the fundamental mode energy couples to the higher order modes. Some fraction of power from higher order modes that survives to propagate through the tapered fiber may recombine and interfere with fundamental mode. This phenomenon can be seen as interference between fundamental mode HE_{11} and its closest higher order mode HE_{12}. This develops an irregular transmission spectrum, this kind of tapered fiber is not suitable to be used in the resultant fabrication of microfiber devices but sometimes it can be used for refractive index measuring and biosensing applications. The coupling from fundamental mode to higher order modes can be minimized by optimizing the shape of the tapers. Most of the time, adiabaticity can be easily achieved by using slow diameter reduction rates or fabrication of tapered fibers with sufficiently long taper transition length.

2.6.2 Evanescent Wave Optical Fiber Sensors

The exponentially decaying evanescent fields in the lower index region of a waveguide have been offering high potential in the design and fabrication of a variety of sensors. The field distribution in the core and cladding regions has the same form and the electric field pattern corresponds to a non-uniform wave traveling along the fiber. Moreover, specifically, it is a standing-wave pattern in the fiber core and a decaying or evanescent wave in the cladding region as illustrated in next figure.

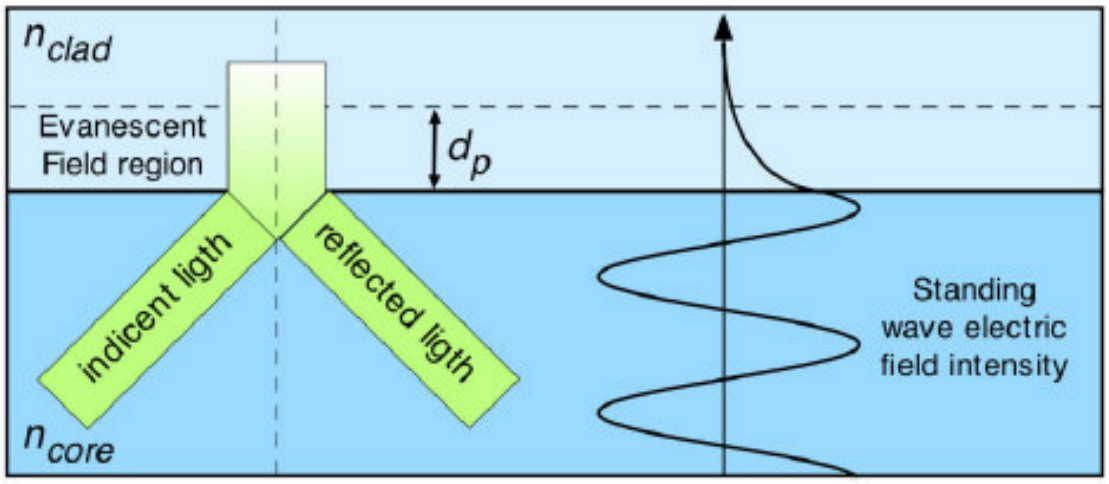

Figure 2.14: Illustration of standing wave pattern and exponentially decaying evanescent wave in core and cladding respectively [53].

This exponentially decaying evanescent field has been utilized for developing different types of intensity modulated fiber optic sensors. More specifically, evanescent waves in the cladding region were exploited for developing evanescent wave absorption sensors. This is achieved by removing a certain region of the cladding of the fiber and allowing interaction with the external medium. Evanescent field absorption occurs when the medium, which forms the cladding of the waveguide absorbs the light at the wavelength being transmitted through the fiber. Compared to other sensing methods these evanescent wave fiber optic sensors have a lot of advantages, which have motivated different groups to work in this field. In evanescent wave fiber optic sensors, the light remains guided in the sensor and no coupling optics are required at the sensing region. Also, these sensors offer the possibility to achieve a considerable miniaturization.

Design of evanescent field absorption based sensor devices requires knowledge about basic parameters of optical sensors that were discussed. For this case a new parameter needs to be considered, the degree of penetration of the evanescent field into the low refractive index medium is very important. This quantity is called penetration depth of the evanescent field, d_p and is defined as the perpendicular distance from the core-cladding interface at which this electric evanescent field amplitude has become 1/e of its value at the waveguide interface. If E_o represents the electric field amplitude at the interface, after a distance d_p, this falls to

$$E(z) = E_0 \, e^{-\frac{y}{d_p}}, \tag{2.26}$$

$$d_p = \frac{\lambda}{2\pi n_1 \sqrt{\left[\sin^2\theta - \left(\frac{n_2}{n_1}\right)^2\right]}}, \tag{2.27}$$

where *y* is the distance from the fiber core, starting at *y* = 0 at the core-cladding interface. θ is the angle of incidence to the normal at the interface (figure 2.15).

Another critical parameter, which has a prominent role in the design is the evanescent power that resides in the cladding, is defined as $= \frac{P_{clad}}{P_{total}}$, this fraction is related to normalized frequency, and its value is maximum for modes close to cut-off and for higher order modes.

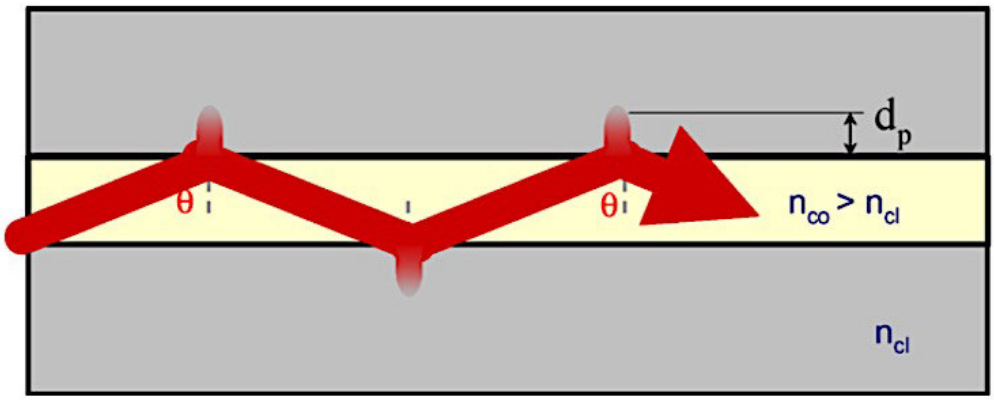

Figure 2.15: Cross-section profile of an optical fiber cut along the long axis [53].

2.6.2.1 Tapered fiber optic biosensors applications

Biosensors are electrical, optical, chemical, or mechanical devices with the capability to detect biological species selectively. They are often modified with biological entities to enhance their selectivity. Examples of biological recognition molecules include enzymes, antibodies, and oligonucleotides.

Fiber-optic biosensors (FOBS) are optical fiber devices which use the optical field to measure biological species such as cells, proteins and DNA. One reliable and sensitive optical method is evanescent sensing. A majority of evanescent FOBS are tapered fiber-optic biosensors (TFOBS). Because of their efficiency, accuracy, low cost and convenience, FOBS are promising alternatives to traditional immunological methods for biomolecule measurements. Tapered fiber-optic biosensors (TFOBS) are a type of FOBS, which rely on special geometries to expose the evanescent field to interact with this kind of samples. In order to amplify sensitivity and selectivity, TFOBS are often used with various optical transduction mechanisms such as changes in refractive index, absorption, fluorescence, and Surface Plasmon Resonance (SPR).

In a uniform-diameter fiber, the evanescent field decays to almost zero within the cladding. Thus, light propagating in uniform-diameter cladded fibers cannot interact with the fiber surroundings. Then, for sensing is required that light interacts with the fiber surroundings. As is seen before, one way to achieve this interaction is to expose the evanescent field to the transmitted light by reducing or removing part of the cladding, then the evanescent field can interact with the surroundings.

Apart from the penetration depth, the properties of light in the fiber core are determined by the number of modes. If the normalized frequency V changes along the fiber due to geometry or local RI changes, the single mode fiber can become multimode, and coupling of modes take place, which increases the evanescent portion. The increase in evanescent field forms the basis for increased sensitivity. In addition, several researchers have attempted to increase the penetration depth of the evanescent field and facilitate mode coupling by bending, tapering, altering the light launching angle and increasing the wavelength [53].

To finish, is well known the evolution of TFOBS, a new effort will be focused on enhancing the sensitivity and selectivity. It appears that methods based on SPR and fluorescence have reached terms of detection limit, and one possible future direction is to combine the two methods so that the SPR signal is enhanced. Improved surface chemical modification and stability of the recognition molecule can also increase the sensitivity and robustness of TFOBS, especially for intensity-based TFOBS because it is the most sensitive when molecules are bound to its surface. Given its promising advantages, TFOBS will remain like a popular choice among researchers and practitioners for detection of biological agents and other applications.

2.6.2.2 Effects of tapering on the evanescent field

Tapering not only exposes the evanescent field to the surroundings, also increases the evanescent field magnitude and penetration depth. Tapering can be performed by removing the cladding and then tapering the core, or keeping both the core and cladding in place and tapering the entire fiber. Fractional power (η) is defined as the fraction of power in the evanescent field compared to the total power in the fiber, and sensitivity is proportional to η, which indicates that tapered fibers are more sensitive [54]. Another way is the use of ratio (*R*) of the power in the evanescent field to the total power of guided light to characterize tapers [55]. In another study by Mackenzie et al., adiabatic tapers as small as 1 μm in diameter produced an optical power intensity in the evanescent field of 100 times bigger than what was achieved with a similarly polished fiber [56].

2.6.2.3 Effects of bending, launch angle and tapered fiber geometries on evanescent field

Bending of optical fiber results in a loss in light and increase in evanescent field. Fiber bending creates higher order modes which results in the evanescent field having greater penetration depth. The number of ray reflections as well as the evanescent absorption coefficient is inversely proportional to the core radius and depends only on because the angle of ray propagation is constant.

For example in a single mode fiber, light is launched over a very small angle because only the lowest order mode is supported. However, in multimode fibers light can be launched at

different angles since these angles correspond to modes, and several modes are supported simultaneously. The evanescent wave penetration was shown by Ahmad et al. to be enhanced by as much as 300% in certain designs of tapered fibers [57].

There are two types of tapered fiber geometries currently used: tapered tips and continuous tapered fibers. A tapered tip consists of an optical fiber, which gradually decreases, in diameter until it becomes a tiny tip, where the tip is the sensing element, the tip itself can transmit the light back to a detector for measurement. On the other hand, a continuous tapered fiber consists of an optical fiber gradually decreasing in diameter, which reaches a constant diameter waist region and then gradually increases back to the original diameter. The waist region is used as the sensing region because the evanescent field is maximum in the region of the smallest diameter. Absorption, scattering, fluorescence, and resonance can occur in the waist region.

2.6.2.4 Detection principles in tapered fiber optic sensors

The mechanisms used in evanescent sensing depend on the application of the sensor. The use of evanescent sensing has been previously investigated with many different sensing principles such as Changes in output power and spectrum due to refractive index changes and other causes, Evanescent field absorption (interaction with the analytes), Fluorescence and Surface Plasmon Resonance (SPR).

Changes in the magnitude of the evanescent field are detected by measuring the changes in output power and spectrum of the fiber. Factors, which influence the sensitivity, include bending, radius, length, and taper ratio. As mentioned, bending of a tapered fiber increases the fraction of evanescent field in the sensing region, and therefore increases sensitivity. In terms of the radius, it was found that smaller diameters cause a larger evanescent field, which increases sensitivity. The tapered region can convert lower order modes to higher order modes that couple deeply and more efficiently into the cladding. Furthermore, it was shown that longer tapers gave the largest deep penetration (d_p). Another factor, which affects the performance of the sensor, is the taper ratio. Taper ratio is the ratio of the waist diameter of a tapered fiber to the total diameter of a uniform fiber.

When taper ratio is large, the evanescent wave is negligible, whereas when taper ratio is small, the mode is so highly spread out that it tends towards a free-space wave [53].

This chapter presented the theory about tapered optical and other components that had been used in this work. The properties and equations of light propagation of optical fibers were described; more specifically about tapered optical fibers and its functioning, detection principle and applications. Moreover, the effects of several parameters on the evanescent field were explained. With these concepts more clear, next chapter will mainly describe the components characterization and methods for fabrication of tapered optical fibers and for implemented setups.

Chapter III: System Implementation and its Characterization

This chapter will describe the system implementation and its characterization by experimental methods with the objective to prove the correct functioning of the devices in the system; each component of the system will be separately studied. In this work tapered optical fibers were used for sensing and laser applications, therefore these systems implementation will be explained.

3.1 Single-Mode Pump Laser Diode Characterization

Single-mode (SM) pump lasers emit low noise, precisely controlled level of light at a specific wavelength out of a small-core fiber. In this case, the brand QPHOTONICS model QFBGLD-980-500 was used. This diode offers fiber Bragg grating (FBG) to stabilize lasers with up to 600 mW rated output power at 974 nm, as well as polarization maintaining (PM) with fiber-coupled lasers, its low noise design enables superior PM combining to attain higher power levels.

SM pumps require a micro-alignment; this alignment must stay stable throughout wide temperature ranges and high shock/vibration environments. SM pumps are most commonly used for EDFAs and fiber laser pumping applications. By selecting and stabilizing the wavelength closely to the doped absorption peak, the pump enables the maximum efficiency and light output from the system.

Next picture shows the implemented simple scheme to characterize the Pump laser diode used in the system. A Temperature Controller protects the diode all the time. This controller is a complete driver package designed to drive and cool pigtailed butterfly laser diodes. It contains a built-in mount for portability and mechanical stability. It accepts fiber-coupled lasers, superluminescent diodes, and laser amplifiers. This unit provides a high degree of output stability and maintains the temperature with 0.005 °C of stability over 24 hours, prolonging the life of the diode. In addition to a full complement of safety features, such as a soft start mode, current and temperature limits, and external interlock compatibility, also includes a switchable noise reduction filter and a modulation input.

Figure 3.1: Scheme of the implemented system for the characterization of the Pump laser diode.

The pump laser diode is coupled to the optical power meter, power characterization is shown in figure 3.2, and also it is compared with the curve of the manual of the manufacturer for ambient temperature, the results are practically the same if we take into account the losses in the splice and in free space. Then, by using an Optical Spectrum Analyzer (OSA) instead of the power meter, threshold current, center wavelength and spectral width were verified (figure 3.3).

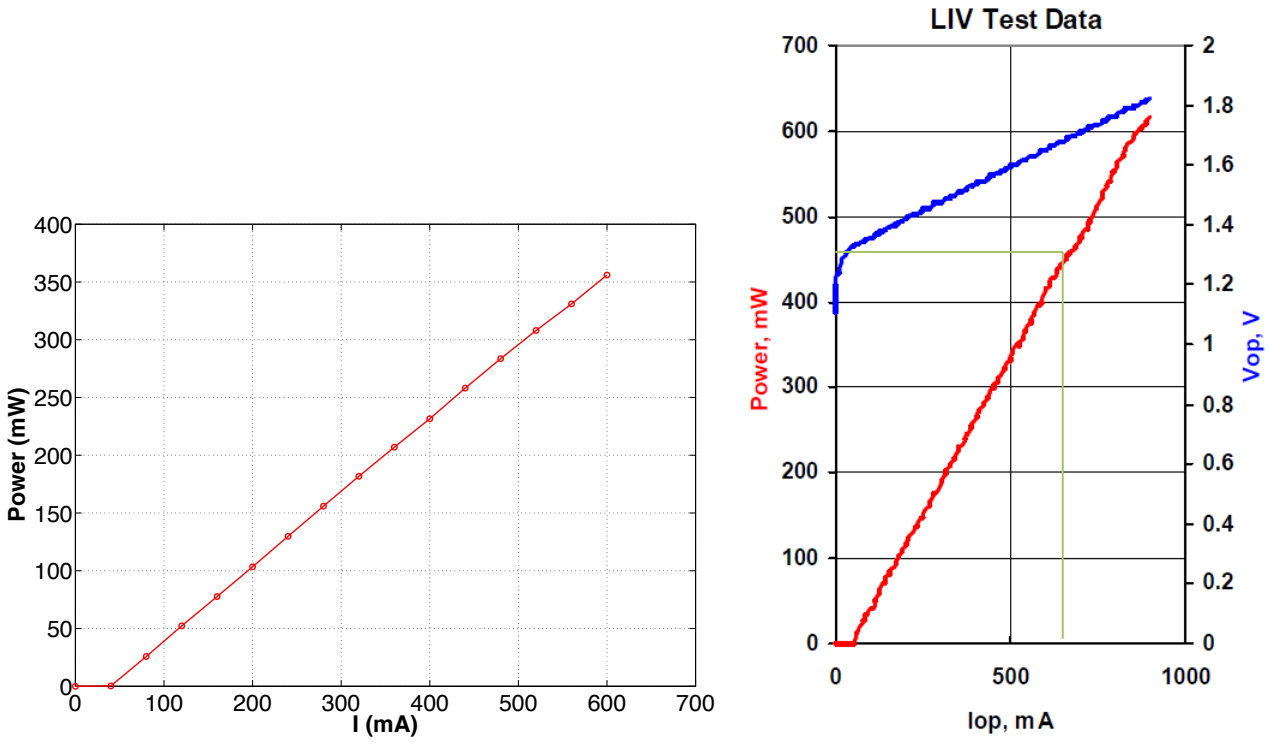

Figure 3.2: Power characterization of the Pump laser diode. Experimental results (left). Manufacturer test (right).

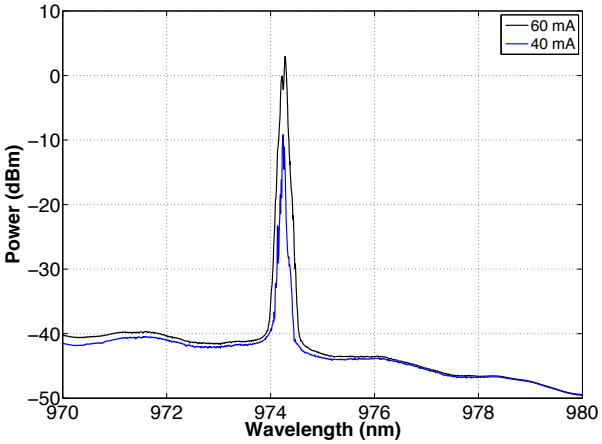

Parameter	Value	Units
Internal Temperature	25	°C
Thermistor Resistance	10.0	k?
Optical Output Power	500	mW
Threshold Current	60	mA
Operating Current	733	mA
Maximum Operating Current	806	mA
Operating Voltage	1.73	V
Monitor Current	1.6	mA
Center Wavelength	974.3	nm
Spectral Width	0.35	nm

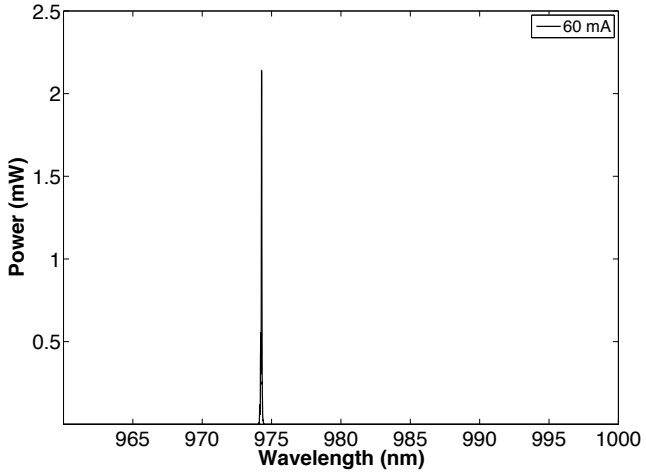

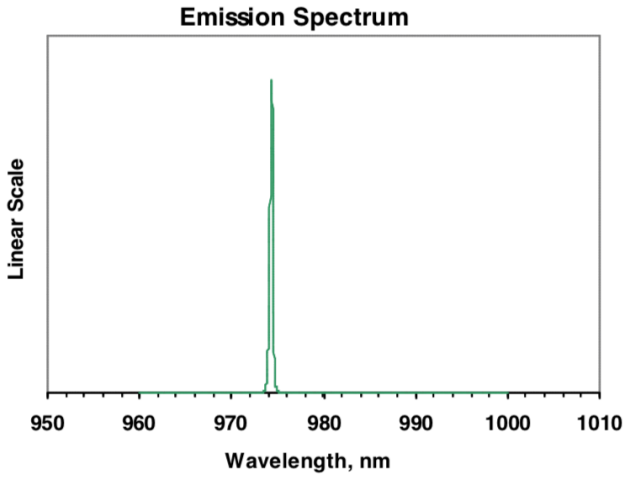

Figure 3.3: Verification of the main parameters of the Pump laser diode. The logarithmic scale of diode spectrum (top left). Manufacturer Datasheet (top right). Linear scale spectrum (bottom right and left figures correspond to the experimental result and manufacturer test respectively).

3.2 Superluminescent Diode Characterization

The Superluminescent Diode (SLD) is a semiconductor device to emit low-coherence light of a broad spectrum like Light Emitting Diode (LED), but high brightness like Laser Diode (LD). SLD is commonly used as incoherent light source for optical. In this case, the brand QPHOTONICS model QSDM-1550-1 was used. The central wavelength at 1534 nm and spectral width of 37 nm were verified in next figure.

The mechanism of SLD emission is the same as a semiconductor laser (LD) and light emitting diode (LED). Emission occurs by flowing forward current to a p-n junction. When a power supply is connected to the p-layer positive and the n-layer negative, electrons enter

from the n-side and holes from the p-side. When the two meet at the junction, an electron drops into a hole and light is emitted. The difference is that while the SLD has the coated end of the active layer to prevent reflected light, both end surfaces of the LD is cleaved to form Fabry-Perot resonator.

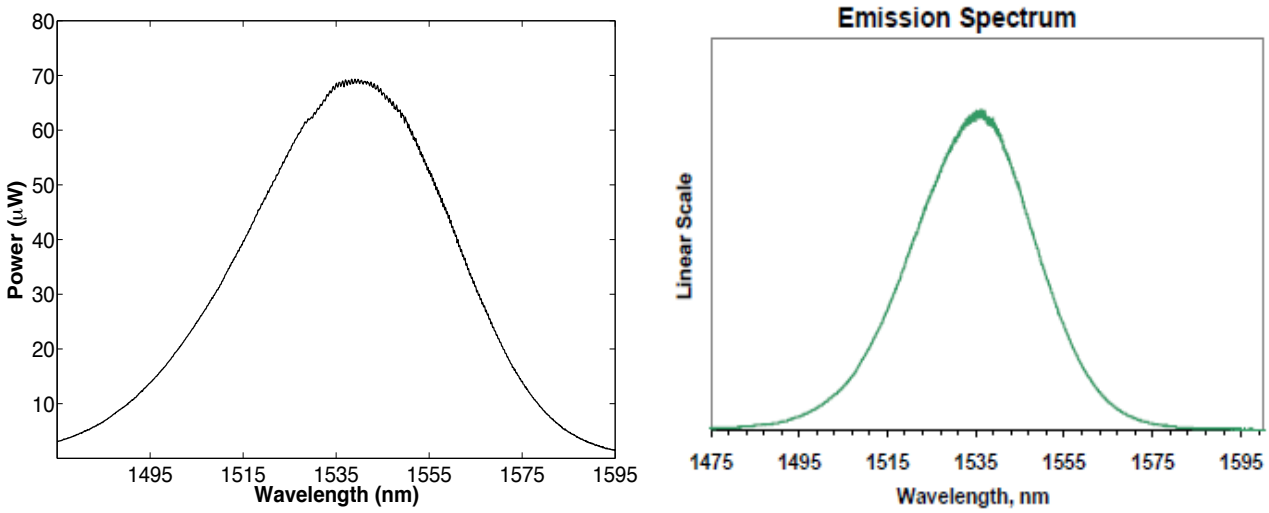

Figure 3.4: Verification of main parameters of Superluminescent diode. Linear scale spectrum (right and left figures correspond to the experimental result and manufacturer test respectively).

The light is called superluminescence and is the same type of light emitted from the rare earth doped fiber referred to as ASE light. Since the spontaneous emission light as a seed light has a random phase and a broad spectrum, the superluminescence also becomes a low-coherence light with a broadband spectrum.

The emission wavelengths of the SLD depend on the band gap energy of the semiconductor as in the case of LD and LED. A semiconductor with a larger band gap emits a shorter wavelength. For example, an AlGaAs emits wavelengths of 0.8 ~0.9 μm, and a GaInAsP with a smaller band gap emits longer wavelengths of 1.3~1.6 μm.

3.3 Erbium Doped Fiber Characterization

Experimental characterization techniques (Refractive Index Profile measurement and Absorption Coefficient measurement by using Cutback technique) and some equations to obtain some important parameters of the utilized EDF (LIEKKI™ Er16-8) will be presented.

3.3.1 Refractive Index Profile Measurement

The main transmission properties of an optical fiber, like bandwidth and dispersion, are dependent on the design of the fiber refractive index profile, which is the base of optical waveguide composition. Also, some properties of both, single and multimode fibers are determined by the refractive index profile of the fiber, which provides information such as core and cladding diameter, and numerical aperture (NA).

Hence, from the design of optical fibers to their fabrication, refractive index profile is an essential basic parameter, and often the practical optical fiber refractive index profile is the key that defines if the above-mentioned transmission performance can accomplish the expected goal. Therefore, the exact measurement of a finished fiber refractive index profile is absolutely indispensable.

The Refractive Index Profile of EDF was characterized by using a Fiber Index Profiler model IFA-100. By scanning the fiber from the side, the IFA-100 measures the refractive index profile of an optical fiber with a submicron spatial resolution. The measurements can be taken in one dimension giving a line plot of the refractive index at any given cross-section of the fiber. This measurement assumes the fiber to be symmetrical for the computation of the refractive index profile. This allows to measure the average refractive index of the irradiated core in a grating region and compare it to unprocessed fiber. Moreover, special waveguide structure written into an optical fiber can be verified.

Next figure shows the measured refractive index profile of used EDF in the system, as a function of Refractive index contrast with fiber diameter. Well, as it was seen before the calculation of some EDF parameters need to be calculated, the analysis of some expressions will be remembered from the previous chapter.

The numerical aperture (NA) is considered a light gathering capacity of an optical fiber. The NA of the fiber is the sine of the maximum angle of an incident ray in relation to the fiber axis, so that the transmitted beam is guided in the core. The NA is determined by the refractive index difference between core and cladding, more specifically by the relation:

$$NA = \sqrt{{n_{core}}^2 - {n_{cladding}}^2}\ , \tag{3.1}$$

which can be derived from the requirement that the transmitted beam at the core/cladding interface propagates with the critical angle for total internal reflection. For a single-mode fiber (SMF), the NA is typically of the order of 0.1, but can vary roughly between 0.05 and 0.4. Multimode fibers normally have a higher numerical aperture around 0.3. Very high values are possible for photonic crystal fibers (PCF).

To calculate NA, the expression of refractive index contrast (Δn) needs to be analyzed:

$$\Delta n = \frac{{n_{core}}^2 - {n_{cladding}}^2}{2{n_{core}}^2}, \tag{3.2}$$

$n_{cladding}$ is well known for SiO2 (silica) at 1550 nm, and from figure 2.11 Δn is 0.017 and n_{core} (erbium doped region) can be calculated using equation 3.2 as well as NA being of approximately 0.13.

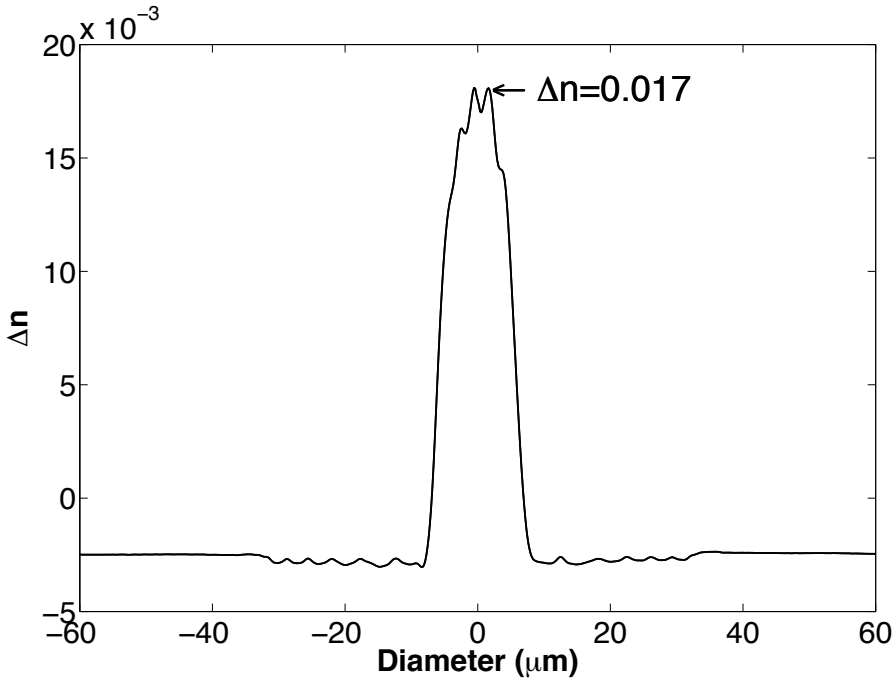

Figure 3.5: Measured Refractive Index Profile of used EDF.

3.3.2 Cutback Technique for Absorption Coefficient Measurement

Optical absorption involves the transfer of energy from the propagating light beam to the material structure, resulting in the excitation of the material to a higher energy state.

The cutback technique is used to experimentally measure the absorption spectrum of an erbium doped fiber. EDF is connected to a white light source and an OSA, and the spectrum is measured (figure 3.6). A known length of fiber is cut and a second spectrum is measured.

The absorption coefficient (α) is calculated by dividing the dB change between the two spectra into the cutback length (equation 3.3):

$$\alpha = \frac{P_2 - P_1}{L_1 - L_2}, \tag{3.3}$$

where $P_2$and $P_1$are the Powers in dB of shorter and larger lengths of fiber respectively, and $L_1$and $L_2$the larger and smaller lengths of fiber respectively.

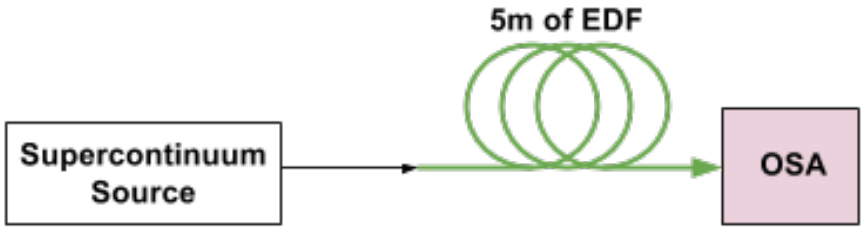

Figure 3.6: Scheme of the implemented system to measure the Absorption coefficient of the EDF.

Figures 3.7 and 3.8 show the obtained spectrums and the calculated Absorption coefficient of the EDF. Also, the emission of this fiber was measured just interchanging the Supercontinuum source with the pump laser at 976 nm (figure 3.9).

It is clear that as traditionally an EDF due to the concentration of erbium material, an EDF has high absorption around 980 nm and 1530 nm (including all the C-Band above 4 dB/m), but also it has high emission at these wavelength regions, to allow the amplification of the signal and to compensate the absorption at the pumping region.

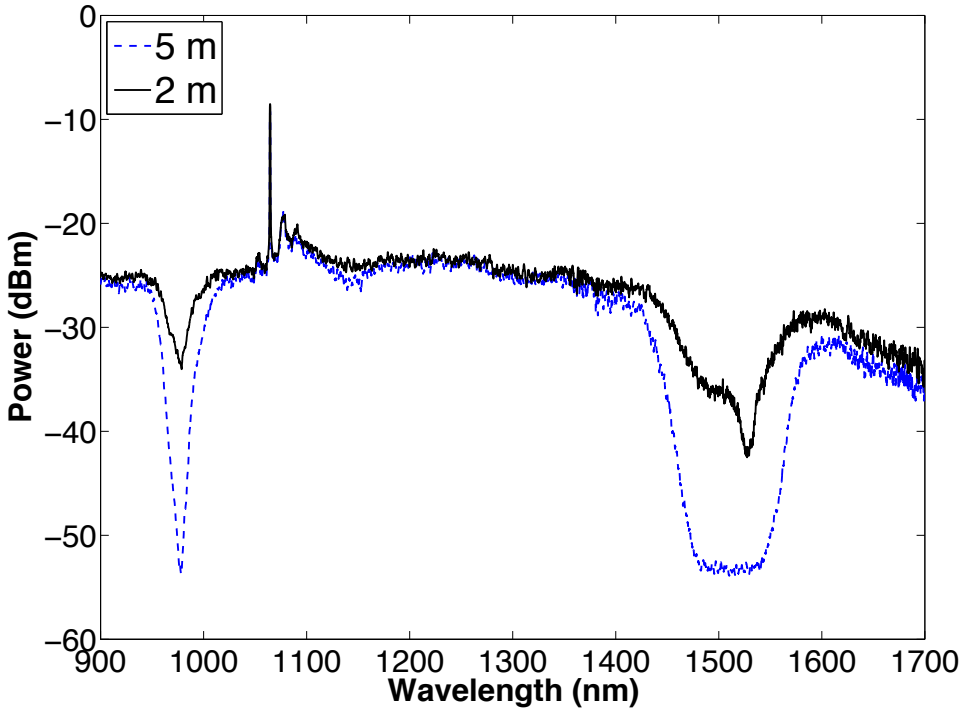

Figure 3.7: OSA spectrum for 5 m and 2 m of fiber length.

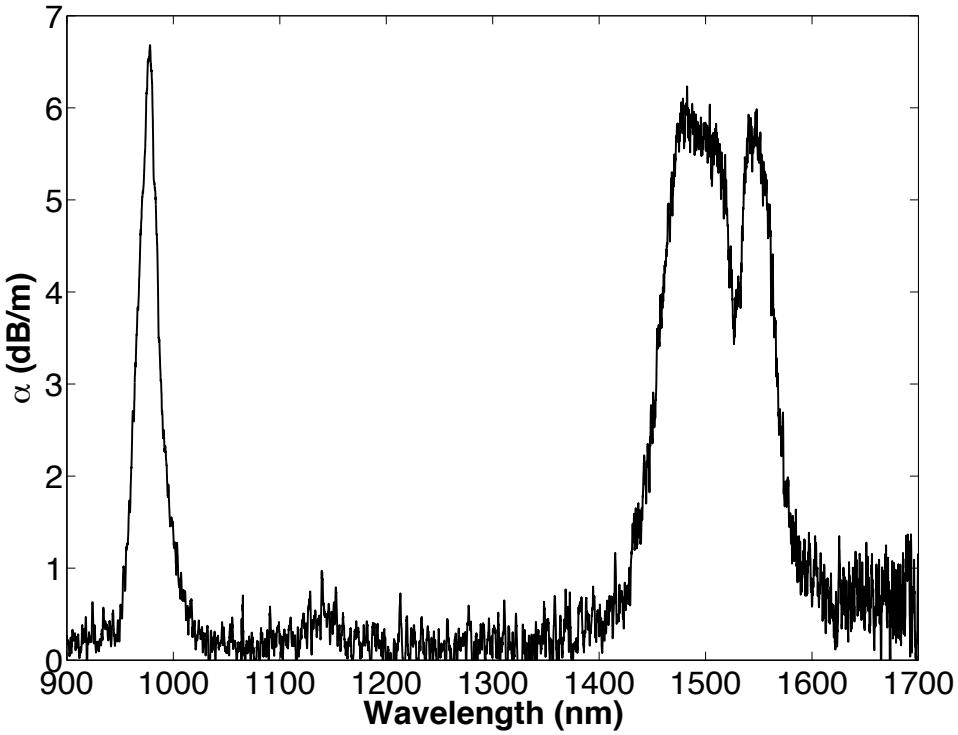

Figure 3.8: Absorption coefficient of the EDF.

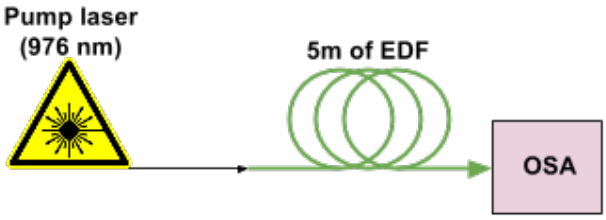

Figure 3.9: Scheme of the implemented system to obtain the Emission spectrum of the EDF.

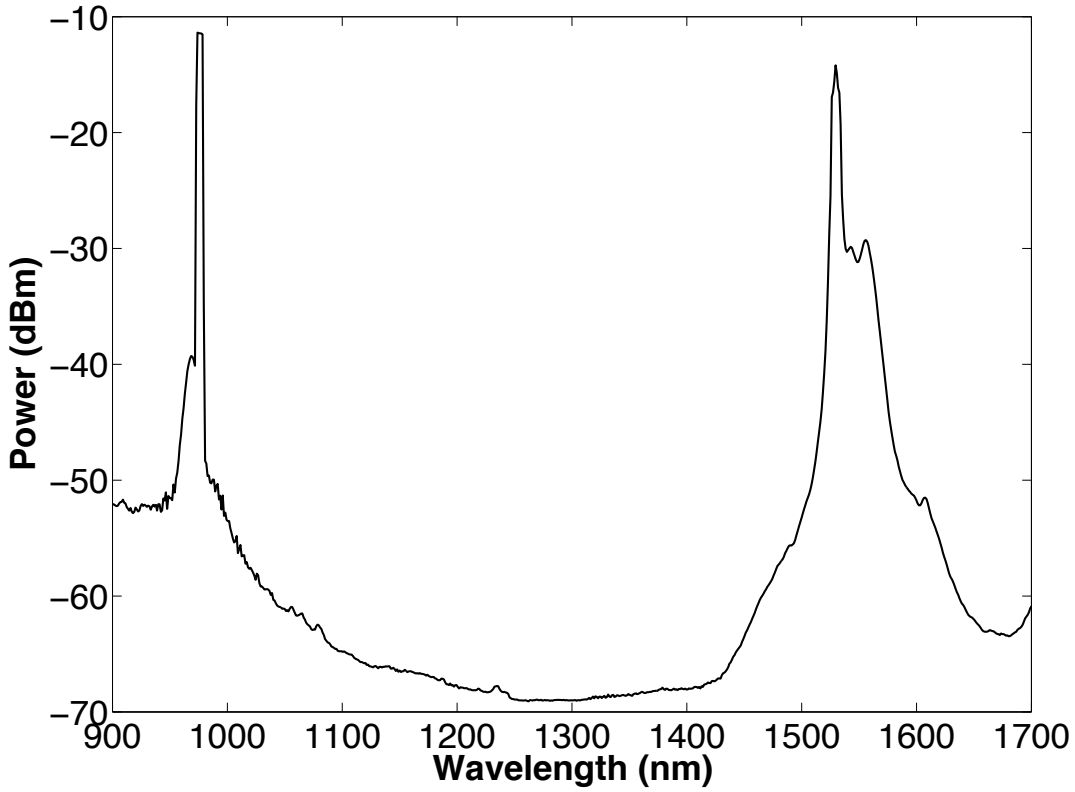

Figure 3.10: Emission spectrum of the EDF.

3.4 Tapered optical fiber Fabrication

This section will provide a brief description of the steps to follow by using the Tapers Fabrication Machine utilized in this work through heating and strain. As is seen in the previous chapter, this machine is made of mechanic elements (flame device, fiber holders) and a control module, which regulates the motors movements and the accurate combination of gases (oxygen and butane).

The software is very simple to use due to the easy navigation for the different menus. The first step is to select the CONTROL box to regulate the gases concentration; in this case, we work with the values presented in the next figure. It is important to wait a few minutes to stabilize the gases mixture before to light up the flame.

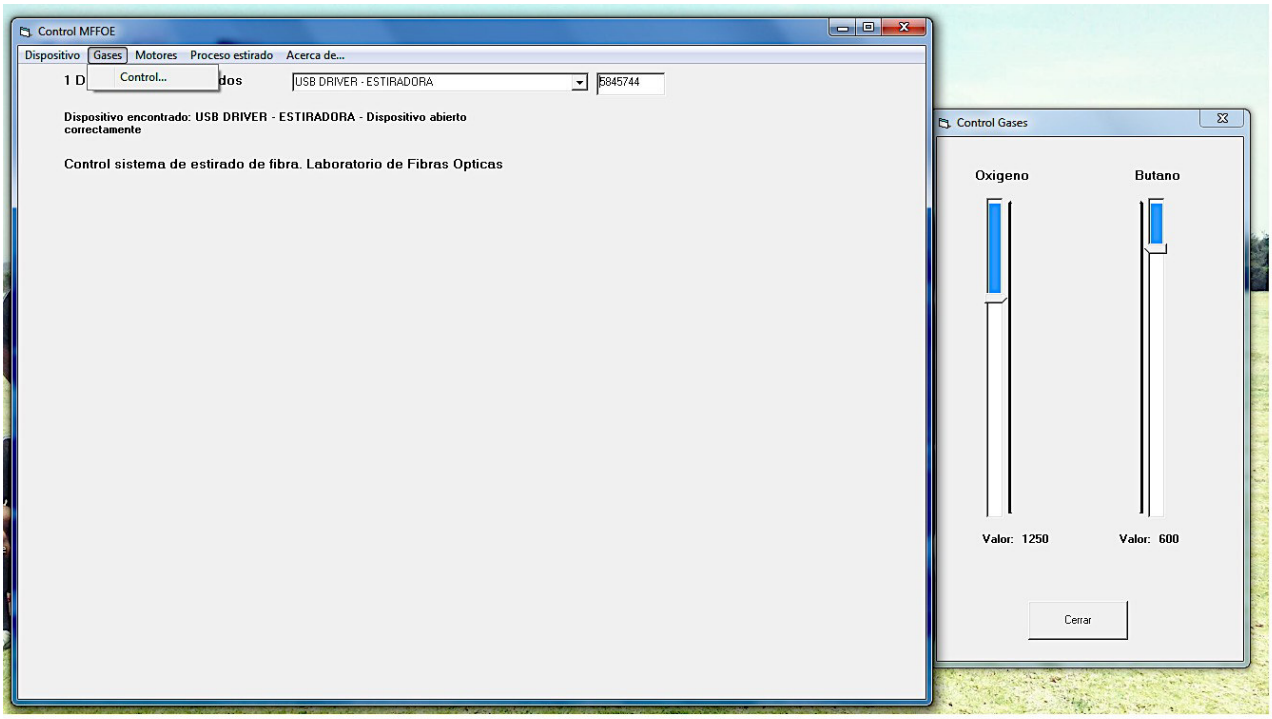

Figure 3.11: Selection of gases concentration.

Next, the tapered optical fiber parameters have to be established (figure 3.12), waist diameter (initial diameter is assumed as 125 microns), stretching velocity (18 mm/min used in this work), burner velocity (4mm/min), initial amplitude of burner oscillation (correspond to the waist length), and transition parameter (to control the taper geometry, value between -1 and 1).

Once all the parameters are settled, we have to click the VALIDATION button; the program will display the elongation length and time for fabrication. Afterward, we start the process (figure 3.13) and just follow step by step the indications.

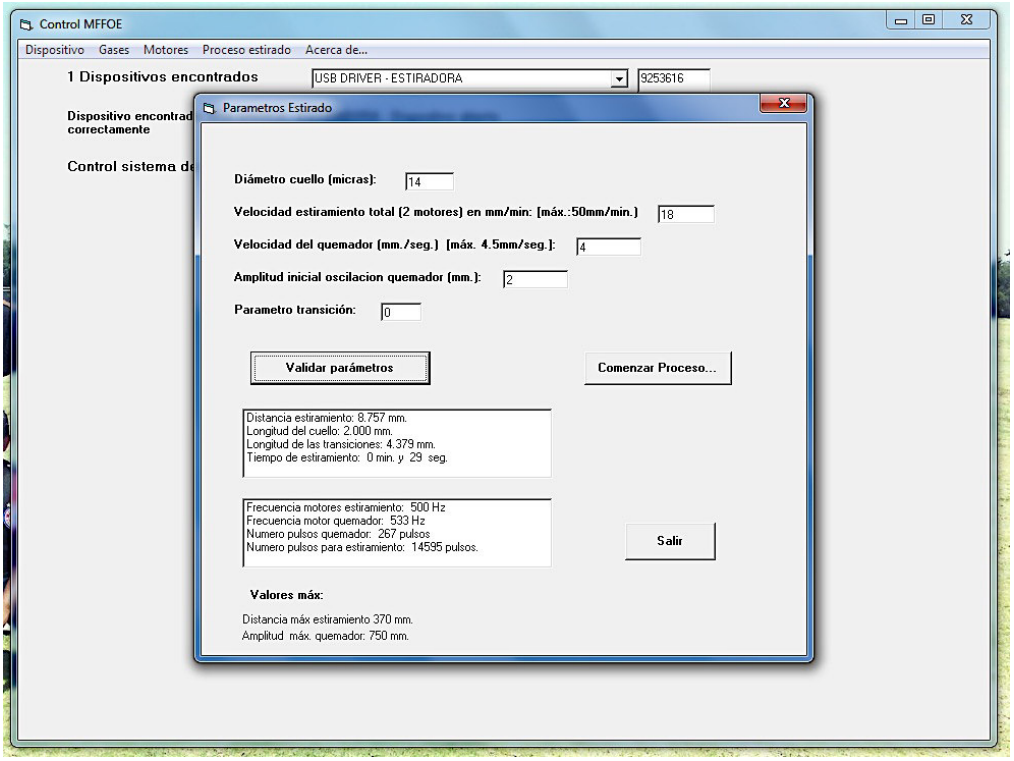

Figure 3.12: Parameters for the tapered optical fiber fabrication.

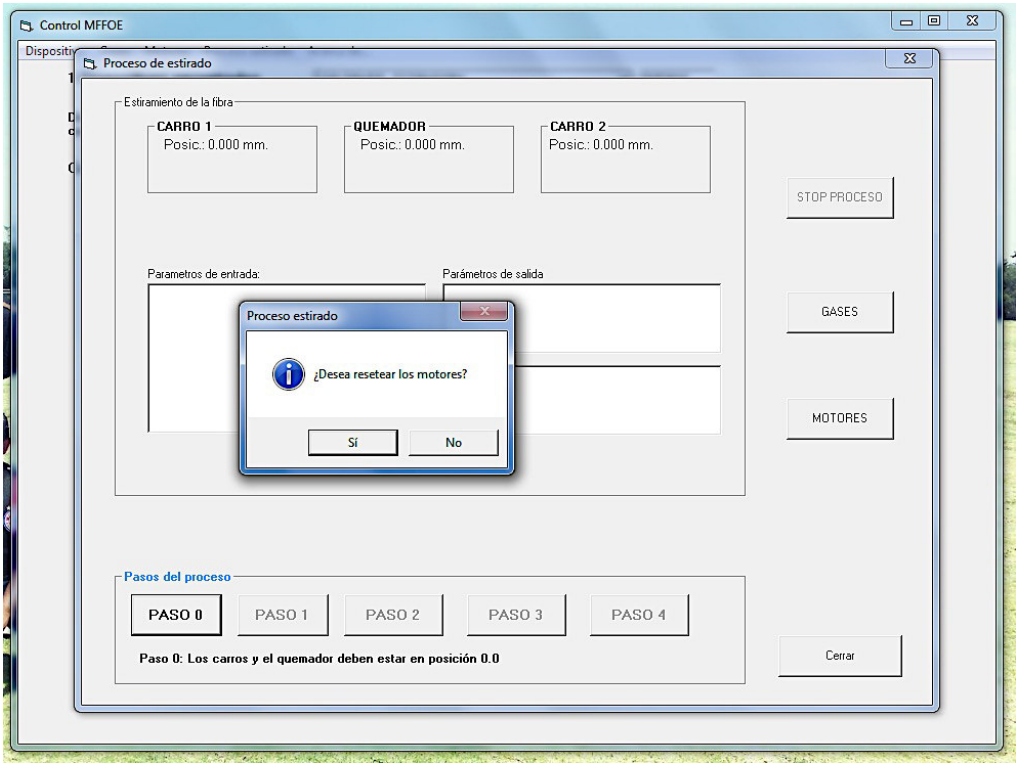

Figure 3.13: Steps to follow for fabrication.

From the information presented above in the previous chapter, the function for the decaying-exponential profile and the transition length t (T_{down} and T_{up} in figure 2.11) are respectively given by (z is the transition length, for more information see equations in chapter 2)

$$r(z) = r_0 e^{-\frac{z}{L_0}}, \tag{2.24}$$

$$t = L_0 \ln\left(\frac{r_0}{r_c}\right), \tag{2.25}$$

At the beginning, we start to work with a fixed value of taper diameter (20 μm) and long transitions t of more than 20 mm, but we noticed that all the light escape in this region and we need more coupling of the high order modes to obtain a good interference pattern. Furthermore, we work with different diameters but below 10 μm it is too difficult to manipulate the fiber due to the elevated fragility, the same thing happens with large waist lengths L_0. Therefore, after several experimental tests, we simulated equation 2.24 in Matlab with L_0=2 mm and t=5 mm in figure 3.14 (obtaining 14 μm as optimum diameter value, it is important to stress out that we used lower values in some experiments but the results had inferior quality), where the exponential change of the taper radius is observed, a promising thing to obtain a probable desired adiabaticity.

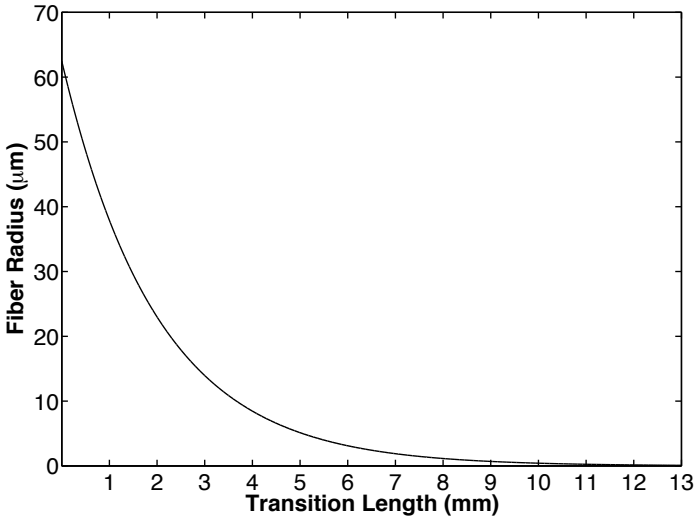

Figure 3.14: Taper radius decrement when transition length is increased.

Moreover, If E_o represents the electric field amplitude at the interface, after a distance d_p (deep penetration), will be

$$E(y) = E_0 \, e^{-\frac{y}{d_p}}, \tag{2.26}$$

$$d_p = \frac{\lambda}{2\pi n_1 \sqrt{\left[\sin^2\theta - \left(\frac{n_2}{n_1}\right)^2\right]}}, \tag{2.27}$$

where *y* is the distance from the fiber core, starting at *y* = 0 at the core-cladding interface. θ is the angle of incidence to the normal at the interface (figure 2.15).

Simulating equation 2.26 (figure 3.15), it is perceived how the evanescent field decays in few microns, because of that it is important the tapering process to approach the fact that the evanescent field could be close or even reach the air, becoming the taper more sensitive to external changes.

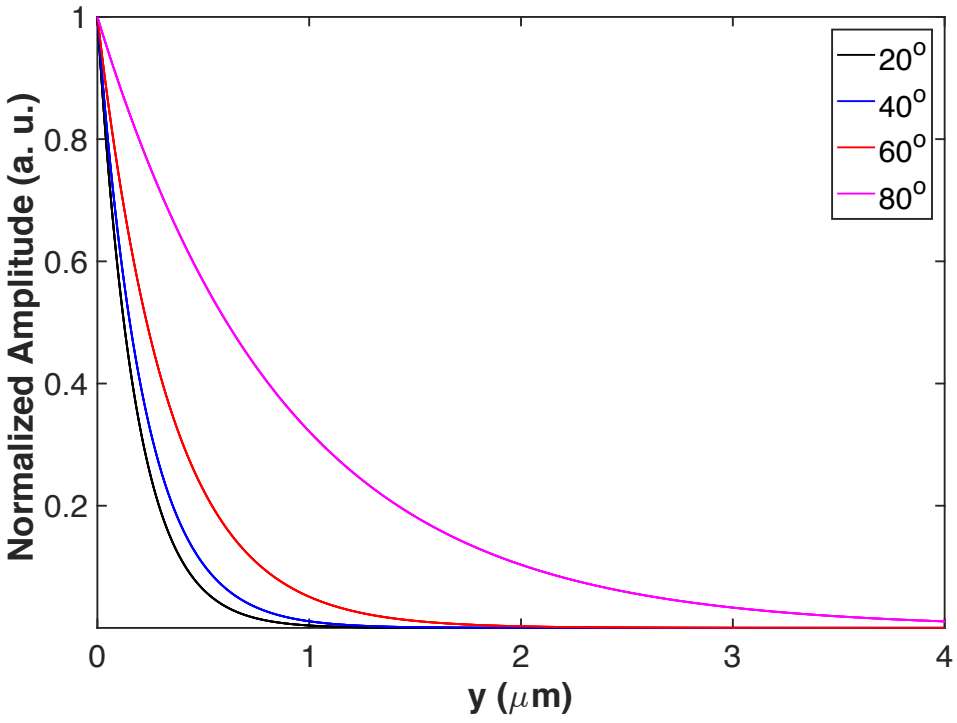

Figure 3.15: Change of the evanescent field with the angle of incidence.

This chapter explained the design of the implemented experimental setups for system components characterization by some experimental methods. One of the most important methods was The Refractive Index Profile measurement due to the fact that the most important transmission properties of an optical fiber can be obtained. The measured Refractive Index resulted to be Graded Index, it is a really great result because that means that the velocities of the different modes will be approximately the same (excellent for communications). Also, the absorption and emission spectrum of the erbium-doped fiber was measured. Furthermore, the software operation of the tapers fabrication machine was described.

Next chapters will present the obtained results for the implemented experimental setups. It will be separated in four main parts, two for sensing of different parameters (curvature, strain, and magnetic field), one for laser applications and the last one for Bragg gratings in tapered optical fibers, used to characterize multimode fibers operating in single mode regime. In some cases, phase analysis was used through Fourier Transform to examine the interference optical spectrum.

Chapter IV: Magnetic Field Sensing Based on Bi-Tapered Optical Fibers Using Spectral Phase Analysis

For several decades, the optical fiber sensor community has spent its efforts proposing many structures and methods to measure physical parameters. Two main measurement modalities are available: phase and intensity. Both methods have pros and cons. For instance, intensity modulation has a simple demodulation process, but the measurement can be affected by source variations and environmental effects around the fiber. On the other hand, phase modulation exhibits immunity to intensity variations, but unfortunately, its demodulation signal requires additional analysis, and there may be phase ambiguity due to phase wrapping. In addition, there are other points to consider in fiber optic sensors such as the reproducibility of the fabrication process and insertion losses affecting the signal-to-noise ratio.

Magnetic field is seen in everyday life, used for motors, electromagnets and more numerous applications, sometimes is necessary to measure its value to control the effects depending on the purpose. Some of the first attempts to detect the magnetic field consisted in analyzing the polarization effects and the intensity changes generated by deforming a single mode fiber using an external sensitive magnetic material. These works use an external material that responds when a magnetic field is applied. Indeed, contemporary works combine special materials with Fabry-Perot interferometers (FPIs) or linear fiber lasers to propose a magnetic field sensor. Nevertheless, in recent years, nanoparticles with special magnetic properties have been studied. These nanoparticles, merged with a liquid, provide a magnetic fluid that, combined with fiber optic structures, generate a magnetic fiber optic sensor; these structures are tapered optical fibers, FPIs, ring fiber lasers, fiber Bragg gratings, multi-mode interferometers, core-offset interferometers, long period gratings, and filled fiber structures. As can be appreciated, the magnetic optical fiber sensors are strongly related to the material involved, many of them are expensive or not commercially available. In addition, most of the above-mentioned works measure the phase modulation to estimate the magnetic field, but other groups measure the intensity modulation. In the latter case, the optical fiber undergoes a chemical treatment that increases the losses in the system when a magnetic field is applied. Nevertheless, intensity

modulation has certain advantages: moreover, the fabrication procedure proposed is more complex, and a special temperature control system is required.

In this work, we propose an alternative signal processing method to detect any physical parameter that presents phase modulation (more information can be founded in the published paper [58]). In this part of the work, we introduce the term “bi-tapered optical fiber” to define the basic tapered fiber, we use this term to make clear that our devices is composed of two transitions (instead of only one) and the waist. To validate the processing signal method, we present a study of a magnetic field fiber optic sensor based on a bi-tapered optical fiber (BTOF). Here, the design of a BTOF, operated in reflection mode, laid over an inexpensive thin magnetic tape as a magnetic field fiber optic sensor. Our design is compact, requiring only a centimeter fiber length, and is insensitive to signal polarization changes, making it suitable for applications outside the laboratory environment. We apply a magnetic field across a range of 30 mT using a permanent magnet that can be moved close to the magnetic tape. The tape bending, induced by the magnetic field, generates phase modulation of the optical signal. From our experiments with specific bi-tapered fiber design parameters, we can extract a maximal wavelength sensitivity around 70 pm/mT and the signal analysis shows low response linearity. We show that this issue can be overcome via phase analysis. As previously demonstrated, the spatial frequency analysis represents an alternative method of exploiting the fiber optic sensor high sensitivity. In our case, we use this technique to improve the detection and the linearity response. Here, the phase analysis offers a better linear response (R^2 = 0.98) and sensitivity (~0.028 rad/mT).

4.1 Experimental Setup and Operation Principle

Our experimental setup consists of three main elements: a superluminescent diode (SLD: QSMD-1550-1), an optical spectrum analyzer (OSA: Yokogawa AQ6370B, Co., LDT, Newman, GA, USA), and a BTOF. We designed our system using standard single-mode optical fibers; the BTOF operates in reflection mode, the aforementioned elements were interconnected using an optical fiber circulator (see figure 4.1). The BTOF operation is based on the interference between fiber modes in the waist region. A single mode fiber is down-tapered (S_1) to launch power into two or more modes in the waist region; each mode

acquires a different phase as it crosses the waist; when the mode recombine to a single mode in the up-taper section (S_2) they interfere constructively or destructively and overlap with the single core mode. As the wavelength is changed, the phase difference between two modes periodically changes.

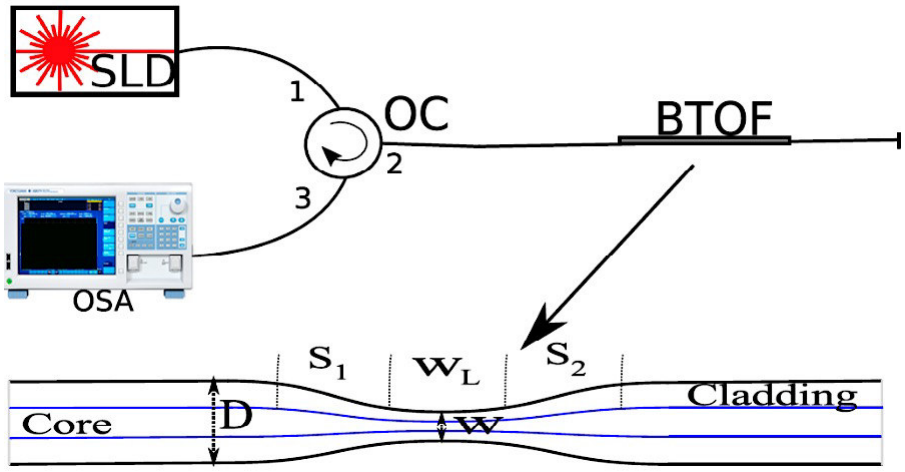

Figure 4.1: Sketch of the experimental setup: SLD: superluminescent diode; OSA: optical spectrum analyzer; OC: optical circulator; BTOF: bi-tapered optical fiber. The bottom inset illustrates the BTOF geometry (up- and down-taper sections: S_1 and S_2; waist length: W_L; waist diameter: W) [58].

Moreover, to validate our proposed method, two BTOFs with quasi-adiabatic tapers were fabricated by the flame brushing technique. These structures have the same physical dimensions (see figure 4.1 inset): a quasi-adiabatic region of 5 mm (down- and up-taper sections S_1 and S_2), a waist around 14 μm (W), and a waist length of 2 mm (W_L) (It is important to mention that all the tapered optical fibers that have been used in this thesis, have the same characteristics). As is well known, reproducibility is a drawback of the fabrication process used in this work. In our particular case, two BTOFs ($BTOF_1$ and $BTOF_2$) were intentionally fabricated using the same process, but different insertion losses ($BTOF_1$ = 2 dB and $BTOF_2$ = 7 dB), and a similar free spectral range (FSR) (20 nm) with a high fringe contrast (FC) around 12 dB, were obtained. The variations of the insertion losses are related to the strain differences applied to the fibers during the fabrication process when a length of fiber is set between the two translation motors. Nevertheless, the fabrication error is small and the FSR is the same, and only the losses between two different fibers are found. In other words, the amplitude changes do not affect the

dominant Fourier component of the interference spectrum. The wavelength spectrums of both samples exhibit different absolute signal phases, but the analysis does not require them to be the same since each fiber is self-referenced for the signal phase analysis (see figure 4.2).

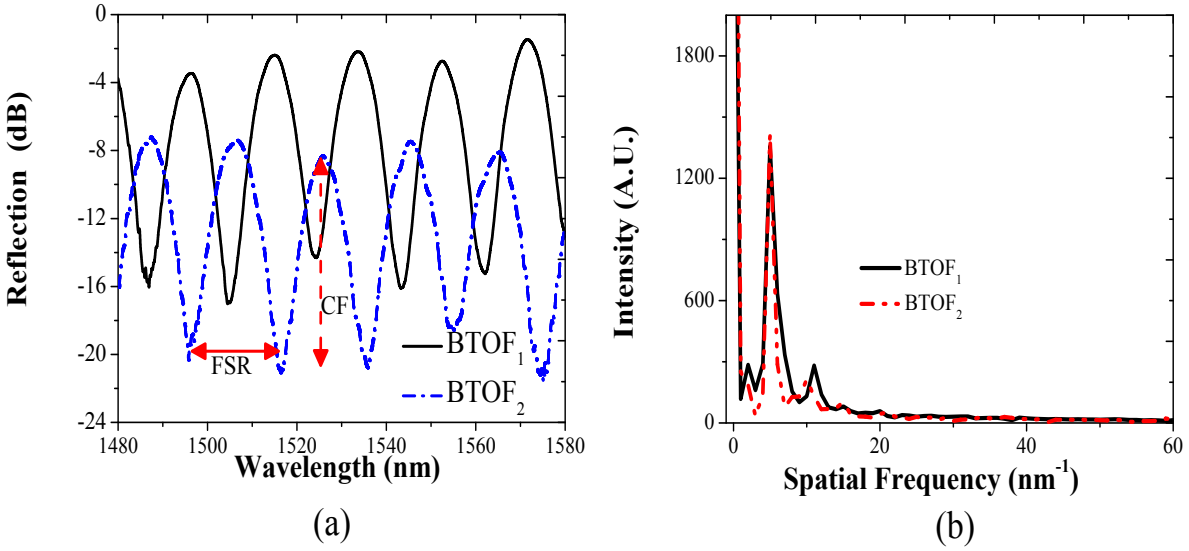

Figure 4.2: (**a**) Reflection spectrum of the fabricated BTOFs (BTOF1 and BTOF2); (**b**) spatial frequency spectra of the BTOFs [58].

Fourier transform signal analysis was applied to the wavelength reflection spectra of the BTOFs; their spatial frequency amplitudes are shown in figure 4.2b. Despite the power level disparity and the difference phase-matching observed in the reflection interference (around π), the spatial frequency spectrum shows similar modal contribution. Both (spatial) frequency spectra exhibit the presence of two, dominant signal frequencies: the component centered at zero frequency (D.C. component) and the interference between a high-order (cladding) mode and the core mode with a peak centered around 5 nm^{-1}. As can be observed in figure 4.2b, the dominant spatial frequencies for both BTOFs are close to one another and their energy content, based on the peak heights and widths, are also very similar. These frequency components are used to implement a magnetic field phase-sensitive analysis. The interference reflection spectrums of the BTOFs (see dot-dash and solid lines in figure 4.2a) generate the strong peaks observed in figure 4.2b.

The interaction between them can be expressed by the following expression:

$$I = I_a + \sum_b I_b + 2\sum_b \sqrt{I_a I_b}\cos(\Delta\phi_{ab}), \tag{4.1}$$

where I_a represents the core mode intensity, and I_b is the intensity of the cladding modes excited in the waist region of the BTOFs. The first two terms represent zero frequency contributions. The differential phase components between the modes involved is represented by $\Delta\phi_{ab}$. This difference phase is related to the difference in propagation constants: $\beta_b - \beta_b$ where $\beta_{a,b} = 2\pi n_{a,b}L/\lambda$, where λ is the wavelength, L is the total length of the BTOFs, and $n_{a,b}$ represents the effective refractive index of the core mode (n_a) and high-order cladding modes (n_b) in the waist. The effective refractive index is related to the BTOF dimensions and is strongly wavelength dispersive.

4.2 Magnetic Field Detection

4.2.1 Wavelength analysis

As a proof of principle for the magnetic field sensor, our BTOF structures were laid over a commercial thin plastic magnetic tape (length: 11.5 cm, width: 12.7 mm and thickness: 25.4 microns), and the principal magnetic element in the magnetic tape is a well-known Fe_3O_4 material. The ends of the magnetic tape and the BTOF were fixed using two translations stages (A and B). The magnetic field was applied using a magnet attached to a vertical translation stage. When the distance between the magnet and magnetic tape decreased, the magnetic field over the magnetic tape surface increased, and the magnetic tape with the attached BTOF bowed toward the magnet (see figure 4.3). The magnetic field was estimated using a Magnetometer E-1008537, and the maximum magnetic field applied was 59 mT and the maximal curvature produced was 2.4 m^{-1}. As the magnet was lowered toward the tape, the tape's bowing curvature above the platform increased. The motion of the tape changed the fiber curvature, and the reflection spectrum was shifted to longer wavelengths. The wavelength shift is related to the effective refractive index

changes generated by the bending induced over the BTOF [59]. To prevent temperature effects from affecting our magnetic field detection system, the experiment was experiment was kept at room temperature, 25 °C. Other authors have reported inducing a magnetic field using current flow through a metal wire coil, which requires a special system to measure the temperature effects at the sensor or to keep its temperature constant. We eliminated the undesirable local heating effects using a permanent magnet in our experiments and directly measured the local magnetic field.

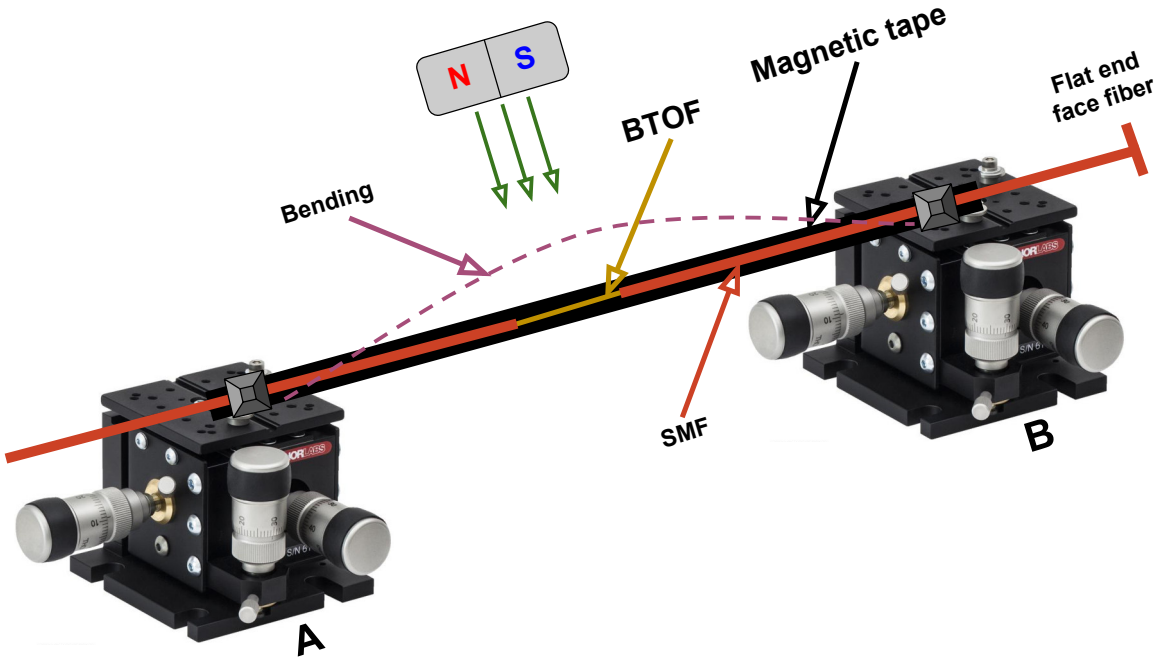

Figure 4.3: (**a**) Schematic diagram of the experimental setup. The magnetic field is changed by moving a permanent magnet close to or further from the magnetic tape [58].

The bending induced in the BTOF altered the effective refractive index of the modes involved, and the refractive index profile can be approximated according to the curvature radius, R_c, by [60,61]:

$$n(R_c) = n_s\left(1 + \frac{x(1+\chi)}{R_c}\right), \tag{4.2}$$

where n_s represents the effective index of the straight tapered length, the strain is applied along the x axis, χ is the strain-optic coefficient (−0.22 for silica), and R_c is the curvature radius. The maximal change of the refractive index estimated from equation 4.2 is of order 0.0004. Figure 4.4a shows the BTOF1 interference reflection response when the magnetic field on the magnetic tape is increased. We observed a uniform wavelength shift across the entire spectrum. The redshift of the waveform is attributed to the decrement of fiber bending and the radius of curvature R_c. As a result, the phase difference phase increases as the magnetic field increases.

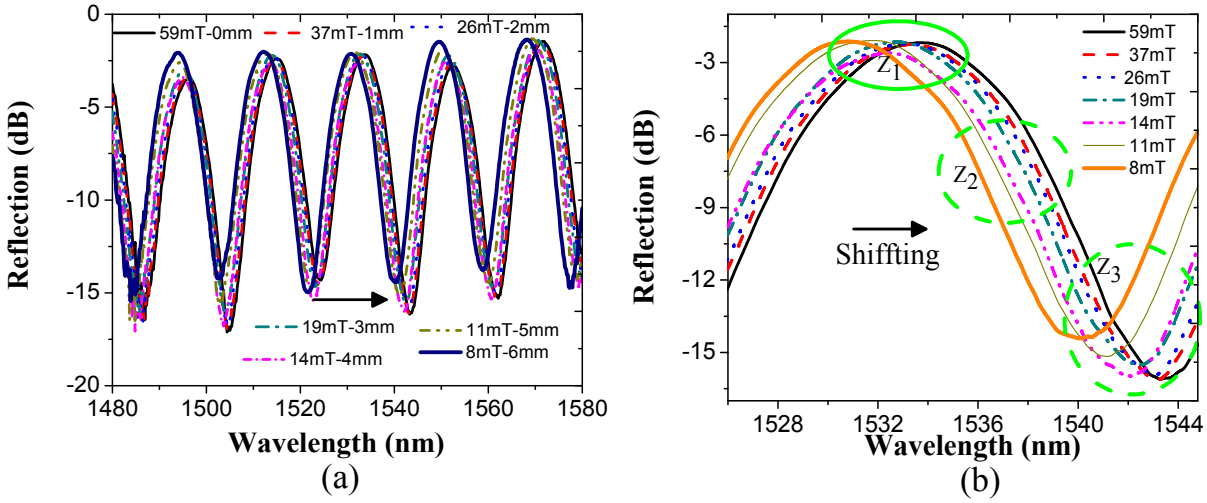

Figure 4.4 (**a**) Magnetic field response for specific magnet positions; (**b**) Particular fringe regions analyzed for magnetic field increments. Z_1 is near the signal maximum, Z_2 is where the signal's slope change is the highest, and Z_3 is at the signal minimum [58].

To make further tests, a specific wavelength region was analyzed to show the reproducibility of the fiber signal. In figure 4b, particular fringe regions were examined to closely analyze the magnetic field effect; three zones were studied to validate our method. The first zone (Z_1) is a peak centered around 1533 nm, where we observe a smaller linear shift of the peak position with magnetic field strength. Due to this effect, the Z_1 region, corresponding to a maximal signal power peak, was limited in terms of analyzing the fiber sensor signal. The second region (Z_2) represent a clear, linear wavelength shift increment for the applied magnetic fields, with a sensitivity extracted from the data around 70 pm/mT. The third region (Z_3), around the signal minimum, also presents a limited linear increment

when the magnetic field is applied. It has the same issues as the Z_1 region; reduced sensitivity in detection is clear for higher magnetic field values. The issues described above are presented in several fiber optic sensors that use a direct analysis of the signal phase modulation.

The two BTOFs were analyzed by considering the region Z_2, for $BTOF_1$ the initial wavelength was 1536 nm and the maximal sensitivity can be estimated around 70 pm/mT (see figure. 4.5). Additionally, the $BTOF_2$ exhibits a sensitivity around 50 pm/mT, both sensitivities are an approximation due to the lower linearity exhibit when the magnetic field is applied, this response is related to the magnetic field-distance association. Indeed, these sensitivities depend on the region and the reproducibility of the fabricated devices. At this point, we detect magnetic field by inducing curvature over a BTOF.

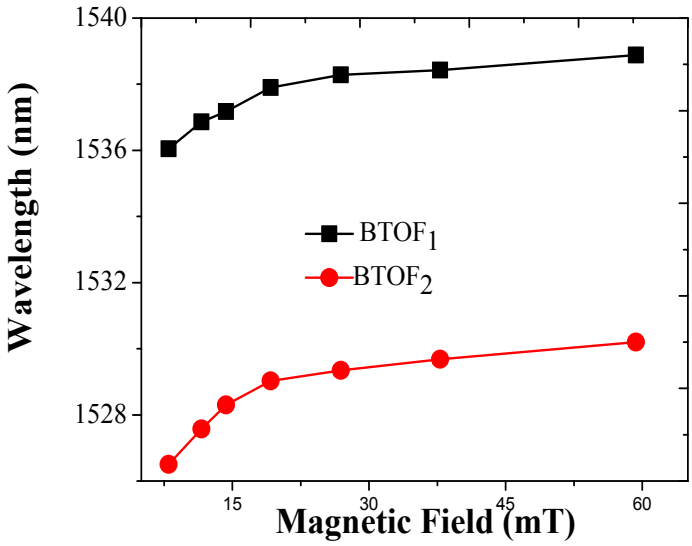

Figure 4.5: Sensitivities responses for $BTOF_1$ and $BTOF_2$. Using a signal analysis in zone Z_2 [58].

4.2.2 Spatial frequency signal analysis

In order to detect magnetic field without the inconveniences mentioned in the wavelength study, we propose an alternative signal analysis method using the dominant spatial frequency extracted from the signal spectrum. In our particular case, we use the interference spatial frequency centered at 5 nm^{-1}, the two BTOFs fabricated show the same centered frequencies. Besides, this peak remains almost constant in frequency and

only some intensity variations are observed. In addition, these intensity changes are not linear and any correspondence can be attributed to the applied magnetic field. To appreciate the magnetic field changes induced in the $BTOF_1$ wavelength spectrum, we filtered the second Fourier component (see figure 4.6a) and its phase was extracted, then this phase is plotted for specific arbitrary wavelength (see figure 4.6b). As observed in figure 4.6b the magnetic field increments can be easily identified by phase changes, and moreover, its sensitivity will not depend on the fringe region.

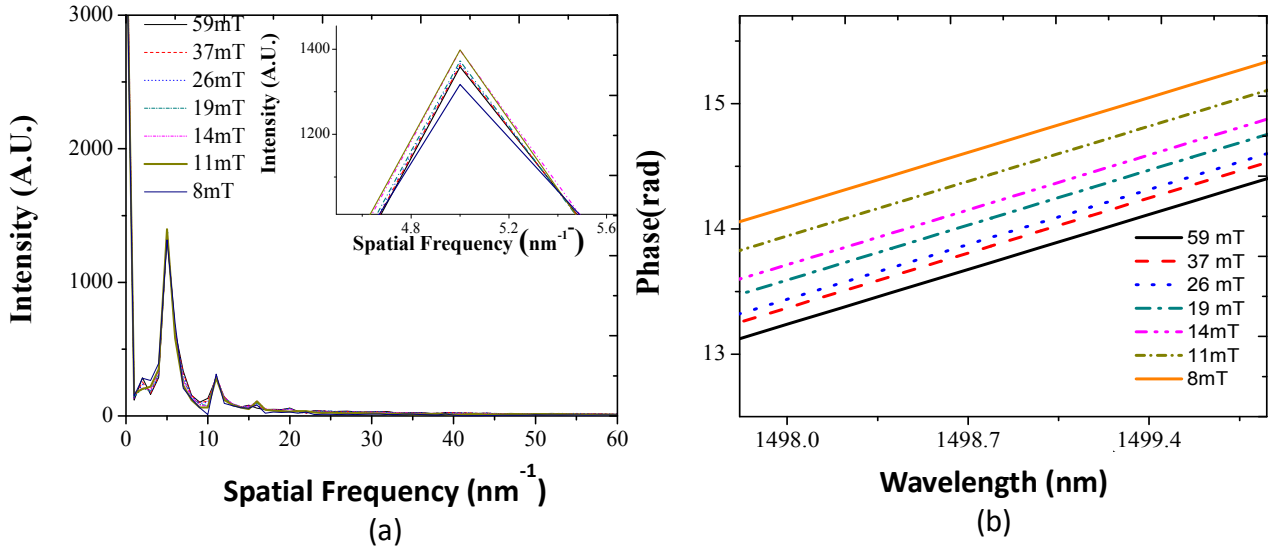

Figure 4.6: (**a**) Spatial frequency spectrum for $BTOF_1$ when magnetic field is applied; (**b**) Phase changes of the filtered $BTOF_1$ Fourier component when the magnetic field is increased [58].

The difference phase generated is extracted in figure 4.6b as the magnetic field is increased and plotted in figure 4.7 (in this case since 5 to 37mT). Here phase change sensitivities of 0.027 rad/mT ($BTOF_1$) and of 0.029 rad/mT ($BTOF_2$) were calculated. The two BTOF interferometers show very similar sensitivities and it can be appreciated a clear linear response (R_1^2=0.9814 and R_2^2=0.9614). Moreover, the phase-matching difference and the power level disparity presented in the fabrication process do not affect the sensitivity values. In addition, these sensitivities probably can be increased by modifying the BTOF physical parameters. However, in this part of the thesis work we focused on a novel signal processing method for magnetic field detection trying to avoid problems presented in the traditional wavelength shifting analysis.

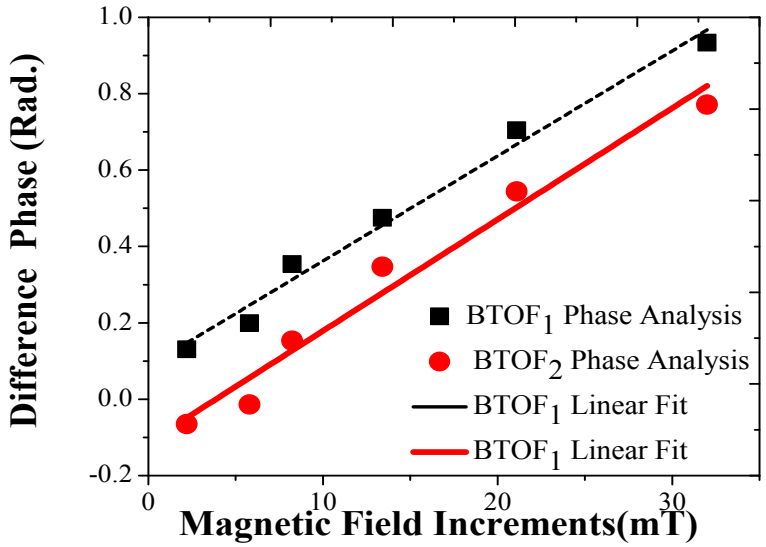

Figure 4.7: Difference phase analysis of both BTOFs for magnetic field increments [58].

Three regions were identified and analyzed and their advantages and disadvantages were explained. The maximal phase shift (wavelength) sensitivity achieved was 70 pm/mT, albeit with lower linearity in the response. The spatial frequency analysis was implemented by filtering the modal interference we found in both tapered fiber spectra. It is important to stress that despite the interference reflection differences, the spatial frequency spectrum shows the same dominating modal interference spatial frequency centered at 5 nm^{-1}. Once the signal is digitally filtered its phase is extracted; the magnetic field can be clearly identified from the phase analysis. The sensitivity presented in both tapered fibers reached by this method is around 0.028 rad/mT. Moreover, the phase difference as the magnetic field is increased shows a linear increment response. Furthermore, BTOF for higher or lower magnetic field sensing can be designed by using different magnetic materials with stiffer or softer bowing responses to the local magnetic field giving a range of applications.

Chapter V: A Dual Modality Optical Fiber Sensor

As is explained before, the field of optical fiber sensors has concurrently grown because of the wide availability and low-cost of the fibers, photonic devices and electronics. In particular tapered optical fibers are a specific class that has been developed for diverse applications; they have found application in fiber lasers, nonlinear optical elements, low-level biomolecule or chemical species sensing and thermodynamic variable sensing such as temperature; specifically, tapered fiber sensors are able to measure refractive index, strain, magnetic field, temperature, acoustic signals, etc. Moreover, it has been demonstrated that several parameters can be simultaneously detected by modifying fiber optic structures such as temperature and curvature, fiber bending and strain, temperature and strain, and temperature and refractive index.

Several published approaches are based on spectral feature modulation (wavelength shifts) and intensity modulation (power variations) in the transmitted signal. Nevertheless, when a physical variable is changed both modulations are often observed for the same variable change, which leads to an ambiguity related to associating the measured signal features with a specific effect if multiple variables are being measured. Moreover, recently reported structures use several fiber optic components that involve complicated fabrication processes as well as undesirable crosstalk effects in the signal measurements.

In this part of the thesis work, we report our design and application of a dual modality fiber sensor using an optical fiber bi-taper fabricated by a low-cost technique that simultaneously detects curvature and strain with no measurable crosstalk between the phase and amplitude signal components (more information can be founded in the published paper [62]). In the same piece of fiber, the strain is applied over a section that contains the tapered region and the curvature is applied over a conventional single-mode fiber placed in a second section of the device. The design allows the application of dual simultaneous sensing instead of two interconnected devices. The phase modulation signal provides an unambiguous estimation of the strain and the intensity modulation is similarly only related to the fiber curvature. Our system presents very high sensitivities and no ambiguity in the measurement of each parameter. Furthermore, it would have application in structural health monitoring and it is really important to build permanent points for system optical

components to avoid measurement deviations, specifically for materials that present strain and bending at the same time.

5.1 Fabrication and Operating Principle

As is seen in the previous section, the down- and up-taper sections of the tapered fiber excite higher order cladding modes by coupling energy of the fundamental core mode into the cladding in the fiber waist section. So, the excited fiber modes have different effective refractive indexes. These multiple waist modes are coupled back into the fundamental fiber mode in the up-taper section. The observed interference pattern is obtained due to the different phases accumulated by each mode crossing the waist section. This accumulated phase is a function of the wavelength. Also, it is important to mention that as a consequence of the fabrication process is not possible to ensure the generation of only one high-order cladding mode.

A typical interference pattern acquired after the tapered fiber is shown in figure 4.8 inset; the spectrum has a sinusoidal shape with a peak-to-valley intensity contrast around 12 dB and a period of 12.5 nm. The Fourier transform of the spectrum has several peaks, the modal sinusoidal interference contribution in the data is observed as a dominant spectral peak at a non-zero frequency.

Changing a physical variable, which modifies the difference phase or the intensity contributions of the modes involved, will uniformly shift the modal interference pattern. Extracting the phase change from the interference pattern is directly correlated to the physical variable changes in the surrounding environment. In this work, we use this information to obtain simultaneous information about curvature and strain measurements, where crosstalk between them lies below the measurement threshold.

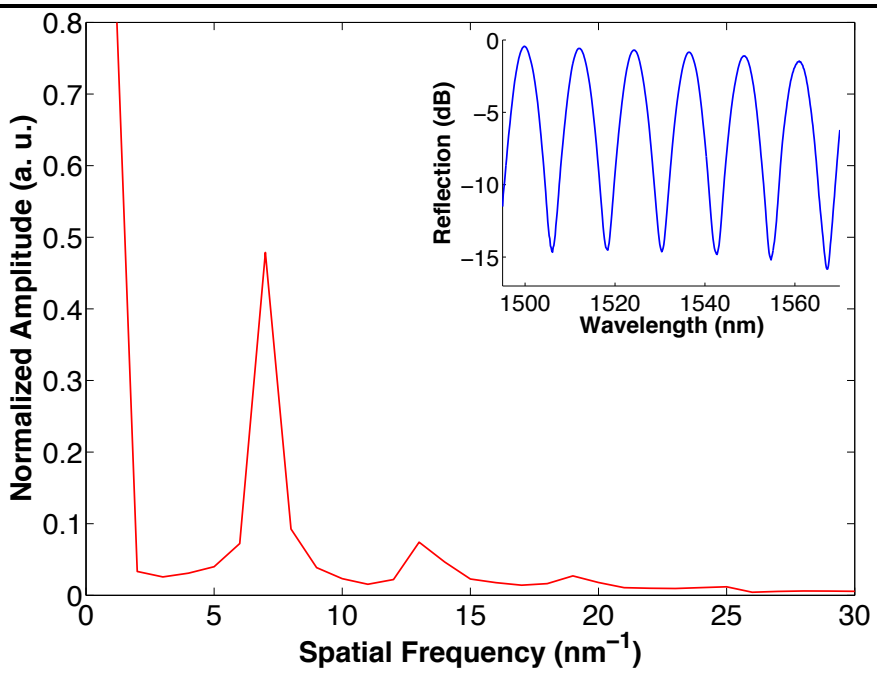

Figure 4.8: The frequency spectrum of the transmission data through the tapered optical fiber [62].

5.2 Results and Discussion

5.2.1 Experimental Setup

We developed the fiber sensor shown in the schematic configuration of figure 4.9 for dual modality operation, i.e. it can simultaneously sense strain and fiber curvature. The sensing elements are a bi-tapered fiber with a bent fiber section. The source of our broad wavelength spectrum is the superluminescent diode (SLD) QSMD-1550-1. The light passes through an optical fiber circulator (OC) into the two sensing elements. The light is reflected at the end of the sensing element by the reflection at the glass/air interface (about 4% reflectivity) and passes through the two sensing segments again. The OC directs the signal into the Optical Spectrum Analyzer (AQ6370B), which measures the spectrum. The tapered fiber is placed between two holders (*A* and *a*). The holder *A* is fixed to an optical element, the holder *a* at another end of the fiber taper is attached to translation stage 1. The second sensing element is a fiber section attached between holder *a* and *b*. The fiber holder labeled *b* is moved by the translation stage 2. When the translation stage 1 is moved in forward direction, strain is applied by affecting the length *D* (15.6 cm), however, at the same time the distance between *a* and *b* (*L* = 3 cm) is reduced and the fiber is bent,

moreover, by moving the translation stage 2 in forward direction the curvature is increased and the strain is not affected.

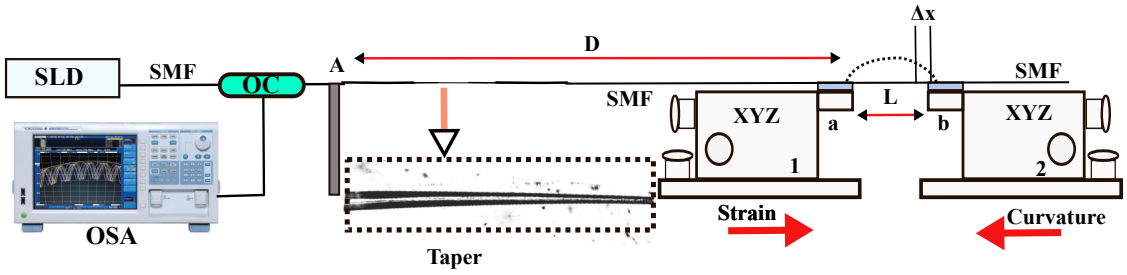

Figure 4.9: Schematic configuration of the experimental set-up [62].

5.2.2 Strain Measurements

The axial strain is controlled by moving the translation stage 1, furthermore, using the relation between strain and the displacement increment, $= \Delta x/D$, the strain value can be estimated. When the strain is applied the wavelength spectrum was measured and analyzed. As the strain is increased the intensity peak is blue shifted (see figure 4.10 inset). By analyzing the labeled peaks P_3 (1524 nm), P_4 (1537 nm) and P_5 (1549 nm) a linear wavelength shifting is observed in response to the increased strain (see figure 4.10). The shifting of the interference pattern is related to the change of the effective refractive indexes of the modes that dominate the interference spectrum, which modify the difference phase of the dominant modes. When strain is applied in the tapered and the un-tapered regions, the relation between the effective refractive index and the strain applied can be expressed by [63]:

$$\Delta n = -0.5p\left[\left(n_{w,eff}(r)\right)^3\left(1-\frac{d_0}{d_1}\right)\right]\varepsilon\,, \tag{4.3}$$

where ε is the strain, p represents the photo-elastic coefficient, $n_{w,eff}(r)$ is the effective refractive index of the tapered fiber waist region with radius r and the ratio between the un-tapered and the tapered fiber diameters is d_0/d_1.

Moreover, by carefully measuring the intensity peaks for different applied strain values, we find only minimal intensity variations of P_3 (around 0.077 dB). This variation is attributed to

a curvature-induced amplitude change by the reduction of the distance between the points *a* and *b*. The wavelength and measured intensity change of P_3 when the strain is applied is plotted in figure 4.11, from the data we find the slope has a sensitivity of −1.64 pm/*με* and the correlation coefficient is 0.999. The analysis shows a highly linear relationship between the wavelength shifting and the applied strain and at the same time, we observe almost constant power for the fringe peak intensities. It is important to mention that for the system experiments performed here, we simultaneously change the curvature and strain because the fiber holder point *b* is held fixed in this setup. For this reason, there is a minimal intensity variation when the strain is applied to the bi-tapered fiber section. In this section, we consider the maximal strain around 6400 *με* due to the strain around 7000 *με* can catastrophically break the fiber. The maximal applied strain on the fiber segment does not exceed its elastic limit, so there is no permanent distortion of the bi-tapered optical fiber; in other words, the deformation induced by our maximal strain is reversible. Nevertheless, the waist diameter of the bi-tapered optical fiber used in this work represents a limit of our capability; however, for larger waist sizes we found a lower sensitivity. In addition, the strain applied in this work is higher than presented in other articles.

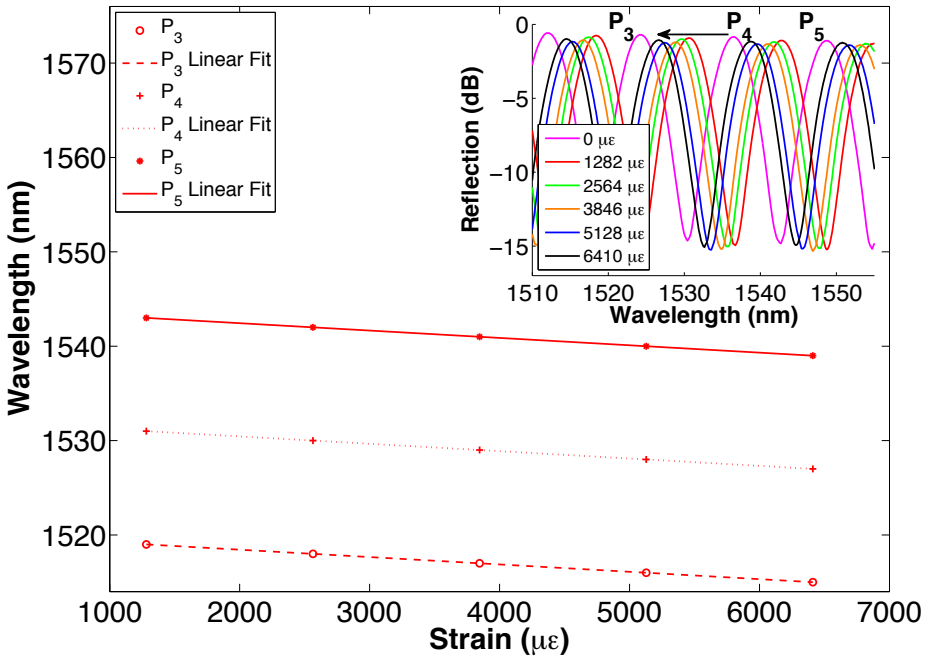

Figure 4.10: Interference spectrum response when the strain is applied [62].

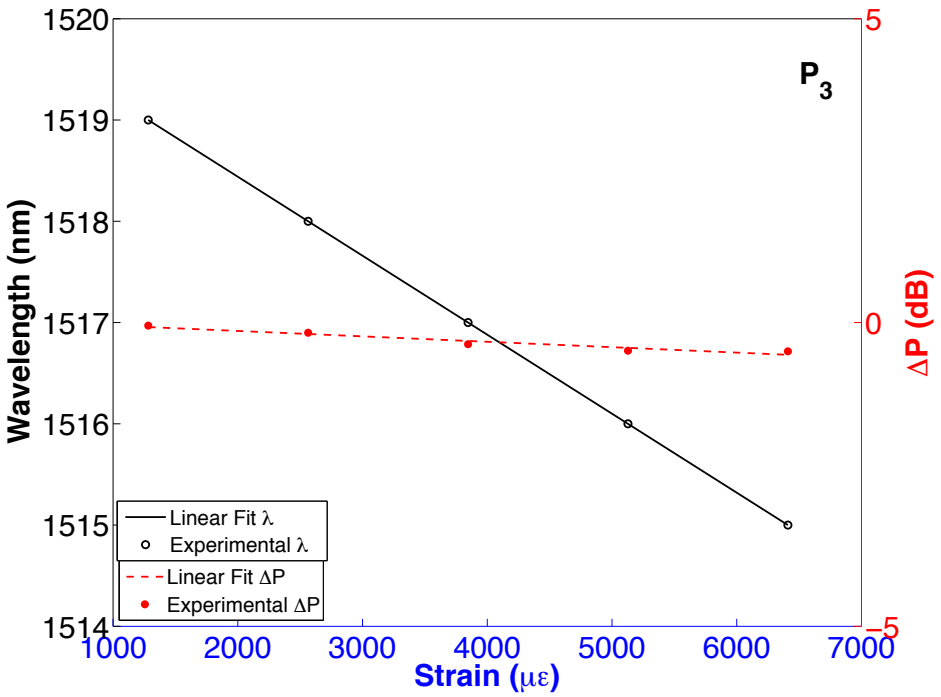

Figure 4.11: Intensity and wavelength response of the peak centered at 1524 nm when the strain is applied [62].

5.2.3 Curvature

The fiber curvature is induced in the system by changing the distance between the fiber holders *a* and *b* (their separation is around 30 mm), this occurs by moving the translation stage 2 in the direction of stage 1. The curvature of the fiber is estimated by [64]:

$$c = \sqrt{\frac{24\,\Delta x}{L^3}}, \tag{4.4}$$

where L is the distance between the fiber holders *a* and *b* and Δx is the forward displacement of the translation stage 2. As the curvature is increased, the intensity extreme of the reflected interference spectrum decreases, as the arrow shows in the figure 4.12 inset. The amplitude changes in the power spectrum are related to the loss of power for the fundamental mode into higher order cladding modes in the bent fiber section. It is

important to note that the tapered optical fiber is not directly affected when the fiber curvature is changed in the system.

Moreover, by analyzing the interference (P_3, P_4 and P_5) when the curvature is applied from 40 to 60 m^{-1} (see figure 4.12), similar power variations are observed. According to the linear fit to the data, correlation coefficient R = 0.999 is exhibited by peak P_3. The analysis of P_3 is summarized in figure 4.13, we estimated a measurement sensitivity around −0.374 dB/m^{-1} and moreover when only the curvature is presented, there is no wavelength shifting, as a result of both measurements it can be inferred that there is no measurable crosstalk between strain and curvature measurements.

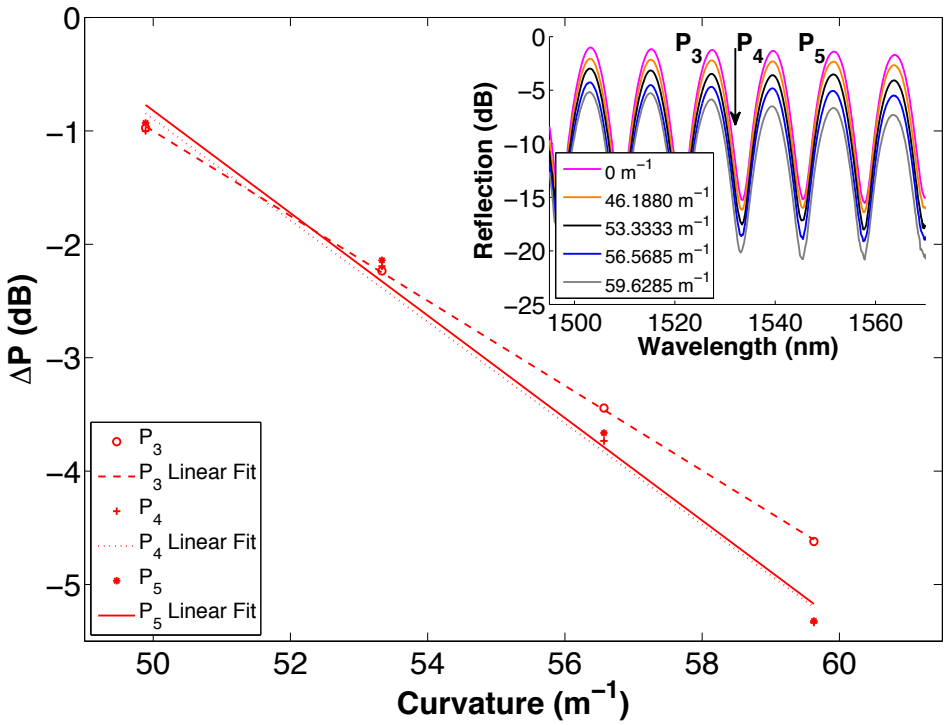

Figure 4.12: Curvature data analysis [62].

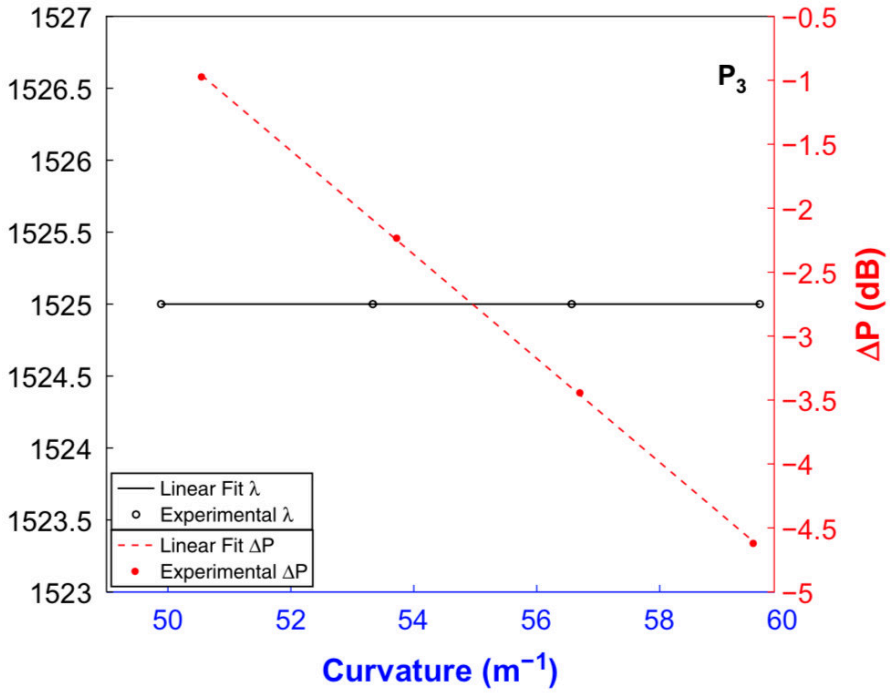

Figure 4.13: Curvature analysis of the peak (P_3) centered at 1524 nm [62].

5.2.4 Simultaneous Detection

The data for curvature and strain changes using the peak P_3 are plotted together in figure 4.14. The results show that simultaneous detection can be obtained by considering the wavelength shifting and the power peak variation of the peak P_3. This means that intensity modulation will provide information about the curvature and phase modulation will provide information about the strain. However, a discrimination matrix can be constructed from the data; the peak is chosen to generate the simultaneous measurement matrix. P_5 has the same response as P_3 and a strong correlation with the applied physical variable, around R = 0.9909 for strain and 0.9916 for curvature.

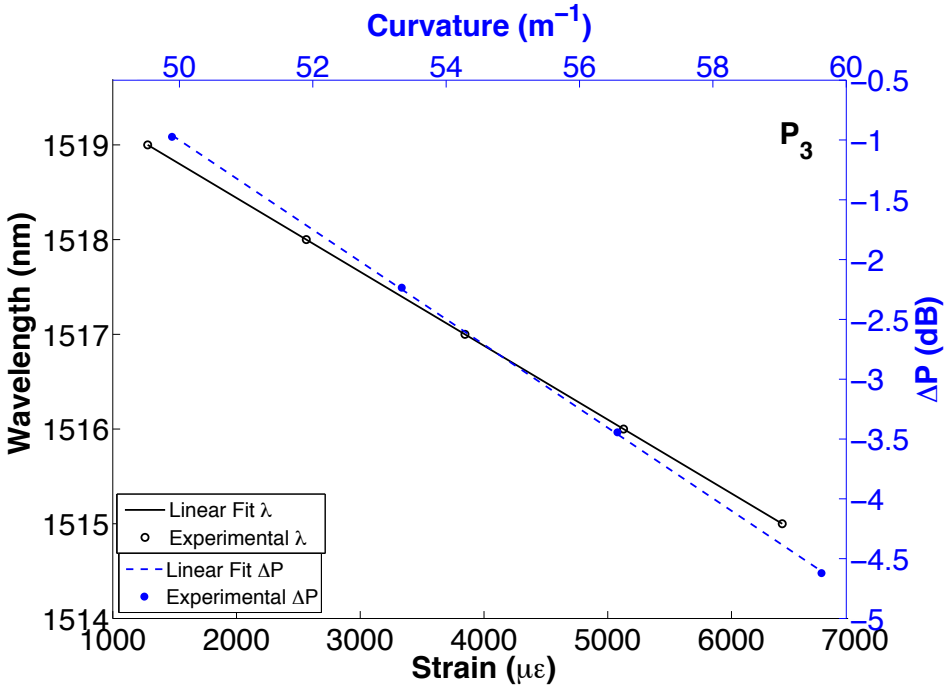

Figure 4.14: Simultaneous curvature and strain analysis of the peak (P_3) centered at 1524 nm [62].

We use peak 3 and peak 5 to generate the simultaneous detection matrix, here using the sensitivities of curvature and strain the matrix can be written as [19]:

$$\begin{matrix}\Delta\lambda \\ \Delta P\end{matrix} = \begin{pmatrix} S_{\varepsilon P3} & S_{cP3} \\ S_{\varepsilon P5} & S_{cP5} \end{pmatrix} \begin{pmatrix} \Delta\varepsilon \\ \Delta c \end{pmatrix}, \tag{4.5}$$

where $\Delta\lambda$ and ΔP are the wavelength shift and change of the peak power extracted from the data of the interference spectrum, respectively. The curvature sensitivities are represented for both of the chosen peaks as S_{cP3}=−0.374 dB/m^{-1} and S_{cP5}=−0.376 dB/m^{-1}; in the strain analysis both peaks present the same sensitivity ($S_{\varepsilon P3}$=$S_{\varepsilon P5}$) around −1.64 pm/*με*, finally, the strain and curvature are represented by $\Delta\varepsilon$ and Δc, respectively. The resolution of the system can be analyzed, using the highest OSA resolution in both wavelength and power, hence a resolution around −10.9 *με* and 0.026 m^{-1} were estimated for strain and curvature, respectively. In order to demonstrate the measurement capability of the proposed analysis, the strain and curvature data were used to probe the matrix, achieving a similar result as it can be appreciated in figure 4.15. By comparing the theoretical and experimental results, based on the standard deviation of the data from the

straight lines, we find that variations from linearity are 0.1% for strain and 0.2% for curvature. The matrix provides a very similar response for other analyses of the peak; in other words, our system has a simple demodulation process for simultaneously determining curvature and strain information. It is important to remember that the system is operated in reflection mode, and higher spectral resolution (HSR) is used in our measurements. The signal-to-noise ratio (SNR) is also an important issue. The tradeoff between HSR and SNR can be compensated in several ways; such as increased light source brightness or increasing the data capture integration time. In the former case, a high-energy pump diode can be used, as well as increasing the reflectivity at the fiber end by applying a reflective thin film to its surface.

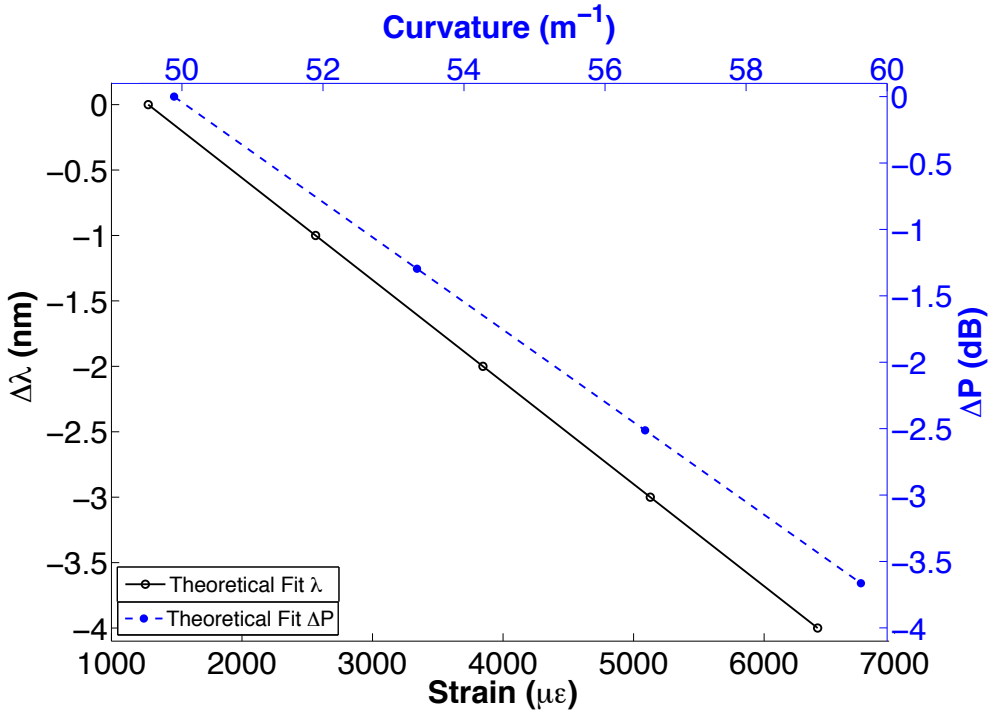

Figure 4.15: Theoretical curvature and strain analysis [62].

By analyzing the output spectrum response data, sensitivity around 1.64 pm/$\mu\varepsilon$ is estimated, it is important to emphasize that the fixed points keep the curvature constant when the strain is induced in the system, as a result, minimal power fluctuations were observed. The curvature is applied by reducing the distance between two fixed points of the bent fiber section; here the tapered fiber is not affected; the curvature is applied to a regular fiber optic section. The fiber bending control analysis shows a power intensity

decrement as the bending is increased and zero shifting of the interference intensity peaks; hence we can estimate a curvature sensitivity around −0.374 dB/m^{-1}.

Both results were estimated using a central wavelength at 1524 nm. However, another peak (1549 nm) shows very similar results. Using these peaks with phase modulation presented when the strain is applied, and intensity modulation when the fiber is bent, simultaneous detection is observed with no measurable crosstalk. The minimal curvature and strain deviations from a linear data fit of 0.259 and 0.128%, respectively, were obtained from our measurements. The interference spectrum analysis shows resolution around −10.9 $\mu\varepsilon$ and 0.026 m^{-1} for curvature and strain, respectively.

Chapter VI: Highly Stable Multi-wavelength Erbium-doped Fiber Linear Laser based on Modal Interference

Erbium-doped fiber lasers (EDFL) have been proposed during more than four decades for different purposes. In recent times, there is growing interest in the use of EDF for pulsed lasers, meanwhile, some research groups have been concentrated on fiber continuous wave lasers operating with fiber optic structures, pursuing a narrower line width and increasing the number of laser lines. Most of the recent works use all-fiber structures such as fiber Bragg gratings, special fibers as photonic crystal, twin-core and polarization maintaining fibers, Mach-Zehnder, Fabry-Perot, Sagnac devices and nonlinear components. One interesting structure is the Fabry-Perot filter (FPF) based on air intra-cavities due to their stable measurement, compactness and simple fabrication. Other important devices widely used in fiber laser arrangements are bi-tapered optical fibers, whose have been developed for controlling the output response.

As it is appreciable from literature, several techniques and components to fabricate a fiber structure filter have been presented to be used in a laser cavity, however, sometimes a complex setup is required to obtain good performance. At that point, we propose competitive laser parameters, specifically low power fluctuations and excellent wavelength stability, better than previously reported works (more information can be founded in the published paper [65]). Despite some works report good symmetrical spacing emissions for more than 4 lasing lines, the pulse width reported is bigger than obtained by our configuration (0.138 nm). In addition, our cavity simplicity does not require sophisticated fibers or components and special pumping sources to generate narrow multi-wavelength emissions. Unfortunately comparing with other multi-wavelength spectrums observed, the symmetry is lower, however, this can be useful to avoid crosstalk in sensing, spectroscopy, or telecommunications applications.

In this work, we link together and air-gap Fabry-Perot interferometer and bi-tapered conventional optical fiber to generate a multi-modal interaction into the fiber laser cavity. From the experimental setup phase modulation is obtained when strain is applied and intensity modulation is presented when a section of untapered fiber is bent, these parameters are studied both individually and combined. By using these parameters, it is

possible to modify the gain-losses profile, polarization, birefringence and modal phase into the laser cavity. The laser presents dual-wavelength emission that can be switched between two specific regions when curvature is applied, and when only strain is applied the lasing lines can be tuned and also the spacing mode can be changed. In addition, when both parameters are applied, a stable multi-wavelength emission is achieved.

6.1 Experimental Setup

6.1.1 Schematic Configuration

The resonant fiber optic linear cavity showed in figure 4.16 was implemented based on four main elements: a pump pigtailed laser diode (QFBGLD-980-500), 4.5 m of erbium-doped fiber as gain medium, the filter device which is composed of a tapered optical fiber and an all-fiber intrinsic FPF, and other inherent components such as a fiber coupler (90/10) and a wavelength division multiplexer (WDM).

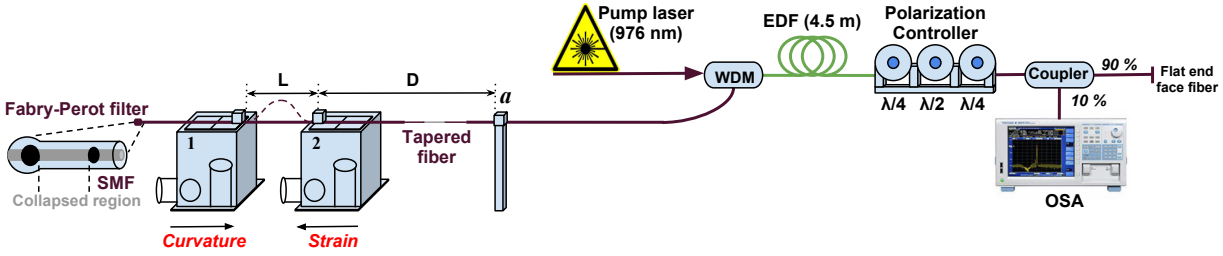

Figure 4.16: Experimental setup [65].

The pumped light is incorporated into the fiber laser cavity by a 980/1550nm WDM, the light goes to the gain medium and amplified spontaneous emission (ASE) into the resonant cavity is generated. This signal passes through a polarization controller (PC: three-paddle fiber polarization in quarter wave plate-half wave plate-quarter wave plate configuration) and by using an optical fiber coupler (90/10), the laser output is monitored by using the 10% port connected to the optical spectrum analyzer (OSA), the rest of the signal (90%) arrives at a fiber with a flat end face, acting as a mirror of the laser cavity, here a Fresnel reflection is obtained and the reflected signal is guided to the 1550 nm WDM port in which the all-fiber modal filter (FPF-Taper) is connected performing as a partial reflection mirror. Curvature and strain are applied by moving two translation stages

(1 and 2) and *a* is a fixed point where the end of the tapered fiber was carefully placed. When the translation stage 2 is moved in the backward direction strain is induced in the system by affecting the length *D* (15.6cm), however, the distance between the two translation stages (*L* = 3 cm) is reduced, as a result, un-tapered fiber is bent. Additionally, by moving the first translation stage in the forward direction the curvature is increased.

6.1.2 Modal Fiber Optic Filter

The modal filter is composed of a Fabry-Perot Interferometer and bi-tapered optical fiber, both of them generate several modes into the laser cavity. To obtain this modal structure a section of conventional single-mode fiber was tapered, then the FPF was fabricated at a small distance from the tapered region. The filter operation in reflection mode was previously reported, with the finality to be used for laser applications, indeed, the properties shown of thin film tips filters can be combined whit air cavities to improve the laser response.

To fabricate the FPF, conventional single mode fiber (SMF28) and special hollow core photonic crystal fiber (HC-1060) were used. These fibers were cleaved and spliced with Fitel S175 fusion splicer. Afterward, using the splicer manual mode, the splice joint was translated a distance of 50 *μ*m from the electrodes. At this point, three discharges were applied, as a result an air cavity was formed. The next step consists of placing this cavity a distance of 500 *μ*m from the electrodes and after several discharges, it was separated into two parts and forming one more cavity. As a consequence, the discharges over all the HC-1060 fiber, generated a collapsed core holey region structure forming a solid material. The FPF generated several reflections modes due to the several air-silica refractive index interfaces. Then, the interaction between the fundamental reflected fiber mode and the several reflected higher-order cladding modes produced by the cavities described above, provide an interference reflection spectrum. As it is seen before, the full manufacturing process and principle operation of the FPF are detailed in [40].

As it is well known bi-tapered optical fiber excites the interaction between the fundamental mode [29] I_c and high-order modes I_m (equation (4.7)) and the phase between these modes can be written as:

$$\Delta\phi_{cm} = \frac{2\pi\Delta nL}{\lambda}, \tag{4.6}$$

where Δn is the refractive index difference between these modes, L the tapered region length and λ the operation wavelength. These modes arrive at the FPF and other several modes are excited by nonsymmetrical Fabr-Perot cavities. It can be inferred that the phase could be denoted by $\Delta\phi_{cn}$ (fundamental mode I_c and high-order modes I_n). The reflected modes by the FPF reach the tapered region and the total modal interaction can be described by:

$$\mathrm{I} = \mathrm{I}_c + \mathrm{I}_m + \mathrm{I}_n + 2\left[\sqrt{\mathrm{I}_c\mathrm{I}_m}\cos(\Delta\phi_{cm}) + \sqrt{\mathrm{I}_c\mathrm{I}_n}\cos(\Delta\phi_{cn})\right], \tag{4.7}$$

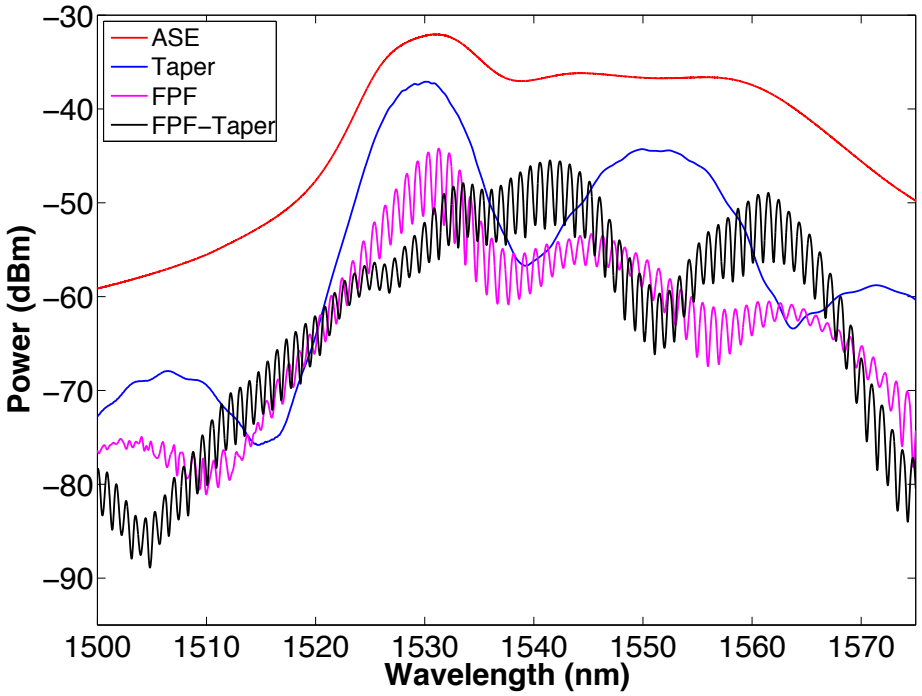

Figure 4.17: Taper-FPF structure reflection spectrum [65].

Then when a matching between $\Delta\phi_{cn}$ and $\Delta\phi_{cm}$ is obtained, it starts to appear regions of probable emission into the cavity (figure 4.18), on the other hand, if these values are not equivalent, only noise is achieved. The reflected modal interaction generates an interference pattern with a fringe contrast visibility and free spectral range (FSR) around 8

dB and 1nm respectively (see figure 4.17). As it was explained before, several and not controllable modes are generated, all the reflected modes generated by the interferometer structures is governed by the polarization and the effective refractive index of the modes involved, moreover, the reflection can be expressed by [63]:

$$\mathrm{R} = 1 - \left[\sin(\theta)\cos\left(\frac{\beta}{2}\right)\right]^2 , \tag{4.8}$$

$$\beta_i = \frac{2\pi l_i(\mathrm{n}_{cm} - \mathrm{n}_{cn})}{\lambda}, \tag{4.9}$$

here l_i is the length of the optical path, n_{cm} and n_{cn} are the effective refractive index of the modes generated by the modal structure section, θ denotes the polarization rotation angle and β_i represents the lasing modes that will interact in our resonant cavity. As is well know the multi-wavelength fiber lasers operation is strongly related to polarization-losses dependence. In our linear laser cavity, the multi-wavelength effect is governed by the PC and the combination of the tapered optical fiber and FPF. It is important to mention that most of the works in the literature use a PC to control any arbitrary state of polarization to adjust the numbers of lasing lines, generating stability in the laser cavity. Moreover, in our particular case, the modes generated by the FPF are arbitrarily polarized due to birefringence changes caused by strain and curvature application.

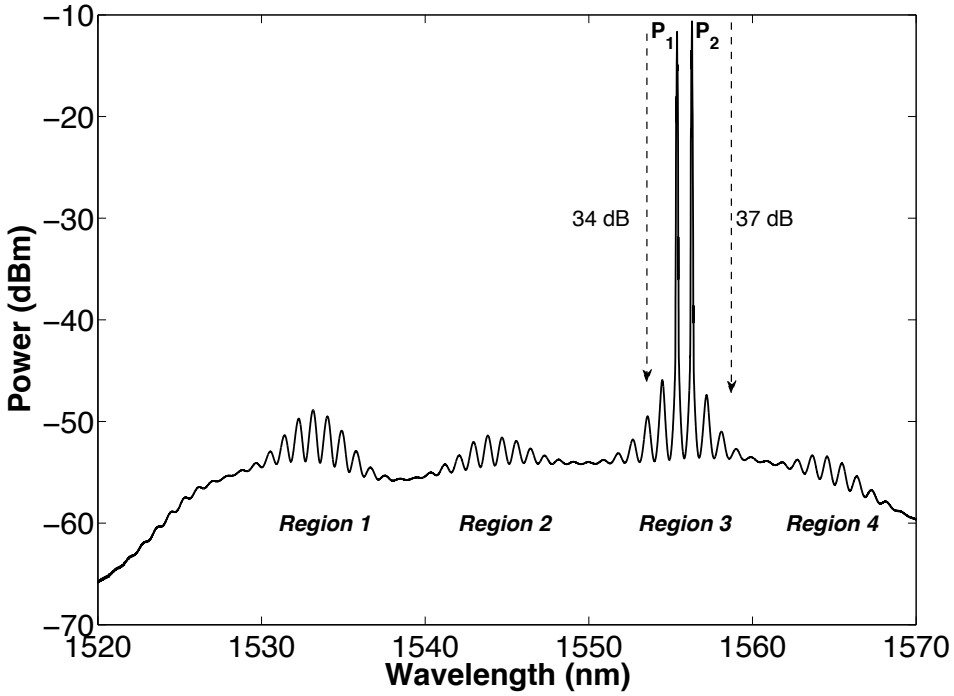

Figure 4.18: Laser lines generation obtained from the linear fiber laser experimental setup [65].

6.2 Results and Discussion

With the pump laser being operated at 500 mA of maximal current two laser lines are achieved at 1555 nm and 1556 nm (figure 4.18), with SMSR of 37 dB and 34 dB for P_1 and P_2 respectively, and 0.14 nm of spectral width. As it can be observed there are four regions with a probability of emission, these regions are the result of the lasing modes generated by the modal interferometer; the regions with the lower probability of emission are related to the higher phase mismatch of the cavity modes. When we applied curvature and strain, physical change in the system occurs due to these perturbations, stimulating birefringence in the system, varying the polarization state of the light and modifying the output spectra. The laser lines appear in the third region, this was expected because it is the area with better energy flatness in the ASE spectrum, hence the modes competition is minor. The laser lines stability is shown in figure 4.19, presenting 1 dB of maximal power variations and no changes in wavelength during 1 h at intervals of 3 min. In addition, the spacing mode between the laser emissions is around 1 nm; this is related to the FSR of the modal interference (see figure 4.17).

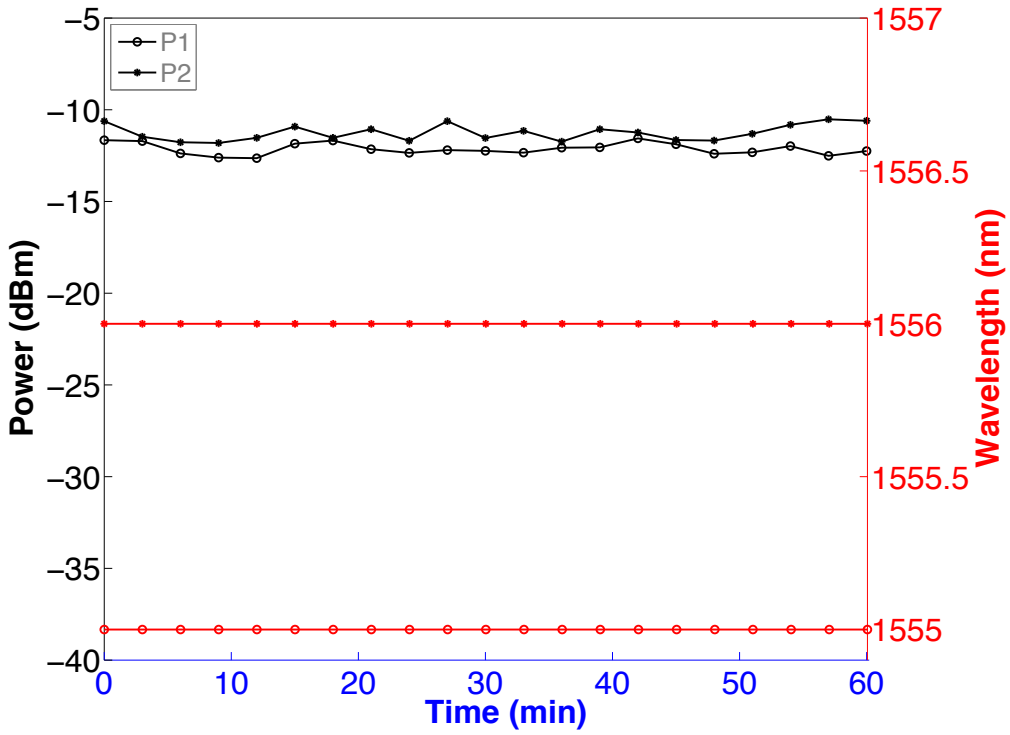

Figure 4.18: Laser lines generation obtained from the linear fiber laser experimental setup [65].

The polarization changes induced by bending the fiber show dual-wavelength emission in regions 3 and 4, here the spacing mode remains almost constant (1 nm), in addition for a specific case (42 m^{-1}), the spacing mode of the dual emission is around 20 nm. The strain applied over tapered optical fiber allows a tuning range from region 3 to 2 and moreover four-wavelength emission can be observed, unfortunately, a high value of strain need to be avoided to keep the integrity of the FPI-Taper structure. The combination of both effects (curvature-strain) provides 5 lasing lines in regions 1, 2 and 3, or triple lasing emission at region 1, here the spacing mode is according to the region. As can be observed the curvature-strain control can be used to modify the number of lasing lines required, moreover, the laser is operated by not complex or high-cost arrangements and the filter structure has a good operating range for curvature and strain. This complete behavior will be detailed in this section.

6.2.1 Curvature

To apply the fiber curvature into the system, the first translation stage is moved in the forward direction. Fiber bending induces polarization changes and wavelength-dependent losses, transforming the gain in the laser cavity and changing the dynamic range in the interference spectrum, as a consequence fringe peaks are suppressed due to the alteration in the loss increment for the higher-order cladding modes and new laser emissions are obtained due to polarization effects and matching phase of lasing modes. According to figure 4.19, this behavior is confirmed, initially, when curvature is increased the laser spectrum does not present changes because the losses are really small. However, the last region of possible emission (after 1560 nm) starts to lose power due to this area is the zone with less energy in the ASE spectrum provided for the EDF. Then, since 42 m^{-1} the laser lines start to be switched to the first region (zone with the higher power of ASE spectrum) and P_1 quickly changes its position to 1533 nm (SMSR of 22 dB). On the other hand, P_2 seems immobile, but for 46 m^{-1} changes to 1532 nm (SMSR of 26 dB), after that, the lines just start to decrease until they totally decay at 53 m^{-1}.

We decided to analyze the stability of the system (figure 6) for 42 m^{-1}; taking in count these are the laser lines with better SMSR. The variations still being of 1 dB of maximal power and there are not changes in wavelength.

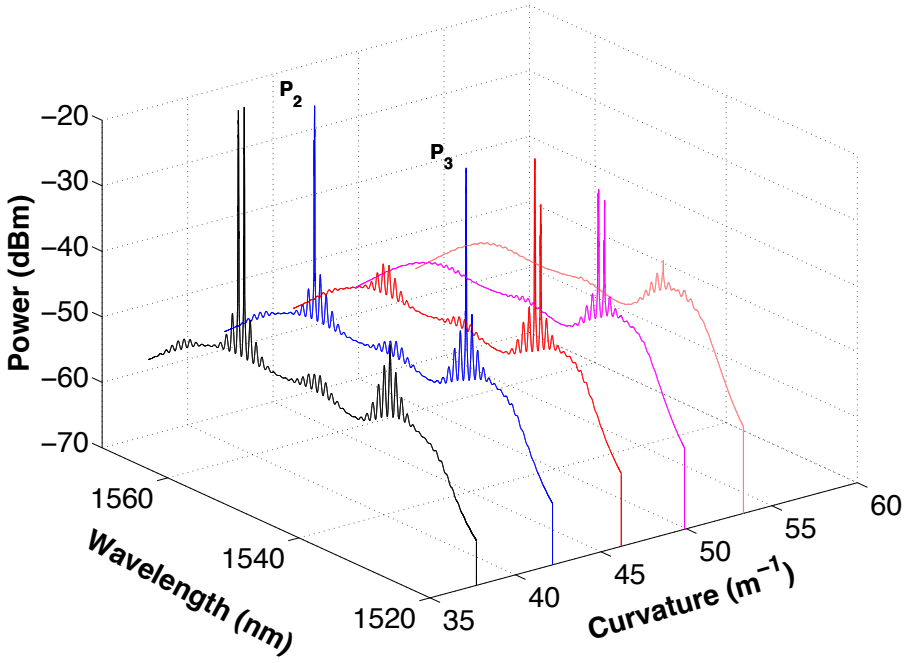

Figure 4.19: Laser spectrum analysis when curvature is applied [65].

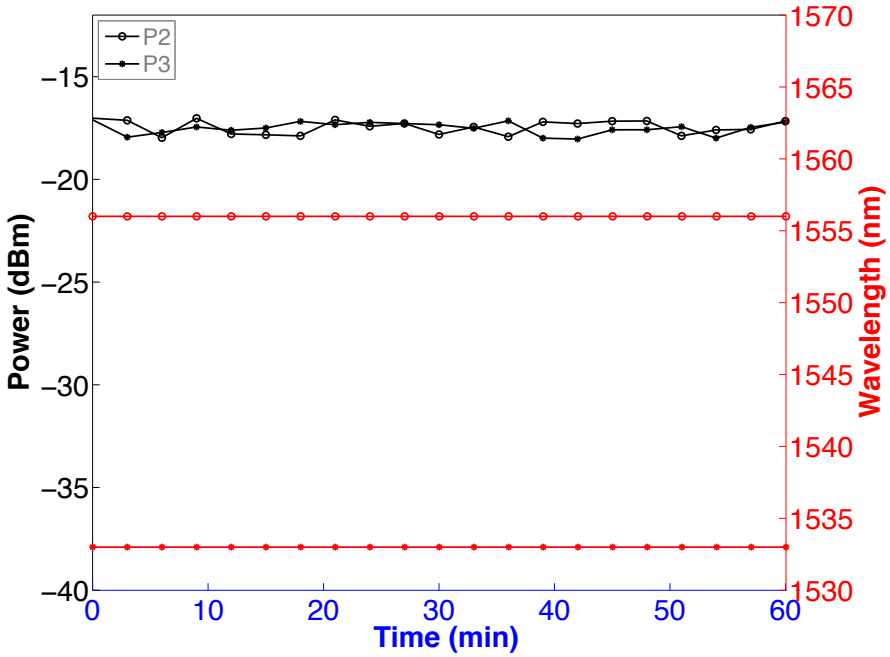

Figure 4.20: Stability analysis of the laser lines obtained with 42 m^{-1} of curvature [65].

6.2.2 Strain

The second translation stage allows controlling the axial strain and the spectrum is measured when this parameter is increased. As it can be observed in figure 4.21, at the beginning a phase modulation is presented at 1282 $\mu\varepsilon$, occurring a shifting of 9 nm in the laser lines and changing the SMSR of original laser lines to 38 dB and 23 dB. This shifting effect is related to the change in the effective refractive indexes of the modes that dominate the interference spectrum. Some wavelengths are under high attenuation and others not, then a sinusoidal profile is achieved to try to equalize the losses produced in the laser cavity due to a homogeneous broadening in the EDF. Consequently, the mode competition becomes stronger and this generates intensification in the lasing power difference between laser lines. As already stated, when strain is applied, a minimal curvature is presented, therefore the laser lines start to switch at 2564 $\mu\varepsilon$ and even at 3846 $\mu\varepsilon$ appear two new ones (SMSR of 36 dB, 24 dB, 28 dB and 20 dB for P_2, P_4, P_5 and P_6 respectively), obtaining a maximum lasing power difference between P_2 and P_6 of 16 dB. It is important to stress that the new modes are produced by the phase alteration between the lasing modes, here the strain and small curvature are applied at the same time.

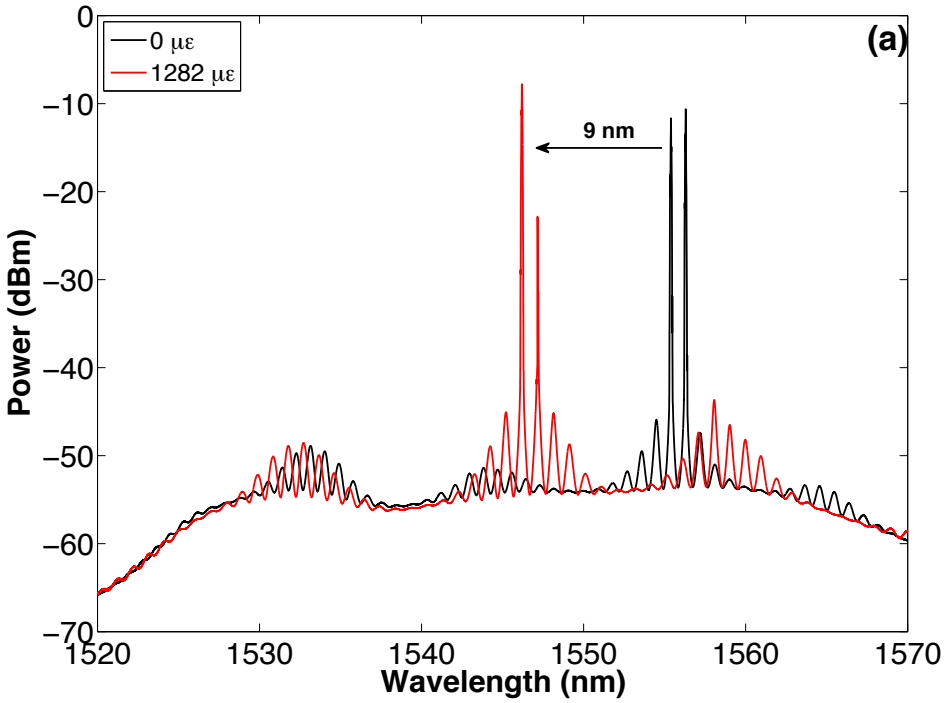

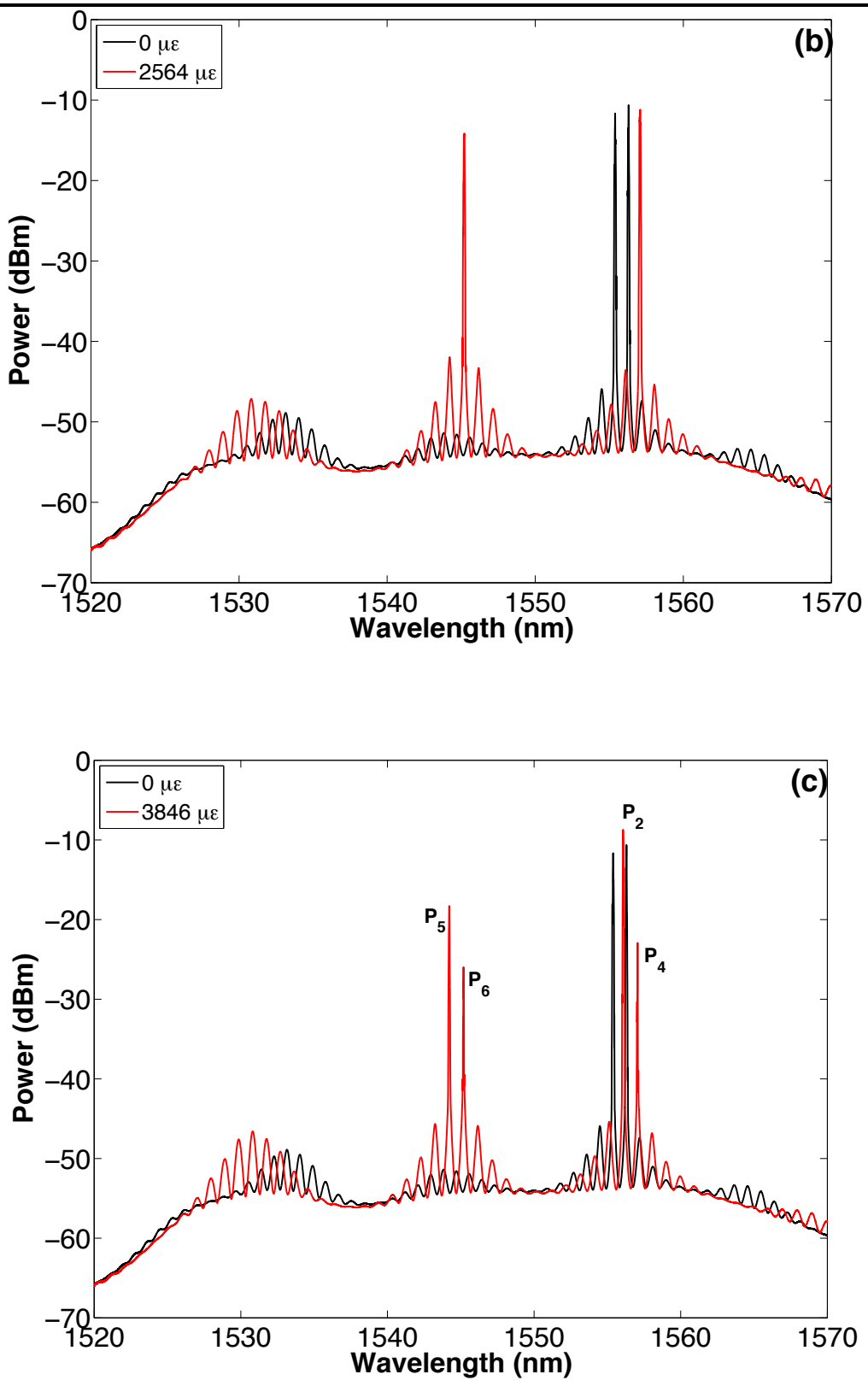

Figure 4.21: Laser spectrum analysis when strain is applied. (a) 1282 *με*. (b) 2564 *με*. (c) 3846 *με* [65].

We consider for this setup the maximal strain around 4000 $\mu\varepsilon$, at this point the tension can break the tapered fiber. Then the stability was measured (figure 4.22) for 3846 $\mu\varepsilon$ to observe the behavior of the system operating with four laser lines. The variations were about 1.2 dB of maximal power and again there are not changes in wavelength.

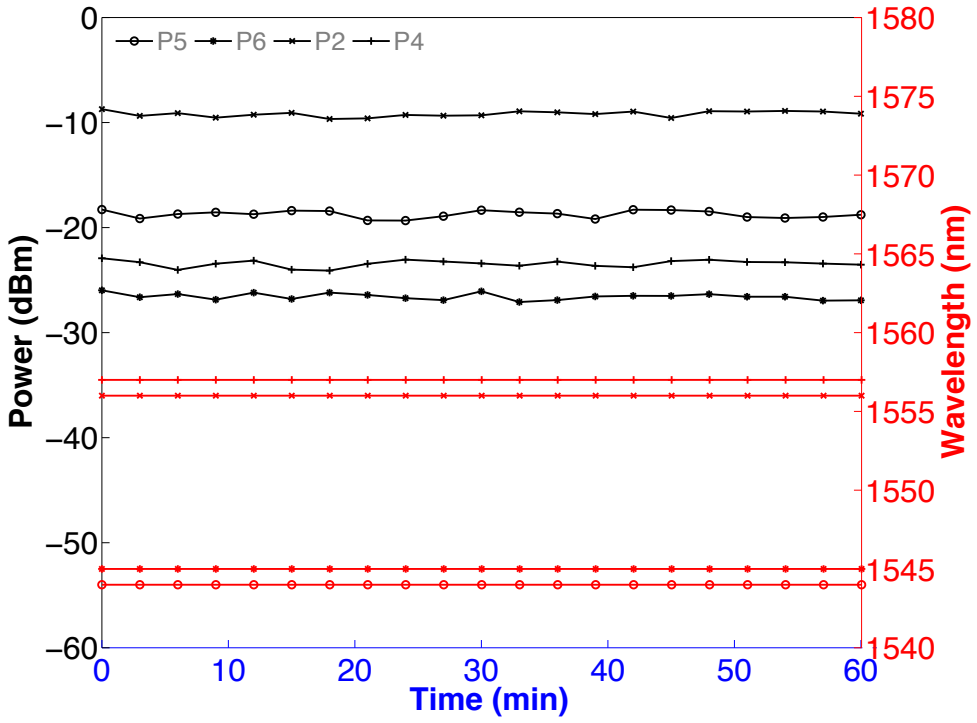

Figure 4.22: Stability analysis of the laser lines obtained with 3846 $\mu\varepsilon$ of strain [65].

6.2.3 Simultaneous Analysis

After observing the behavior of the system under curvature and strain changes by separated, the next step was to apply simultaneously these physical parameters. The objective was to obtain a major number of laser lines at different frequencies to increase the applications of the work.

Figure 4.23 shows the acquired spectrum of the fiber laser; first of all, the strain is increased with a fixed curvature and vice versa. As it is noted, when the strain is increased P_3 stays immobile, but P_2 is switched and appears with another line, achieving a triple laser emission around 1532nm (blue plot (a)), then at maximal strain these three lines are separated at 1527, 1535 and 1550nm (magenta plot (a)). On the other hand, when

curvature is changed, the line with larger wavelength (P_4 at 1557nm) is switched and shows up next to a second line at 1530 and 1531nm. The other lines remain in the same position achieving a quintuple laser emission (blue plot (b)). Unfortunately, after 52 m^{-1} this performance starts to disappear, obtaining only three lines (red plot (b)) due to the high losses in the system induced by maximal curvature.

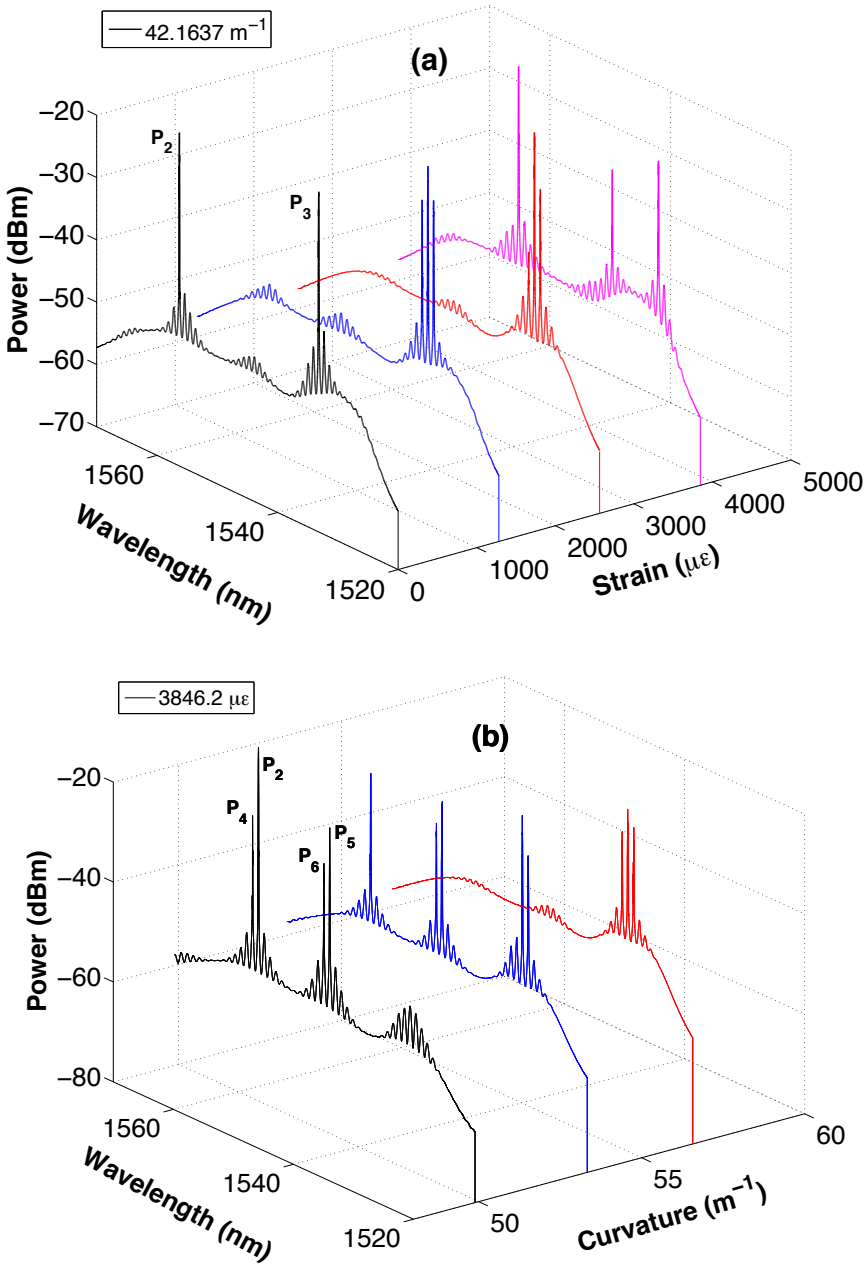

Figure 4.23: Laser spectrum simultaneous analysis when (a) strain is applied at 42 m−1, (b) curvature is applied at 3846 *με* [65].

Furthermore, we decided to connect a nonlinear fiber (NLF) between the tapered fiber and the 1550 nm port of the WDM, to stimulate four-wave mixing (FWM) effect between the lasing modes, growing the number of laser lines. Figure 4.24 displays until nine laser lines, unluckily the system is not really stable for the reason that the wavelength lasing oscillations are competing rigorously for the homogeneity of the whole gain medium spectrum (EDF). Probably an appropriated manner to improve the system behavior would be connecting another polarization controller before the NLF.

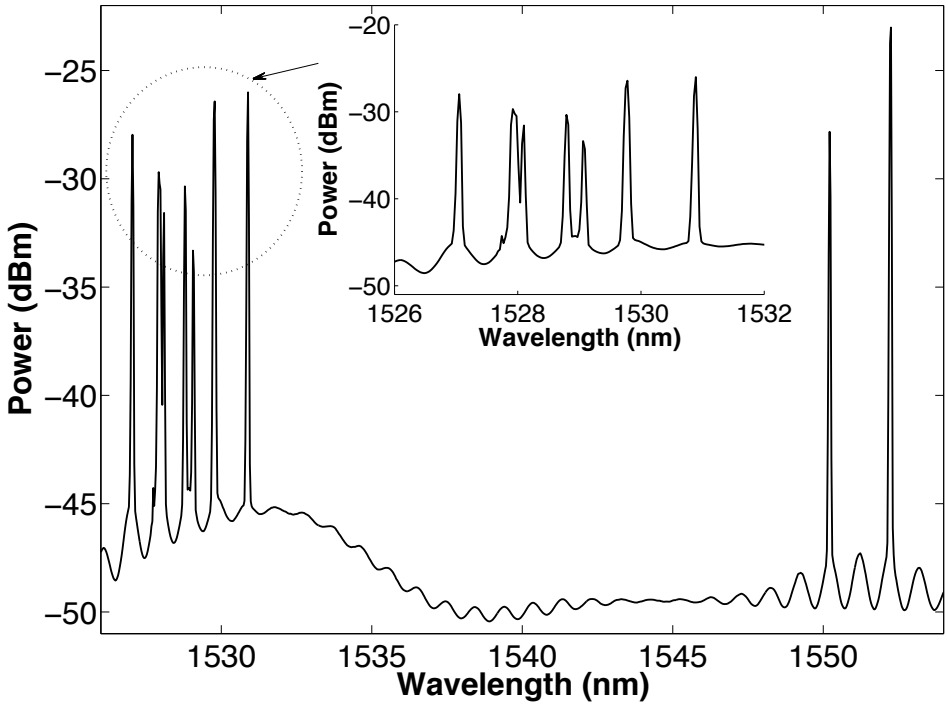

Figure 4.24: Laser spectrum when NLF is connected [65].

Subsequently, this laser configuration offered in this work can be adapted for many applications like ultra-short pulses by adding a saturable absorber, for nonlinear spectroscopy investigation and communications.

Chapter VII: Single-mode Bragg Reflectors in Tapered Few-Mode and Multimode Fibers

Telecommunications and laser technologies have been recently related with few-mode, Large Modal Area (LMA) and multimode fibers (MMF). More specifically, photonic lanterns, pump combiners and MMF have been newly proposed for high power lasers and communications, additionally, fiber Bragg gratings allow to obtain better efficiency and stabilize the emission spectrum of these laser devices. Furthermore, some research groups have been concentrated on fiber continuous wave lasers operating with fiber optic structures like Bragg gratings, pursuing a narrower line width and increasing the number of laser lines. Moreover, a Bragg high-reflectivity response in MMF can be used for spectral control of a laser having a relatively large beam diameter and difficult to couple with single-mode fibers (SMF), also Bragg gratings in few-mode and MMF are used for sensing using high-order modes.

As is seen before, another device frequently used in lasers, sensing and other systems communications is tapered optical fiber. A few years ago, a solution presented to diminish the signal degradation in MMF due to modal dispersion, was the restriction of the signal transmission in the fundamental mode of MMF, performing mode conversion between the fundamental mode in SMF and fundamental mode in MMF. Alternative progress in this area was an efficient multi-to-single mode converter as a convenient solution to couple the light from a diode laser to SMF. Additionally, it was necessary to maximize the optical power collected in a waveguide from the diffracting field of a semiconductor laser. The conformal mapping technique permitted the reshaping of the captured field into the fundamental mode of the output waveguide.

After an extensive review of the literature, it is clear the growing interest in the necessity of managing individual modes to improve their performances and eliminate high order modes to achieve single-mode operation in power fiber lasers. Moreover, gratings in multimode or LMA fibers present several reflection bands related to the coupling between different propagating modes, diminishing the correct functioning of laser devices. In this work, we demonstrate a single band reflector based on tapered 4-modes and multimode fibers with potential applications in fiber lasers and sensing applications (more information can be

founded in the published proceeding [66].

The experimental setup used for fibers characterization and the filter structure are shown in figure 4.25 and it was implemented in Valencia, Spain. The pumped polarized light of the diode is incorporated into the port 1 of the circulator; our filter device is connected at port 2 where the transmission is monitored, and the reflection spectrum is analyzed in port 3 of the circulator, both with an optical spectrum analyzer.

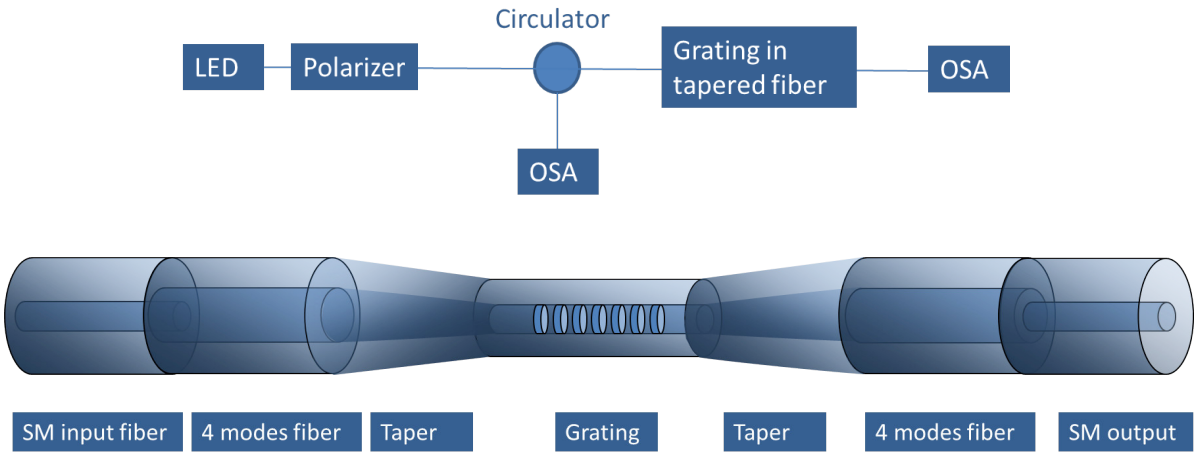

Figure 4.25: Top: Testing setup. Bottom: Diagram of the Bragg grating in the tapered fiber.

The filter is composed of a Bragg grating in a tapered optical fiber, linking these structures together we obtained only the fundamental mode and eliminated the high-order modes in the fiber core (we start our work with a 4-modes fiber provided by OFS).

The 4-modes OFS fiber has a step-index profile and an estimated normalized frequency (*V*) value of 5 at 1550nm (figure 4.26 shows the four modes for *V*=5). The first step was to plot the changes in refractive index with variations of wavelength for each mode (using dispersion equations for LP modes [67], to calculate the approximated value of the effective refractive index (n_{eff}) for these four modes, LP01, LP11, LP21 and LP02 (equation 4.10). We obtain this refractive index value (figure 4.27) making a zoom of figure 4.26 (right).

$$\frac{J_m(u)}{uJ_{m-1}(u)} = -\frac{K_m(w)}{wK_{m-1}(w)}, \qquad (4.10)$$

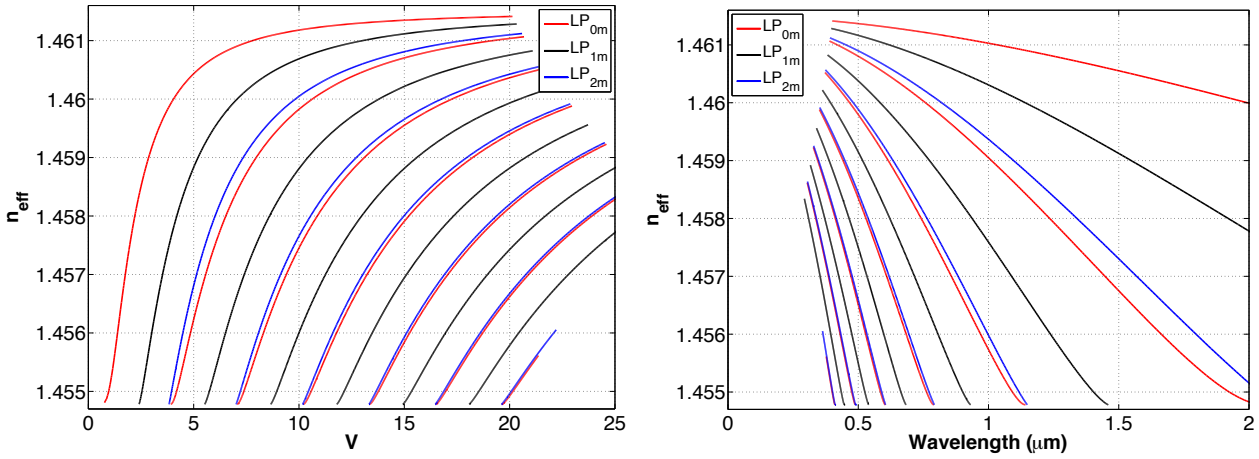

Figure 4.26: Simulation of Dispersion equation of LP modes for OFS fiber. Right: Conversion to plot Effective index vs wavelength.

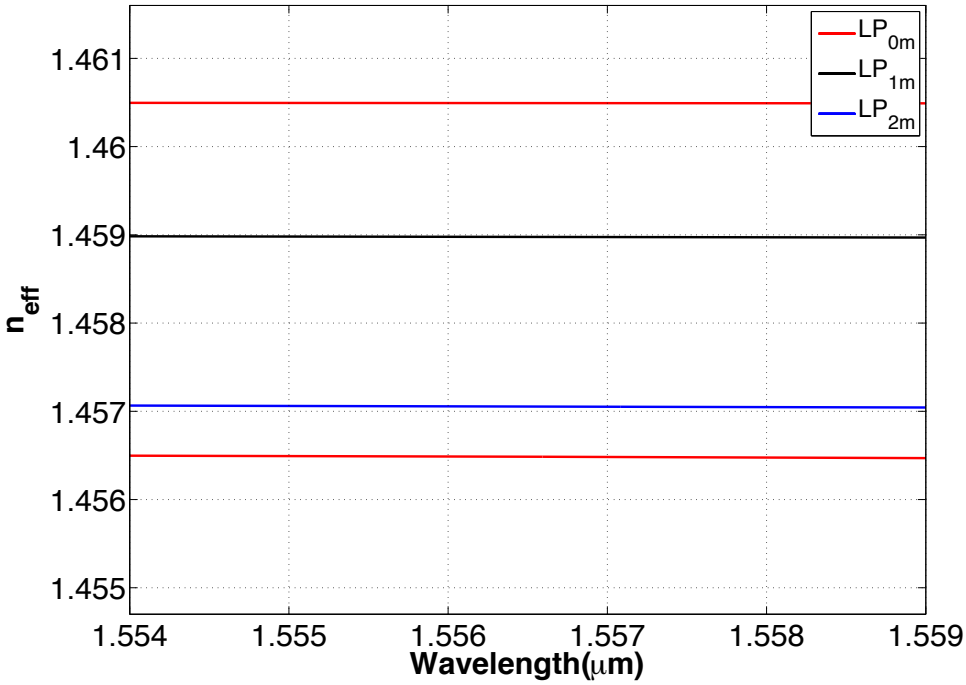

Figure 4.27: Zoom to obtain the effective refractive index values of LP modes.

Then, we recorded a Bragg grating in this fiber using a phase mask with a period (Λ) of 1076.25nm and 2.5cm of length. Since the fiber holds four modes, the grating in the fiber has to produce ten different resonances, matching with the coupling between these modes. Figure 4.28 shows the expected resonant wavelengths calculated from the effective indices of the modes coupling (equation 4.11), it can be seen two overlapping, the coupling of the

LP02 mode is degenerated with the crossed coupling between the LP02 and the LP21 modes; the same happens between the LP11 coupling and the crossed coupling LP01-LP21. It is important to mention that the observation of the corresponding resonances is dependent on the illumination of the fiber as well as on the axial symmetry of the gratings. Asymmetric excitation and blazed gratings are required to observe the full set of resonances. The grating was written with a small tilt angle between the fiber and the diffractive phase-mask, and ultraviolet (UV) light was launched into the fiber by a SMF with a slight offset between fiber cores. If standard (not blazed) gratings (figure 4.28) are written and the fiber is symmetrically illuminated (standard splice to the SMF), even modes have weaker resonances, but not null due to the residual asymmetries in the gratings; subsequently some resonances are really difficult to be observed in reflection because the splice between the SM feeding fiber and the few-mode fiber acts as a modal filter for asymmetric modes.

$$\lambda = \Lambda\left(n_{eff1} + n_{eff2}\right), \tag{4.11}$$

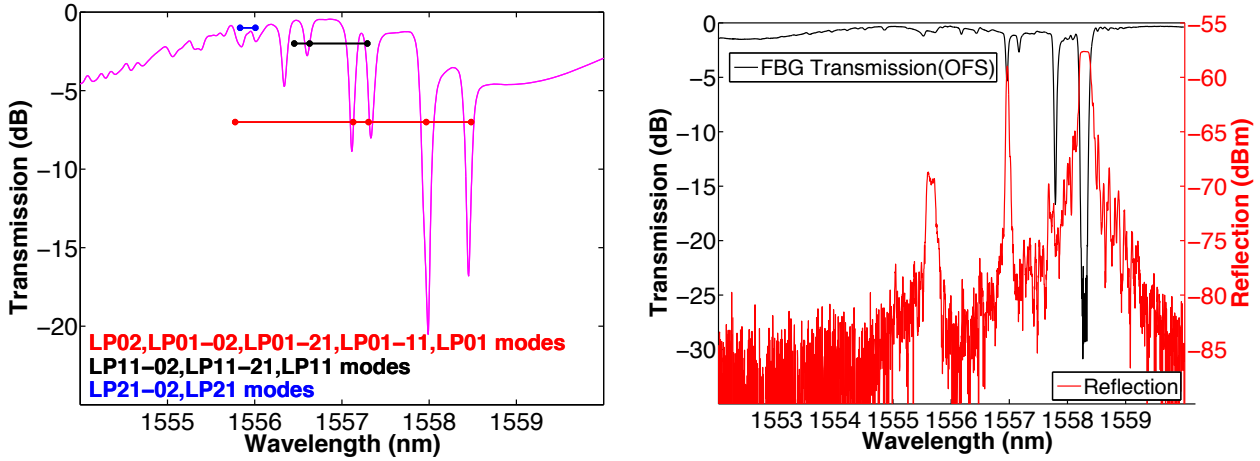

Figure 4.28: Left: OFS Few-mode fiber grating spectrum (tilted grating measured with asymmetric illumination, the dots show the calculated resonant wavelengths of LP modes coupling). Right: Standard grating with symmetric illumination.

Next, the fiber was tapered to reduce the fiber diameter and achieve single mode operation, after that, standard Bragg grating was written in the taper waist (figure 4.25). The tapered fiber waist has 50 microns of diameter, resulting in a *V* value of about 2, and

40 mm of length. Each transition has 37 mm and the tapers were made long enough to prevent sharp cut-off of high order modes and consequently diminish the attenuation. In addition, the attenuation measured during the grating fabrication was less than 1dB in the L+C bands.

The measured spectra with symmetric illumination are displayed in figure 4.29. The transmission demonstrates single mode operation at the fiber core due to we can only perceive one resonance. Unfortunately there are small transmission deeps at shorter wavelengths, some of which can be more clearly observed in the reflection spectrum; these parasitic resonances can be removed by covering the fiber with a fluid (oil) of matched refractive index, therefore they correspond to core-cladding resonances in reflection; these cladding modes are evidence of a small transfer of energy between the core modes of the pristine fiber and the cladding modes of the tapered fiber, this transfer takes place within the transitions between the two sections of uniform fiber, and as is seen, the removal of the cladding modes does not affect significantly the transmitted power level.

Afterward, we repeat the process now in a MMF (graded index) provided by Spectran Corporation, to validate the good performance of our technique in a fiber with multiples modes. It is essential to state that the difference between graded and step index does not affect our method, besides, the fiber profiles determining the fiber diameter changes of few-mode and MMF after being tapered have the same shape (measured profiles of the fibers can be seen in figure 4.30, unfortunately, the device only allows to measure until 26 μm).

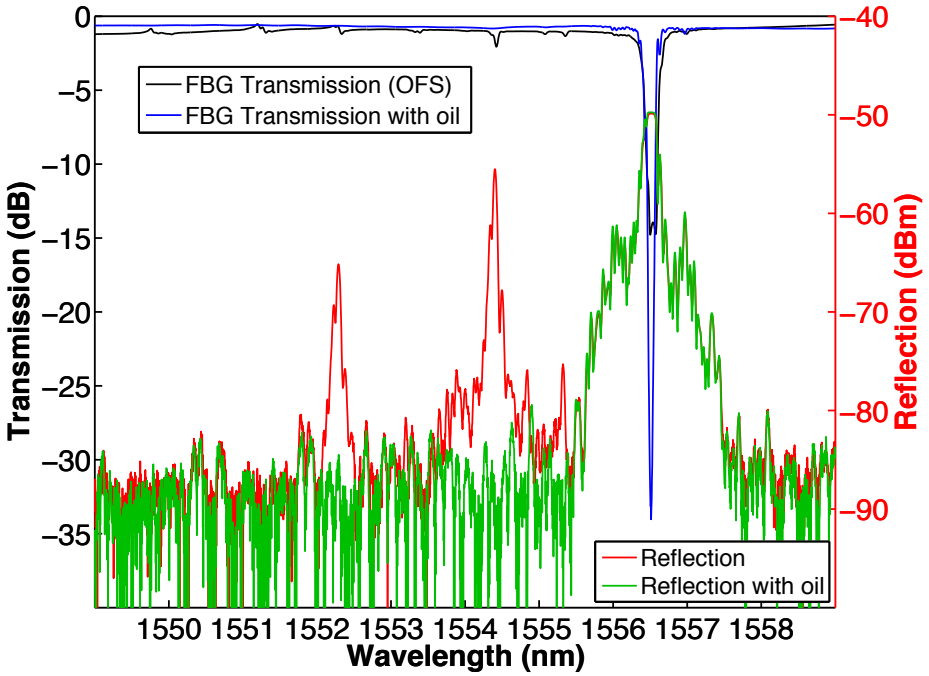

Figure 4.29: Spectra of the Bragg grating in the tapered 4-modes OFS fiber. Transmission and reflection have been measured with the fiber surrounded by air and an index matching fluid (oil with n=1.456).

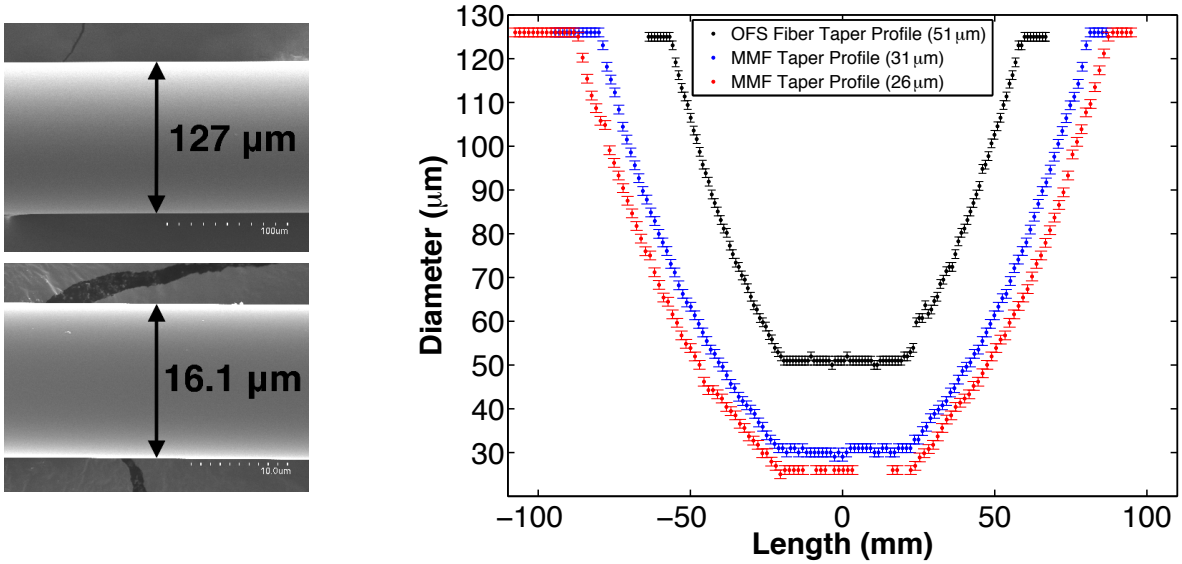

Figure 4.30: Left: Initial (top) and final fiber diameter (bottom) for MMF, scales of 100 μm and 10 μm were respectively used. Right: Profiles of the fibers used in our experiment. Black and red dots correspond to tapered OFS fibers with 51 and 31 μm respectively. Blue dots represent the MMF with 26 μm of waist diameter.

In this case, the tapered fiber with better results has a waist of 20 microns of diameter, and 40 mm of length. Moreover, like the OFS fiber, the attenuation measured during the tapering and grating fabrication was less than 1dB in the L+C bands (figure 4.31). Figure 4.32 displays the transmission spectrum with oil for three different taper MMF diameters and figure 4.33 shows the measured spectra (transmission and reflection with and without oil) for 20 μm with symmetric illumination, as is seen, single mode operation is demonstrated and cladding modes are similarly eliminated with the mentioned oil without affecting the transmitted power level. It is important to mention that the same tests were realized for the othrs tapers with different diameter, obtaining single mode operation as well.

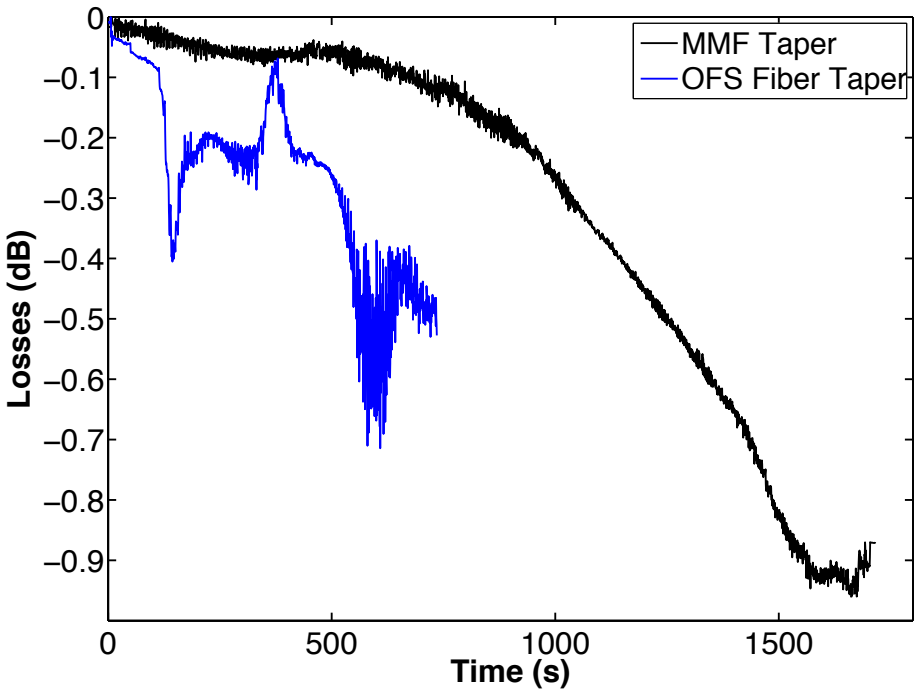

Figure 4.31: Losses of MMF and OFS 4-modes fiber Taper during fabrication.

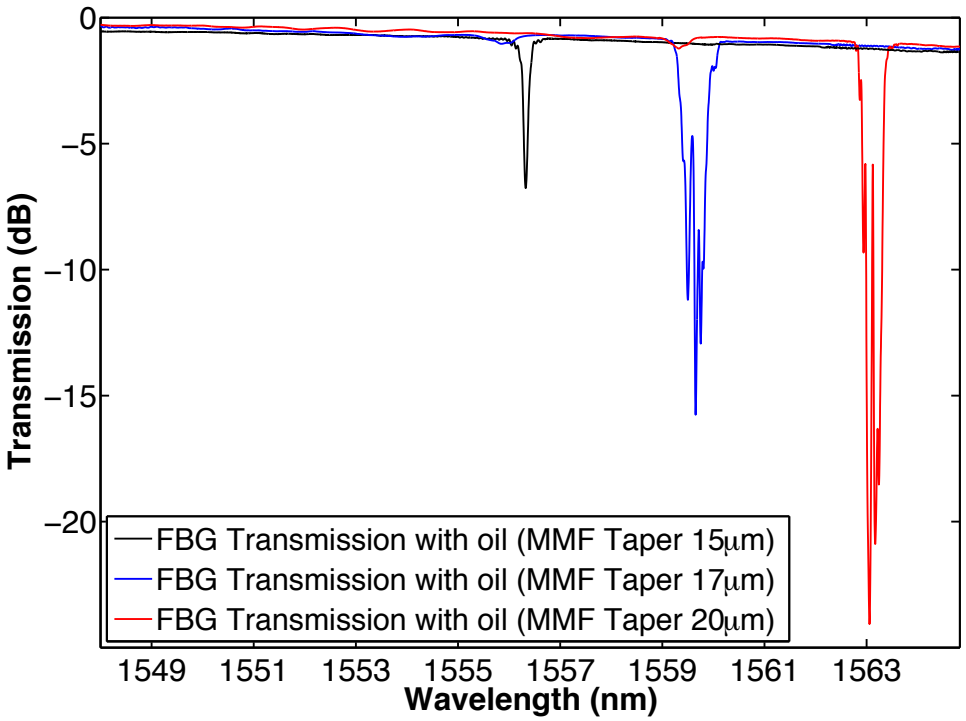

Figure 4.32: Transmission spectra of the Bragg gratings in the tapered MMF with three different diameters. Fibers surrounded for an index matching fluid (oil with n=1.456).

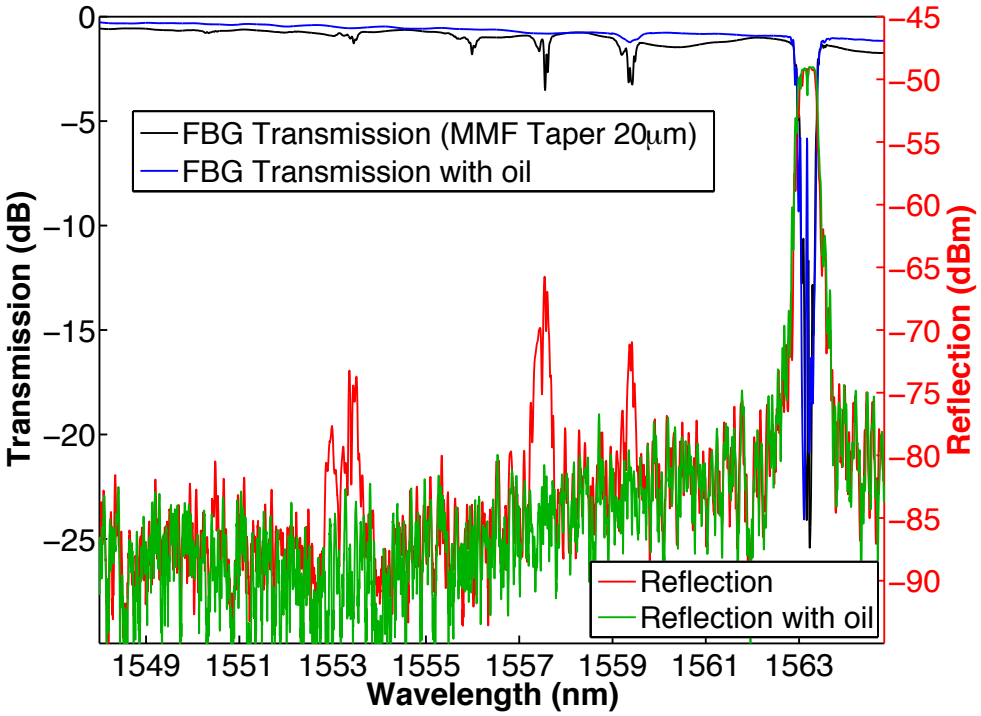

Figure 4.33: Spectra of the Bragg grating in the tapered MMF fiber. Transmission and reflection have been measured with the fiber surrounded by air and an index matching fluid (oil with n=1.456).

Furthermore, we measure the transmission losses of the device by introducing an offset between SMF (from the SLD) and MMF. Fig 4.34 shows this losses behavior of more than 40 dB, because of this a symmetric illumination is crucial to accomplish good results. As is observed a parabolic fit can be adjusted the losses data.

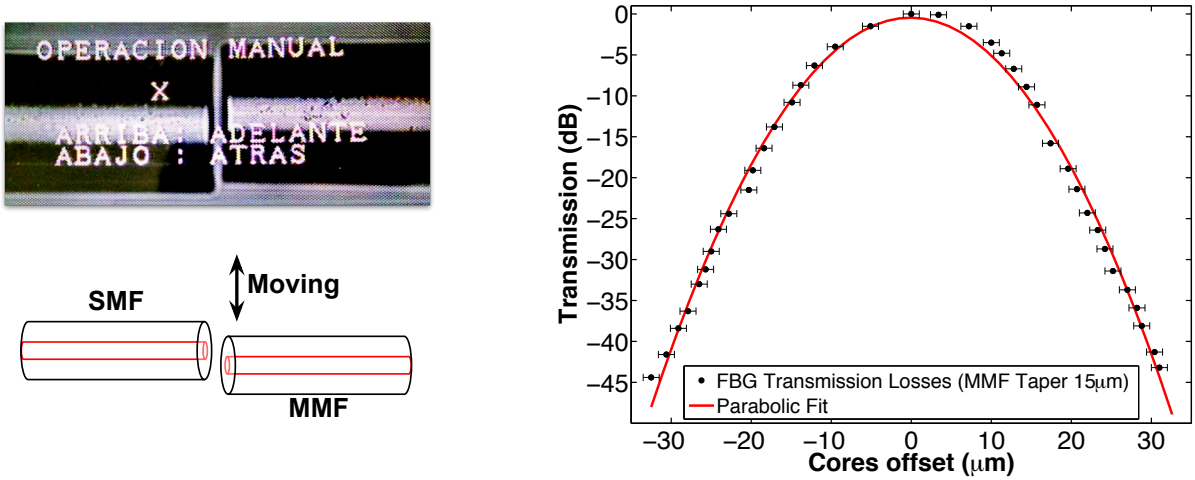

Figure 4.34: Transmission losses when offset between SMF (from the SLD) and MMF is induced in the system (left: real picture of the splicer and diagram of the core offset introduced).

This previous chapters described the experimental setups for the applications with the tapered optical fibers of this work and their optimum results. Sensing and laser applications were implemented and after the results analysis, it is perceptible that the collected data is very competitive compared with the obtained other research groups. We propose the use of sensor systems consisting of a tapered optical fiber and curved fiber sections for simultaneous detection of bending and strain, and magnetic field as well with good sensitivity and resolution. Moreover tapered optical fiber was used in a multi-wavelength laser and Single-Mode Bragg reflectors for Multimode-Singlemode applications.

Chapter VIII: Conclusions and Future Work

Compared with the conventional fiber structures, tapered optical fibers can provide numerous valuable features in laser technologies and other applications. Additionally, tapered fiber sensors are able to measure several physical and chemical parameters.

This investigation about the modal interaction in tapered optical fibers allowed finding the optimum geometry, improving laser technologies and sensing applications from our laboratory and introducing this new field of investigation in our campus. After this research it is expected that the systems presented for our group have better stability and offer more quality of the output signal and other parameters, approaching the advantages that tapers provide.

The implemented experimental setups permitted to obtain excellent results for sensing applications of different parameters (curvature, strain, and magnetic field), a highly stable multi-wavelength laser and a study of Bragg gratings in tapered optical fibers, used to characterize multimode fibers operating in single mode regime.

We proposed the use of a fiber sensor system consisting of a tapered optical fiber and curved fiber sections for simultaneous detection of bending and strain. Using special fixed points the fiber optic system is operated to generate a signal that can measure curvature and strain changes without crosstalk interference, to eliminate ambiguity to the measurement. When strain was applied in the system by stretching the length of a bi-tapered fiber section; this generated a blue shift in the interference pattern reflection due to modal interference in the bi-tapered fiber section. The system offers low cost and simple implementation and it can be used for structural health monitoring but needs to be improved in the case of some particular composite materials that suffer simultaneously strain and bending.

Besides, we constructed a bi-tapered fiber optic sensor to sense magnetic fields using inexpensive transducer material. Our sensor is immune to signal polarization changes and requires only a short fiber length to achieve high sensitivity. To demonstrate the sensor design, we characterized two bi-tapered optical fibers with different insertion losses and mismatched phase. Each tapered fiber was analyzed, here they were set and fixed over a

thin magnetic tape using translation stages, then by using a permanent magnet set over a vertical translation stage, magnetic field is applied. As the magnet is placed close to the sensor platform, the magnetic field increases and the magnetic tape is attracted near to the magnet, as a result, the bi-tapered optical fiber is bent. The bending of the tapered fiber affects the reflection interference spectrum and a wavelength shifting to longer wavelengths is observed.

Furthermore, a stable and reproducible multiwavelength erbium-doped fiber linear laser was proposed. An all-fiber Fabry-Perot interferometer and a tapered optical fiber were inserted into the laser cavity, this combined structure allowed to obtain an interference pattern capable of generating a dual emission with power fluctuations of 1 dB and no wavelength variations. The system output can be controlled by applying curvature and strain, and the laser lines are switchable or tunable depending on which physical parameter is being applied. Monitoring the laser response under these parameters by separated; we obtain a quadruple laser emission with good stability (1.2 dB of power fluctuations and no frequency changes). Additionally, when curvature and strain are simultaneously applied we achieved a multiple laser emission with five laser lines. Finally, our setup bids a low-cost implementation, compactness, really good laser parameters, needs minimal components for its implementation and it can find many uses in communications and other applications where multiple laser lines are required.

Moreover, the coupling of energy to cladding modes in the tapered section of the fibers has been observed and prevented. This kind of devices can be used in several potential applications such as sensors using cladding modes, and lasers taking advantage of the bigger modal area of these fibers.

For future work, it is pretended to scale this study to the improvement of the theoretical part, to complement these and future experiments. Furthermore, it is projected the implementation of the Singlemode Bragg Reflectors in a laser using multimode fibers, to improve the light coupling and then increase the power of these devices.

References

1. J. M. Senior, *Optical Fiber Communications Principles and Practice* (Pearson Education Limited, 2009).

2. A. W. Naji, B. A. Hamida, X. S. Cheng, M. A. Mahdi, S. Harun, S. Khan, W. F. AL-Khateeb, A. A. Zaidan, B. B. Zaidan, and H. Ahmad, "Review of Erbium-doped fiber amplifier," Int. J. Phys. Sci. **6**, (2011).

3. M. Movassaghi, *Characterization of Erbium Doped Fibers* (1996).

4. S. Lacroix, F. Gonthier, R. J. Black, and J. Bures, "Tapered-fiber interferometric wavelength response: the achromatic fringe.," Opt. Lett. **13**, 395 (1988).

5. J. A. Alvarez-Chavez, A. B. Grudinin, J. Nilsson, P. W. Turner, and W. A. Clarkson, "Mode selection in high power cladding pumped fibre lasers with tapered section," Proc. CLEO 247 (1999).

6. B. S. Kawasaki, K. Hill, and R. G. Lamont, "Biconical-taper single-mode fiber coupler," Opt. Lett. **6**, 327–328 (1981).

7. T. A. Birks, D. Bahloul, T. P. M. Man, W. J. Wadsworth, and P. S. Russell, "Supercontinuum generation in tapered fibres," Summ. Pap. Present. Lasers Electro-Optics. CLEO ’02. Tech. Dig. **25**, 486–487 (2002).

8. Z. M. Hale and F. P. Payne, "The single mode tapered optical fibre immunosensor. I. Characterisation with model analytes," **2131**, 484–494 (n.d.).

9. C. Veilleux, R. J. Black, J. Lapierre, and L. W. Reeves, "Nematic liquid crystal clad tapered optical fiber with temperature sensing properties," J. Appl. Phys. **67**, 6648–6653 (1990).

10. R. G. Lamont, D. C. Johnson, and K. O. Hill, "Power transfer in fused biconical-taper single-mode fiber couplers: dependence on external refractive index," Appl. Opt. **24**, 327–332 (1985).

11. D. Jauregui-Vazquez, J. W. Haus, A. B. H. Negari, J. M. Sierra-Hernandez, and K.

Hansen, "Bitapered fiber sensor: Signal analysis," Sensors Actuators, B Chem. **218**, 105–110 (2015).

12. D. Monzon-Hernandez, A. Martinez-Rios, I. Torres-Gomez, and G. Salceda-Delgado, "Compact optical fiber curvature sensor based on concatenating two tapers," Opt. Lett. **36**, 4380 (2011).

13. M. Deng, D. Liu, and D. Li, "Magnetic field sensor based on asymmetric optical fiber taper and magnetic fluid," Sensors Actuators, A Phys. **211**, 55–59 (2014).

14. P. Lu, L. Men, K. Sooley, and Q. Chen, "Tapered fiber Mach-Zehnder interferometer for simultaneous measurement of refractive index and temperature," Appl. Phys. Lett. **94**, 18–21 (2009).

15. Y. Xu, P. Lu, Z. Qin, J. Harris, F. Baset, V. R. Bhardwaj, and X. Bao, "Vibration sensing using a tapered bend-insensitive fiber based Mach-Zehnder interferometer.," Opt. Express **21**, 3031–42 (2013).

16. Y. M. Raji, H. S. Lin, S. A. Ibrahim, M. R. Mokhtar, and Z. Yusoff, "Intensity-modulated abrupt tapered Fiber Mach-Zehnder Interferometer for the simultaneous sensing of temperature and curvature," Opt. Laser Technol. **86**, 8–13 (2016).

17. A. Sun and Z. Wu, "Multimode Interference in Single Mode – Multimode FBG for Simultaneous Measurement of Strain and Bending," IEEE Sens. J. **15**, 3390 (2015).

18. M. Song, "Simultaneous Measurement of Temperature and Strain Using Two Fiber Bragg Gratings Embedded in a Glass Tube," Opt. Fiber Technol. **3**, 194–196 (1997).

19. R. Oliveira, J. H. Osório, S. Aristilde, L. Bilro, R. N. Nogueira, and C. M. B. Cordeiro, "Simultaneous measurement of strain, temperature and refractive index based on multimode interference, fiber tapering and fiber Bragg gratings," Meas. Sci. Technol. **27**, (2016).

20. L. Tong, R. R. Gattass, J. B. Ashcom, S. He, J. Lou, M. Shen, I. Maxwell, and E. Mazur, "Subwavelength-diameter silica wires for low-loss optical wave guiding," Nature **426**, 816–819 (2003).

21. P. Wang, H. Zhao, X. Wang, G. Farrell, and G. Brambilla, "A Review of Multimode Interference in Tapered Optical Fibers and Related Applications," Sensors **18**, 858 (2018).

22. M. J. F. Digonnet and H. J. Shaw, "Analysis of a Tunable Single Mode Optical Fiber Coupler," IEEE Trans. Microw. Theory Tech. **30**, 592–600 (1982).

23. S. K. Sheem and T. G. Giallorenzi, "Single-mode fiber-optical power divider: encapsulated etching technique," Opt. Lett. **4**, 29–31 (1979).

24. R. G. Lamont, K. O. Hill, and D. C. Johnson, "Tuned-port twin biconical-taper fiber splitters: fabrication from dissimilar low-mode-number fibers," Opt. Lett. **10**, 46 (1985).

25. J. Bures, S. Lacroix, and J. Lapierre, "Analyse d'un coupleur bidirectionnel a fibres optiques monomodes fusionnees.," Appl. Opt. **22**, 1918 (1983).

26. R. J. Black, E. Gonthier, S. Lacroix, J. Lapierre, and J. Bures, "Tapered Fibers: An Overview," **V**, 2 (1987).

27. D. T. Cassidy, D. C. Johnson, and K. O. Hill, "Wavelength-dependent transmission of monomode optical fiber tapers," Appl. Opt. **24**, 945 (1985).

28. W. J. Stewart and J. D. Love, "Design limitations on tapers and couplers in single-mode fibres," in *Proc. IOOC-ECOC* (1985), pp. 559–562.

29. G. P. Agrawal, *Fiber Optic Communication Systems*, Third (John Wiley & Sons, Inc., 2002).

30. P. K. Choudhury and T. Yoshino, "TE and TM modes power transmission through liquid crystal optical fibers," Optik (Stuttg). **115**, 49–56 (2004).

31. A. Kumar, K. Thyagarajan, and A. K. Ghatak, "Analysis of rectangular-core dielectric waveguides: an accurate perturbation approach," **8**, 63–65 (1983).

32. P. K. Shukla, P. Khastgir, S. P. Ojha, and P. K. Choudhury, "Comparative aspects of a metal loaded triangular waveguide with uniform and non-uniform distribution of

Goell's matching points," IETE J. Res. **41**, 217–220 (1995).

33. P. K. Choudhury, "Tapered Optical Fibers – An Investigative Approach to the Helical and Liquid Crystal Types," Fiber Opt. Sensors 185–232 (2012).

34. R. I. Laming, "Efficient Pump Wavelenghts of Erbium Doped Fibre Optical Amplifiers," Electron. Lett. **25**, 12–14 (1989).

35. O. Ziemann, "Index Profiles and Types of Fibers," http://www.springer.com/978-3-540-76628-5.

36. C. Kao and P. S. J. Russell, *Guided Rays, Fiber Optics* (1997).

37. G. Rajan, *Optical Fiber Sesors* (2014).

38. M. Bass and E. W. Van Stryland, *Fiber Optics HandBook* (2008).

39. Ji. Sirkis, "Phase-Strain-Temperature Model for Structurally Embedded Interferometric Optical Fiber Strain Sensors with Applications," in *Fiber Optic Smart Structures and Skins IV* (1991), Vol. 1588.

40. D. Jauregui-Vazquez, Y. Lopez-Dieguez, J. M. Sierra-Hernandez, M. Perez-Maciel, M. S. Avila-Garcia, E. Vargas-Rodriguez, R. Rojas-Laguna, and J. M. Estudillo-Ayala, "Modified all-fiber fabry-perot interferometer and its refractive index, load, and temperature analyses," IEEE Photonics J. **7**, (2015).

41. R. W. Waynant and M. N. Ediger, *Electro-Optics Handbook* (2000).

42. S. W. Harun, K. S. Lim, C. K. Tio, K. Dimyati, and H. Ahmad, "Theoretical analysis and fabrication of tapered fiber," Optik (Stuttg). **124**, 538–543 (2013).

43. T. A. Birks and Y. W. Li, "The Shape of Fiber Tapers," J. Light. Technol. **10**, 432–436 (1992).

44. O. Frazao, M. Melo, P. V. S. Marques, and J. L. Santos, "Chirped Bragg grating fabricated in fused fibre taper for strain–temperature discrimination," Meas. Sci. Technol. **16**, 984–988 (2005).

45. Z. Liu, C. Guo, J. Yang, and L. Yuan, "Tapered fiber optical tweezers for microscopic particle trapping: fabrication and application," Opt. Express **14**, 12510–12516 (2006).

46. A. M. Morales and C. M. Lieber, "A Laser Ablation Method for the Synthesis of Crystalline Semiconductor Nanowires," Am. Assoc. Adv. Sci. **279**, 208–211 (2016).

47. J. Chen, M. A. Reed, A. M. Rawlett, and J. M. Tour, "Large On-Off Ratios and Negative Differential Resistance in a Molecular Electronic Device," Science (80-.). **286**, 1550–1553 (1999).

48. J. Westwater, D. P. Gosain, S. Tomiya, S. Usui, and H. Ruda, "Growth of silicon nanowires via gold/silane vapor–liquid–solid reaction," J. Vac. Sci. Technol. B **15**, 554 (2015).

49. A. M. Clohessy, N. Healy, D. F. Murphy, and C. D. Hussey, "Short low-loss nanowire tapers on singlemode fibres," Electron. Lett. **41**, (2005).

50. X. Xing, Y. Wang, and B. Li, "Nanofiber drawing and nanodevice assembly in poly(trimethylene terephthalate)," Opt. Express **16**, (2008).

51. L. Ding, C. Belacel, S. Ducci, G. Leo, and I. Favero, "Ultralow loss single-mode silica tapers manufactured by a microheater," Appl. Opt. **49**, 2441–2445 (2010).

52. P. Wang, M. Ding, L. Bo, C. Guan, Y. Semenova, Q. Wu, G. Farrell, and G. Brambilla, "Fiber-tip high-temperature sensor based on multimode interference," Opt. Lett. **38**, 4617 (2013).

53. A. Leung, P. M. Shankar, and R. Mutharasan, "A review of fiber-optic biosensors," Sensors Actuators, B Chem. **125**, 688–703 (2007).

54. A. G. Mignani, R. Falciai, and L. Ciaccheri, "Evanescent Wave Absorption Spectroscopy by Means of Bi-tapered Multimode Optical Fibers," Appl. Spectrosc. **52**, 546–551 (1998).

55. J. Villatoro, D. Luna-Moreno, and D. Monzón-Hernández, "Optical fiber hydrogen sensor for concentrations below the lower explosive limit," Sensors Actuators, B

Chem. **110**, 23–27 (2005).

56. H. S. MacKenzie and F. P. Payne, "Evanescent Field Amplification in a tapered single-mode optical fibre," Electron. Lett. **26**, 130–132 (1990).

57. M. Ahmad and L. L. Hench, "Effect of taper geometries and launch angle on evanescent wave penetration depth in optical fibers," Biosens. Bioelectron. **20**, 1312–1319 (2005).

58. L. Herrera-Piad, J. Haus, D. Jauregui-Vazquez, J. Sierra-Hernandez, J. Estudillo-Ayala, Y. Lopez-Dieguez, and R. Rojas-Laguna, "Magnetic Field Sensing Based on Bi-Tapered Optical Fibers Using Spectral Phase Analysis," Sensors **17**, 2393 (2017).

59. L. C. Bobb, P. M. Shankar, and H. D. Krumboltz, "Bending Effects in Biconically Tapered Single-Mode Fibers," J. Light. Technol. **8**, 1084 (1990).

60. H. F. Taylor, "Bending Effects in Optical Fibers," J. Light. Technol. **2**, 617–628 (1984).

61. L. Yao, T. Birks, and J. Knight, "Low bend loss in tightly-bent fibers through adiabatic bend transitions.," Opt. Express **17**, 2962–2967 (2009).

62. L. A. Herrera-Piad, J. W. Haus, D. Jauregui-Vazquez, Y. Lopez-Dieguez, J. M. Estudillo-Ayala, J. M. Sierra-Hernandez, J. C. Hernandez-Garcia, and R. Rojas-Laguna, "A dual modality optical fiber sensor," J. Mod. Opt. **65**, 342–347 (2018).

63. C. Y. Lin, L. A. Wang, and G. W. Chern, "Corrugated long-period fiber gratings as strain, torsion, and bending sensors," J. Light. Technol. **19**, 1159–1168 (2001).

64. Y. Wang, D. Richardson, G. Brambilla, X. Feng, M. Petrovich, M. Ding, and Z. Song, "Bend sensors based on periodically-tapered soft glass fibers," in *21st International Conference on Optical Fiber Sensors* (2011), Vol. 7753, pp. 1–4.

65. L. A. Herrera-Piad, D. Jauregui-Vazquez, Y. Lopez-Dieguez, J. M. Estudillo-Ayala, J. C. Hernandez-Garcia, J. M. Sierra-Hernandez, M. Bianchetti, and R. Rojas-Laguna, "Highly stable multi-wavelength erbium-doped fiber linear laser based on modal

interference," Laser Phys. **28**, (2018).

66. L. Herrera-Piad, M. Delgado-Pinar, J. L. Cruz, A. Díez, and M. V. Andrés, "Single-mode Bragg Reflectors in Tapered 4-Modes Fiber," in *OSA Latin America Optics & Photonics Conference* (2018), p. 2.

67. K. Okamoto, *Fundamentals of Optical Waveguides*, Second (Academic Press, Elsevier, 2006).

Conference Proceedings *(It is important to mention that there are more several conference proceedings, but not related to tapered optical fibers or with less impact)*

1. Lopez-Dieguez, Y., Jauregui-Vazquez, D., Estudillo-Ayala, J.M., Herrera-Piad, L.A., Sierra- Hernandez, J.M., Hernandez-Garcia, J.C., Rojas-Laguna, R., "DISEÑO DE UN INTERFERÓMETRO MULTIMODAL", **Book Chapter**, CIO, León, México (2018).

DISEÑO DE UN INTERFERÓMETRO MULTIMODAL

Lopez-Dieguez, Y., Jauregui-Vazquez, D., Estudillo-Ayala, J.M., Herrera-Piad, L.A., Sierra-Hernandez, J.M., Hernandez-Garcia, J.C., Rojas-Laguna, R.

Departamento de Electrónica, División de Ingenierías Campus Irapuato-Salamanca, Universidad de Guanajuato, Carretera Salamanca-Valle de Santiago Km 3.5+1.8 Km, Comunidad de Palo Blanco, Salamanca, Gto., 36885, México.

Catedrático CONACYT, Consejo Nacional de Ciencia y Tecnología (CONACYT), Av. Insurgentes Sur No.1582, Col. Crédito Constructor, Del. Benito Juárez, C. P.039040 México, DF, México.

y.lopezdieguez@ugto.mx.

RESUMEN

En este trabajo se presenta una técnica para la fabricación de interferómetros multimodales por medio de descargas eléctricas. El procedimiento propuesto es de bajo costo y de una alta repetitividad en los patrones de interferencia obtenidos, además, la estructura puede adaptarse a diversos entornos debido a que está compuesto totalmente de fibra óptica convencional. El método propuesto sólo requiere la utilización de una empalmadora de arco eléctrico convencional operada en modo manual con la cual se realiza un empalme entre una fibra óptica convencional y una sección de fibra óptica estrechada. Posteriormente, se realizan descargas eléctricas de manera controlada con el objetivo de manipular la respuesta del patrón de interferencia. Para la validación de esta técnica se fabricaron numerosos interferómetros con características físicas similares los cuales presentan respuestas espectrales similares: un rango espectral libre entre 18nm y 25nm y un contraste de franja máximo de 13dB. Esta técnica de muy bajo costo ofrece la posibilidad de controlar la respuesta de los interferómetros mediante la aplicación de descargas eléctricas y garantiza la repetitividad de los patrones obtenidos. Las características de los interferómetros fabricados hacen posible la aplicación de estas estructuras en el ámbito de sensores.

INTRODUCCIÓN

En los últimos años, el desarrollo alcanzado en el área de las comunicaciones con fibras ópticas ha conllevado al desarrollo de muchísimas áreas relacionadas con las fibras, una de las más importantes es el área de sensores ópticos, que se han hecho muy competitivos en cuanto a sus costos y por las facilidades que ofrecen [1]. Los sensores de fibra óptica pueden ser utilizados para medir una gran cantidad de parámetros tales como: detección de proteínas [2], presión [3], tensión [4], desplazamiento [5], curvatura [6], peso [7], campo magnético [8], [9], índice de refracción [10], temperatura [11], [12], humedad [13], detección simultánea de parámetros tales como temperatura e índice de refracción [14], [15], etc. Existen diversas técnicas para la obtención de interferómetros de fibra óptica que han resultado del interés de muchos investigadores, algunas de ellas utilizan fibras micro-estructuradas [12], [16]–[18] lo que encarece el dispositivo o el proceso de fabricación es complejo [19], [20].

En este trabajo, se propone un procedimiento de bajo costo basado en la técnica de arco eléctrico que permite obtener estructuras interferométricas usando fibra óptica convencional y una sección de fibra óptica convencional estrechada mediante la técnica de arco eléctrico. El rango espectral libre de los interferómetros multimodales obtenidos mediante el procedimiento descrito oscila entre

2. T. Lozano-Hernandez, D. Jauregui-Vazquez, J.M. Estudillo-Ayala, L. A. Herrera-Piad, R. Rojas-Laguna, J.C. Hernández García and J.M. Sierra-Hernandez “Study of nonlinear liquid effects into Ytterbium-doped fiber laser for multi-wavelength generation” **Proc. of SPIE Vol. 105161L-1** 2018, San Francisco, California, United States.

Study of nonlinear liquid effects into Ytterbium-doped fiber laser for multi-wavelength generation

T. Lozano-Hernandez [1], D. Jauregui-Vazquez [*1], J.M. Estudillo-Ayala [1], L. A. Herrera-Piad [1], R. Rojas-Laguna[1], J.C. Hernández García[1] and J.M. Sierra-Hernandez[1]
[1] Departamento de Electrónica, División de Ingenierías Campus Irapuato-Salamanca, Universidad de Guanajuato, Carretera Salamanca-Valle de Santiago Km 3.5+1.8 Km, Salamanca,Gto. 3688. Mexico

ABSTRACT

We present an experimental study of liquid refractive index effects into Ytterbium ring fiber laser cavity configuration. The laser is operated using a bi-tapered optical fiber immersed in water-alcohol concentrations. When the tapered fiber is dipped into a distilled water, a single lasing line with a peak power centered at 1025 nm is achieved. Afterward, by changing the polarization state into the cavity the lasing line can be switched. Moreover, by modifying the refractive index liquid surrounding media the lasing lines can be controlled and special liquid provide nonlinear response. The laser offers compactness, low effective cost and good stability.

Keywords: Ring laser, multi-wavelength, Ytterbium doped fiber, bi-tapered optical fibers

1. INTRODUCTION

Ring fiber laser cavities have been received special attention due its several applications, and the wavelength operation of these cavities depends of the active medium. Here, Ytterbium doped fiber have been used to generate near-infrared spectrums whose are applied in several medical applications, laser cutting and materials processing. As a result, several schemes have been propose based on an all fiber interferometers [1-3]. In addition, some research groups are pursing to obtain multi-wavelength [4], pulsed [5] and switched [2,6] fiber laser for appropriated applications. However, wavelength and power stability is required to achieve a reliable application. In this work we present a stable Ytterbium doped ring fiber laser that generated several lasing lines from 1020 nm to 1027 nm, the lines can be controlled by applying surrounding refractive index media change using a bi-tapered optical fiber. Moreover, the nonlinear effects of special liquid that provide triple simultaneous lasing lines is presented.

2. EXPERIMENTAL SETUP

Our ring fiber laser cavity is composed of a pigtailed laser diode with a centered peak at 976nm and maximal power of 700mW (BL976-PAG700). The pumped signal is integrated into the ring-cavity using an optical fiber Wavelength Division Multiplexer (WDM 980-1060). Then an active medium (28cm of Highly Doped Ytterbium fiber YB1200-4/125) is splice to the to the WDM 980nm port, here Amplified Spontaneous Emission (ASE) is obtained, this signal is launched to an optical fiber coupler 90/10, and by connecting the 10% port to an Optical Spectrum Analyzer (OSA) the fiber laser response is monitoring. The rest of the signal (90%) goes to an optical fiber isolator to set a direction into the cavity. The signal from the isolator is launched to the Bi-Tapered Optical Fiber (BTOF), this element is an optical fiber filter and its fabrication process as well principle operation are mentioned bellow. Finally, a polarization controller is connected between the BTOF and the WDM 1060 port (Fig. 1), here the ring laser cavity is closed.

*jaureguid@ugto.mx

Nonlinear Frequency Generation and Conversion: Materials and Devices XVII, edited by Konstantin L. Vodopyanov, Kenneth L. Schepler, Proc. of SPIE Vol. 10516, 105161L
© 2018 SPIE · CCC code: 0277-786X/18/$18 · doi: 10.1117/12.2291034

3. L. Herrera-Piad, M. Delgado-Pinar, J.L. Cruz, A. Díez, M.V. Andrés “Single-mode Bragg Reflectors in Tapered 4-Modes Fiber ” **Latin America Optics and Photonics Conference, OSA Vol. Th4A.2** 2018, Lima, Peru.

Single-mode Bragg Reflectors in Tapered 4-Modes Fiber

L. Herrera-Piad[(1)], M. Delgado-Pinar[(2)], J.L. Cruz[(2)], A. Díez[(2)], M.V. Andrés[(2)]

(1) Department of Electronics, Universidad de Guanajuato, Campus Irapuato-Salamanca, Carretera Salamanca-Valle de Santiago km 3.5, Salamanca, Gto. 36885, Mexico.

(2) Department of Applied Physics, University of Valencia, Dr. Moliner 50, Burjassot 46100, Spain.

e-mail address: cruz@uv.es

Abstract: In this paper we report on the fabrication of fiber Bragg gratings in tapered 4-modes fibers whose diameter have been reduced to achieve single mode operation. The gratings present a single reflection band, and the device has low insertion loss and reduced coupling to cladding modes when the fiber is symmetrically illuminated.

OCIS codes: (060.3735) Fiber Bragg gratings; (060.2400) Fiber properties.

1. Introduction

Few modes and LMA fibers have been currently introduced in telecommunication and laser technologies [1, 2]; there is a need of handling individual modes to improve their performances. In particular high order modes must be suppressed to achieve single mode operation in power fiber lasers. Furthermore, gratings in either few modes or LMA fibers present several reflection bands corresponding to the coupling between different propagating modes which can spoil the performance of fiber lasers. Here we demonstrate a single band reflector based on a tapered 4-modes fiber with potential applications in fiber lasers.

2. Experiment and results

A 4-modes fiber provided by OFS was used in this experiment; the fiber has a step-index profile and an estimated V-value of near 5 at 1550nm. Since the fiber holds four modes, a Bragg grating in the fiber produces ten different couplings between modes. The observation of the corresponding resonances is dependent on the illumination of the fiber as well as on the axial symmetry of the gratings. Asymmetric excitation and blazed gratings are required to observe the full set of resonances shown in figure 1. The grating was written with a small tilt angle between the fiber and the diffractive phase-mask and light was launched into the fiber by a SM-fiber with a slight offset between fiber cores. The figure shows the expected resonant wavelengths calculated from the effective indices of the modes, and it can be seen that the coupling of the LP_{02} mode is degenerated with the crossed coupling between the LP_{02} and the LP_{21} modes; the same happens between the LP_{11} coupling and the crossed coupling LP_{01}-LP_{21}. If standard (not blazed) gratings are written and the fiber is symmetrically illuminated (standard splice to the SM fiber), even modes have weaker resonances, but not null, due to the residual asymmetries in the gratings; in particular it is relevant the LP_{01} to LP_{11} as it is seen fin figure 1 (right); this resonance can hardly be observed in reflection because the splice between the SM feeding fiber and the few modes fiber acts as a modal filter for asymmetric modes.

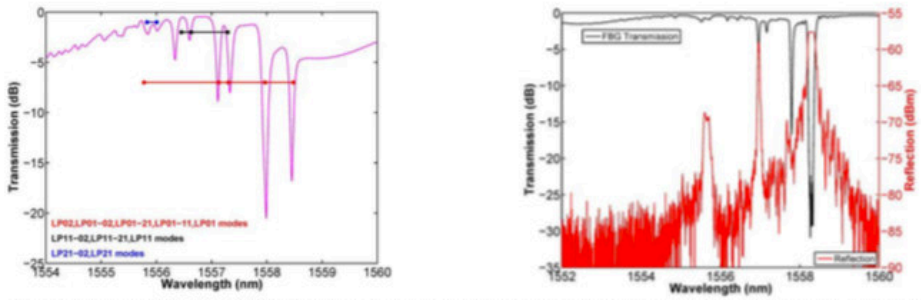

Fig. 1. Few modes fiber gratings spectra. Left: tilted grating measured with asymmetric illumination, the dots show the calculated resonant wavelengths of LP modes coupling. Right: standard grating with symmetric illumination.

The fiber was tapered to reduce the fiber diameter and achieve single mode operation in the fiber waist where gratings have been written. A scheme of the device is shown in figure 2. The fiber waist has 50 microns in diameter, resulting in a V-value of about 2, and 40 mm in length. Each transition has 37 mm in length, the tapers were made long enough to prevent sharp cut-off of high order modes and, consequently, reduce the attenuation [3]. The attenuation measured during the grating fabrication was less than 1dB in the L+C bands.

Published Articles *(It is important to mention that there are two more articles, but not related to tapered optical fibers)*

1. Luis A. Herrera-Piad, Joseph W. Haus, Daniel Jauregui-Vazquez, Juan M. Sierra-Hernandez, Julian M. Estudillo-Ayala, Yanelis Lopez-Dieguez and Roberto Rojas-Laguna "Magnetic Field Sensing Based on Bi-Tapered Optical Fibers Using Spectral Phase Analysis" ***Sensors 2017, 17, 2393.***

sensors

MDPI

Article

Magnetic Field Sensing Based on Bi-Tapered Optical Fibers Using Spectral Phase Analysis

Luis A. Herrera-Piad [1], Joseph W. Haus [2], Daniel Jauregui-Vazquez [1,*], Juan M. Sierra-Hernandez [1], Julian M. Estudillo-Ayala [1], Yanelis Lopez-Dieguez [1] and Roberto Rojas-Laguna [1]

[1] Departamento de Ingeniería Electrónica, División de Ingenierías, Universidad de Guanajuato, Carretera, Salamanca-Valle de Santiago km 3.5 + 1.8, Comunidad de Palo Blanco, Salamanca Gto. C.P. 36885, Mexico; la.herrerapiad@ugto.mx (L.A.H.-P.); jm.sierrahernandez@ugto.mx (J.M.S.-H.); julian@ugto.mx (J.M.E.-A.); y.lopezdieguez@ugto.mx (Y.L.-D.); rlaguna@ugto.mx (R.R.-L.)

[2] Department of Electro-Optics and Photonics, University of Dayton, Dayton, OH 45469, USA; jhaus1@udayton.edu

* Correspondence: jaureguid@ugto.mx; Tel.: +52-46-4647-9940 (ext. 2345)

Received: 4 September 2017; Accepted: 12 October 2017; Published: 20 October 2017

Abstract: A compact, magnetic field sensor system based on a short, bi-tapered optical fiber (BTOF) span lying on a magnetic tape was designed, fabricated, and characterized. We monitored the transmission spectrum from a broadband light source, which displayed a strong interference signal. After data collection, we applied a phase analysis of the interference optical spectrum. We here report the results on two fabricated, BTOFs with different interference spectrum characteristics; we analyzed the signal based on the interference between a high-order modal component and the core fiber mode. The sensor exhibited a linear response for magnetic field increments, and we achieved a phase sensitivity of around 0.28 rad/mT. The sensing setup presented remote sensing operation and low-cost transducer magnetic material.

Keywords: tapered optical fibers; magnetic fiber optic sensor; optical signal processing

1. Introduction

For several decades, the optical fiber sensor community has spent its efforts proposing many structures and methods to measure physical parameters. Two main measurement modalities are available: phase and intensity. Both methods have pros and cons. For instance, intensity modulation has a simple demodulation process, but the measurement can be affected by source variations and environmental effects around the fiber. On the other hand, phase modulation exhibits immunity to intensity variations, but unfortunately its demodulation signal requires additional analysis, and there may be phase ambiguity due to phase wrapping. In addition, there are other points to consider in fiber optic sensors such as the reproducibility of the fabrication process and insertion losses affecting the signal-to-noise ratio.

Some of the first attempts to detect the magnetic field consisted in analyzing the polarization effects and the intensity changes generated by deforming a single mode fiber using an external sensitive magnetic material [1–3]. These works use an external material that responds when a magnetic field is applied. Indeed, contemporary works combine special materials with Fabry–Perot interferometers (FPIs) [4,5] or linear fiber lasers [6] to propose a magnetic field sensor. Nevertheless, in recent years, nanoparticles with special magnetic properties have been studied. These nanoparticles, merged with a liquid, provide a magnetic fluid that, combined with fiber optic structures, generate a magnetic fiber optic sensor; these structures are tapered optical fibers [7–13], FPIs [5,14–18], ring fiber lasers [19–21], fiber Bragg gratings [22–26], multi-mode interferometers [27], core-offset interferometers [28], long period

2. Luis A. Herrera-Piad, Joseph W. Haus, Daniel Jauregui-Vazquez, Yanelis Lopez-Dieguez, Julian M. Estudillo- Ayala, Juan M. Sierra-Hernandez, Juan C. Hernandez-Garcia and Roberto Rojas-Laguna "A dual modality optical fiber sensor" ***Journal of Modern Optics, 2017.***

JOURNAL OF MODERN OPTICS, 2017
https://doi.org/10.1080/09500340.2017.1397220

A dual modality optical fiber sensor

Luis A. Herrera-Piad[a], Joseph W. Haus[b], Daniel Jauregui-Vazquez[a], Yanelis Lopez-Dieguez[a], Julian M. Estudillo-Ayala[a], Juan M. Sierra-Hernandez[a], Juan C. Hernandez-Garcia[a] and Roberto Rojas-Laguna[a]

[a]Departamento de Electrónica, División de Ingenierías Campus Irapuato-Salamanca, Universidad de Guanajuato, Salamanca, Mexico; [b]Department of Electro-Optics and Photonics, University of Dayton, Dayton, OH, USA

ABSTRACT

We propose and demonstrate a fibre optic system based on bi-tapered silica fibre that can simultaneously measure strain and fibre curvature. Both modalities on the signal can be extracted with no measurable crosstalk between them. The experimental signal has a pure phase modulation when strain is applied to the tapered fibre optic section of the sensor and the signal shows only intensity modulation when an un-tapered fibre section is bent. High sensitivity is achieved from the experimental results for strain and bending losses and the estimation of measurement errors is 0.2 and 0.1%, respectively. This system offers low-cost, compactness and it can be adapted for structural health monitoring.

ARTICLE HISTORY
Received 2 July 2017
Accepted 13 October 2017

KEYWORDS
Fibre optic sensor; tapered optical fibre; simultaneous independent measurement; curvature; strain

Introduction

Optical fibres have developed into a mature and ubiquitous technology primarily for optical communications systems. The field of optical fibre sensors has concurrently grown because of the wide availability and low-cost of the fibres, photonic devices and electronics. In particular tapered optical fibres are a specific class that has been developed for diverse applications (1–3); they have found application in fibre lasers (2), non-linear optical elements (4), low level biomolecule or chemical species sensing (5) and thermodynamic variable sensing such as temperature (6); specifically, tapered fibre sensors are able to measure refractive index (7,8), strain (9), magnetic field (10), temperature (11), acoustic signals (12), etc. Moreover, it has been demonstrated that several parameters can be simultaneously detected by modifying fibre optic structures such as temperature and curvature (13), fibre bending and strain (14), temperature and strain (15), and temperature and refractive index (11,16).

Several published approaches are based on spectral feature modulation (wavelength shifts) and intensity modulation (power variations) in the transmitted signal. Nevertheless, when a physical variable is changed both modulations are often observed for the same variable change, which leads to an ambiguity related to associating the measured signal features with a specific effect if multiple variables are being measured. Moreover, recently reported structures use several fibre optic components that involve complicated fabrication processes as well undesirable crosstalk effects in the signal measurements.

In this paper, we report our design and application of a dual modality fibre sensor using an optical fibre bi-taper fabricated by a low-cost technique that simultaneously detects curvature and strain with no measurable crosstalk between the phase and amplitude signal components. In the same piece of fibre, the strain is applied over a section that contains the tapered region and the curvature is applied over a conventional single-mode fibre placed in a second section of the device. The design allows the application of dual simultaneous sensing instead of two interconnected devices. The phase modulation signal provides an unambiguous estimation of the strain and the intensity modulation is similarly only related to the fibre curvature. Our system presents very high sensitivities and no ambiguity in the measurement of each parameter. Furthermore, it would have application in structural health monitoring and it is really important to build permanent points for system optical components to avoid measurement deviations, specifically for materials that present strain and bending at the same time.

CONTACT Daniel Jauregui-Vazquez jaureguid@ugto.mx

3. L A Herrera-Piad, D Jauregui-Vazquez, Y Lopez-Dieguez, J M Estudillo-Ayala, J C Hernandez-Garcia, J M Sierra-Hernandez, M Bianchetti and R Rojas-Laguna "Highly stable multi-wavelength erbium-doped fiber linear laser based on modal interference" ***Laser Phys. 28 (2018) 035101 (7pp).***

IOP Publishing | Astro Ltd — Laser Physics
Laser Phys. **28** (2018) 035101 (7pp) — https://doi.org/10.1088/1555-6611/aa9d9c

Highly stable multi-wavelength erbium-doped fiber linear laser based on modal interference

L A Herrera-Piad[1], D Jauregui-Vazquez[1], Y Lopez-Dieguez[1], J M Estudillo-Ayala[1], J C Hernandez-Garcia[2], J M Sierra-Hernandez[1], M Bianchetti[3] and R Rojas-Laguna[1]

[1] Departamento de Electrónica, División de Ingenierías Campus Irapuato-Salamanca, Universidad de Guanajuato, Carretera Salamanca-Valle de Santiago km 3.5 + 1.8 km, Salamanca, Gto. 36885, Mexico
[2] Catedrático CONACYT, Consejo Nacional de Ciencia y Tecnología (CONACYT), Av. Insurgentes Sur No. 1582, Col. Crédito Constructor, Del. Benito Juárez, C. P. 039040, Mexico
[3] Departamento de Estudios Multidisciplinarios, División de Ingenierías Campus Irapuato-Salamanca, Universidad de Guanajuato, Av. Universidad s/n, Col. Yacatitas, Yuriria, Gto. 38940, Mexico

E-mail: la.herrerapiad@ugto.mx

Received 29 April 2017, revised 28 November 2017
Accepted for publication 28 November 2017
Published 1 February 2018

Abstract

We report a linear fiber laser cavity based on an all-fiber Fabry–Perot interferometer and bi-tapered optical fiber for multi-wavelength emission generation. Curvature and strain are used to operate the laser system and the number of lines as well, the emission regions are stronger related to the physical effect applied, due to the phase alteration between the multiple fiber optic modes involved. The original laser emissions present zero wavelength variations, minimal power fluctuations and small spacing mode (1 nm). Additionally, a nonlinear fiber was employed trying to improve the performance of the multiple lasing lines. This system offers a low implementation cost, compactness and good laser parameters.

Keywords: erbium-doped fiber laser, tapered optical fiber, Fabry–Perot interferometer, curvature, strain

(Some figures may appear in colour only in the online journal)

1. Introduction

Erbium-doped fiber lasers (EDFL) have been proposed during more than four decades for different purposes. In recent times, there is growing interest in the use of EDF for pulsed lasers [1, 2], meanwhile, some research groups have been concentrated on fiber continuous wave lasers operating with fiber optic structures, pursuing a narrower linewidth and increasing the number of laser lines. Most of the recent works use all-fiber structures such as fiber Bragg gratings [3–7], special fibers as photonic crystal [3, 5, 6, 8–10], twin-core [11] and polarization maintaining fibers [12, 13], Mach–Zehnder [10, 11, 14–16], Fabry–Perot [17, 18], Sagnac [9, 12, 19] devices and nonlinear components [14, 20]. One interesting structure is the Fabry–Perot filter (FPF) based on air intra-cavities due to their stable measurement, compactness and simple fabrication [17, 18]. Other important devices widely used in fiber laser arrangements are bi-tapered optical fibers, whose have been developed for controlling the output response [16, 21–23].

As it is appreciable from literature, several techniques and components to fabricate a fiber structure filter have been presented to be used in a laser cavity, however, sometimes a complex setup is required to obtain good performance. At that point, we propose competitive laser parameters, specifically low power fluctuations and excellent wavelength stability, better than previously reported works [7, 9, 13, 16, 18, 19]. Despite some works report good symmetrical spacing emissions for more than 4 lasing lines [7, 9, 13, 18, 19], the pulse width reported is bigger than obtained by our configuration (0.138 nm). In addition, our cavity simplicity does not require

4. Yanelis Lopez-Dieguez, Julian M. Estudillo-Ayala, Daniel Jauregui-Vazquez, Luis A. Herrera-Piad, Juan M. Sierra-Hernandez , Juan C. Hernandez-Garcia, Marco Bienchetti , Jose R. Reyes-Ayona , and Roberto Rojas-Laguna "Tip Fiber-Optic Intermodal Interferometer for Refractive Index Sensing" ***IEEE PHOTONICS TECHNOLOGY LETTERS, VOL. 30, NO. 1, JANUARY 1, 2018.***

Tip Fiber-Optic Intermodal Interferometer for Refractive Index Sensing

Yanelis Lopez-Dieguez, Julian M. Estudillo-Ayala, Daniel Jauregui-Vazquez, Luis A. Herrera-Piad, Juan M. Sierra-Hernandez, Juan C. Hernandez-Garcia, Marco Bienchetti, Jose R. Reyes-Ayona, and Roberto Rojas-Laguna

***Abstract*—We propose an all-fiber-optic multimode interferometer for measuring liquid refractive index. The interferometer was manufactured by using the arc splice technique between standard single-mode fiber and optical microfiber. A maximum refractive index sensitivity of 112 dB/RIU is experimentally demonstrated. In addition, thermal effects exhibit low phase modulation (12 pm/°C) with minimal intensity variations (-10.7×10^{-3} dB/°C); as a result, cross sensitivity around 0.05×10^{-6} RIU/°C and 0.9×10^{-6} RIU/°C is obtained for intensity and phase modulation. The stability analysis shows minimal wavelength and power variations, 0.01 nm and 0.27 dB respectively, for constant temperature and refractive index. Spatial frequency analysis was explored as an alternative method to measure liquid refractive index avoiding thermal effects.**

***Index Terms*—Modal interference, refractive index, optical fiber sensors.**

I. Introduction

REFRACTIVE index is an important factor which is related to several research and industrial applications. As a result, the optical-fiber sensor community pays special attention in measuring this parameter using fiber structures with high sensitivity, long dynamic range, lower ambiguity detection and zero cross-sensitivity [1]–[3]. Thus, several fiber-optic structures have been proposed such as: Sagnac loop [4], Fabry-Perot interferometers [5], tapered fiber-optic [6], tapered fiber-optic coupler [7], photonic crystal fibers structures [8], Mach-Zehnder interferometers [9], long period fiber gratings [3], and multimode interference effects [10]. One alternative explored in recent decades is the well-known arc splice technique [5], [8], this method has been used by some research groups to propose highly sensitive refractive index sensors based on phase [4], [7] and intensity [11], [12] modulation. Nevertheless, it is important to analyze the modulation benefits and risks, before proposing a reliable fiber optic sensor. For instance, phase modulation has good accuracy and immunity to intensity variation, unfortunately ambiguity detection (for instance thermal sensitivity) and complicated demodulation process are involved. By another hand, intensity modulation offers low cost demodulation process, but the measurements can be affected by power source variations or bending fiber effects. The disadvantages for intensity or phase modulation can be solved using computational methods or optical signal processing [13]. In this letter, an approach to measuring liquid refractive indices based on a simply manufactured fiber-optic interferometric structure is presented. Our proposed structure consists on the splice joint between conventional single mode optical fiber and optical microfiber. The reflection spectrum exhibits phase-intensity modulation for the refractive index changes and temperature, here the response is analyzed to present a reliable refractive index fiber optic sensor.

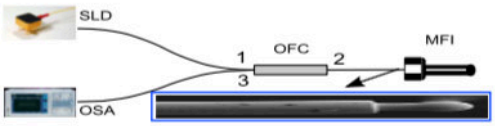

Fig. 1. Schematic diagram of the experimental setup used to fabricate and characterized the modal interferometer. Inset: Micrograph of Modal interferometer.

II. Fabrication Method and Principle Operation

A. Manufacturing Process

The experimental setup used during the manufacturing process and physical characterization is shown in Fig. 1. An optical fiber circulator (OFC) is used to interconnect all the components involved: a broadband source was connected to the port 1 (super-luminescent diode QPHOTONICS QSDM-1550-1), this signal is launched to the proposed interferometer by port 2, and by an Optical Spectrum Analyzer (Yokogawa AQ6370) located at Port 3 the reflected signal is monitored.

To obtain the proposed interferometer, a stretched SMF28 with 30μm radius (microfiber) and standard optical fiber are cleaved, set, and aligned into the commercial splicer (FITEL S-175 V.2000). The microfiber was fabricated

Manuscript received August 6, 2017; revised September 17, 2017; accepted October 25, 2017. Date of publication November 6, 2017; date of current version December 19, 2017. This work was supported in part by UGTO-PTC541. The work of Y. Lopez-Dieguez was supported by the Consejo Nacional de Ciencia y Tecnología under Student Research Grant 577494/307127. *(Corresponding author: Jose R. Reyes-Ayona.)*

Y. Lopez-Dieguez, J. M. Estudillo-Ayala, D. Jauregui-Vazquez, L. A. Herrera-Piad, J. M. Sierra-Hernandez, J. R Reyes-Ayona, and R. Rojas-Laguna are with the División de Ingenierías Campus Irapuato-Salamanca, Departamento de Electrónica, Universidad de Guanajuato, Salamanca 36885, Mexico (e-mail: y.lopezdieguez@ugto.mx; julian@ugto.mx; jaureguid@ugto.mx; la.herrerapiad@ugto.mx; jm.sierrahernadez@ugto.mx; jchernandez@ugto.mx; jr.reyes@ugto.mx; rlaguna@ugto.mx).

J. C. Hernandez-Garcia is with the División de Ingenierías Campus Irapuato-Salamanca, Departamento de Electrónica, Universidad de Guanajuato, Salamanca 36885, Mexico, and also with the Consejo Nacional de Ciencia y Tecnología, Del. Benito Juárez 039040, Mexico.

M. Bienchetti is with the División de Ingenierías Campus Irapuato-Salamanca, Departamento de Estudios Multidisciplinarios, Universidad de Guanajuato, Yuriria 38940, Mexico (e-mail: mb@ugto.mx).

Color versions of one or more of the figures in this letter are available online at http://ieeexplore.ieee.org.

Digital Object Identifier 10.1109/LPT.2017.2771409

5. Yanelis Lopez-Dieguez, Julian M. Estudillo-Ayala, Daniel Jauregui-Vazquez, Luis A. Herrera-Piad, Juan M. Sierra-Hernandez, Diego F. Garcia-Mina, Eloisa Gallegos-Arellano, Juan C. Hernandez-Garcia, and Roberto Rojas-Laguna "Erbium Ring Fiber Laser Cavity Based on Tip Modal Interferometer and Its Tunable Multi-Wavelength Response for Refractive Index and Temperature" ***Appl. Sci. 2018, 8, 1337.***

applied sciences

MDPI

Article

Erbium Ring Fiber Laser Cavity Based on Tip Modal Interferometer and Its Tunable Multi-Wavelength Response for Refractive Index and Temperature

Yanelis Lopez-Dieguez [1], Julian M. Estudillo-Ayala [1], Daniel Jauregui-Vazquez [1,*], Luis A. Herrera-Piad [1], Juan M. Sierra-Hernandez [1], Diego F. Garcia-Mina [2], Eloisa Gallegos-Arellano [3], Juan C. Hernandez-Garcia [1,4] and Roberto Rojas-Laguna [1]

[1] Departamento de Electrónica, División de Ingenierías Campus Irapuato-Salamanca, Universidad de Guanajuato, Carretera Salamanca-Valle de Santiago km 3.5 + 1.8 km, Salamanca Gto. 36885, Mexico; y.lopezdieguez@ugto.mx (Y.L.-D.); julian@ugto.mx (J.M.E.-A.); la.herrerapiad@ugto.mx (L.A.H.-P.); jm.sierrahernandez@ugto.mx (J.M.S.-H.); jchernandez@ugto.mx (J.C.H.-G.); rlaguna@ugto.mx (R.R.-L.)

[2] Departamento de Física, Facultad de Ciencias Básicas, Universidad Autónoma de Occidente, Calle 25 # 115-85, Cali 760030, Colombia; dmina@uao.edu.co

[3] Departamento de Tecnologías de la Información y Comunicación, Universidad Tecnológica de Salamanca, Avenida Universidad Tecnológica 200, Ciudad Bajío, Salamanca Gto. 36766, Mexico; egallegos@utsalamanca.edu.mx

[4] Catedrático CONACYT, Consejo Nacional de Ciencia y Tecnología (CONACYT), Av. Insurgentes Sur No. 1582, Col. Crédito Constructor, Del. Benito Juárez C.P. 039040, México

* Correspondence: jaureguid@ugto.mx; Tel.: +52-46-4647-9940 (ext. 2345)

Received: 29 June 2018; Accepted: 7 August 2018; Published: 10 August 2018

check for updates

Abstract: A tunable multi-wavelength fiber laser is proposed and demonstrated based on two main elements: an erbium-doped fiber ring cavity and compact intermodal fiber structure. The modal fiber interferometer is fabricated using the cost-effective arc splice technique between conventional single-mode fiber and microfiber. This optical fiber structure acts as a wavelength filter, operated in reflection mode. When the refractive index and temperature variations are applied over the fiber filter, the ring laser cavity provides several quad-wavelength laser spectra. The multi-wavelength spectra are tuned into the C-band with a resolution of 0.05 nm. In addition, the spectra are symmetric with minimal power difference between the lasing modes involved, and the average of the side mode suppression ratio is close to 37 dB. This laser offers low-cost implementation, low wavelength drift, and high power stability, as well as an effect of easy controllability regarding tuned multi-wavelength.

Keywords: fiber laser; ring laser cavity; tunable multi-wavelength laser

1. Introduction

For several decades, the ability to generate tunable or switched multi-wavelength fiber lasers has been one of the focuses pursued by the fiber laser community. These lasers are associated with many reliable applications related to multi-wavelength spectra such as optical fiber sensors [1–9], spectroscopy systems [10], biomedical imaging [11], telecommunications [12], microwave photonics [13], and radio frequency optical domain systems [14]. These applications require achieving compact configuration, stable emission, narrow linewidth, and adequate spacing mode. All these features prevent crosstalk, error measurement, and low resolution. To this end, many methods have been proposed, most of them based on fiber interferometers (Fabry-Perot, Mach-Zehnder, Michelson, and Sagnac) [15–19], comb filters [20,21], Raman effect [20], Brillion scattering [22,23], nonlinear loop mirrors [24], saturable optical absorber elements [25,26], and extrinsic interferometers [27].